A STUDY OF HYDROGEN/OXYGEN RECOMBINATION CATALYSTS AND THEIR APPLICATION IN ELECTROCHEMICAL SYSTEMS.

A thesis submitted for the degree of Doctor of Philosophy

of

The City University

by

T. M. HO

April 1984.

ACKNOWLEDGEMENTS

I would like to thank my supervisor, Professor A.C.C. Tseung for his advice, help and stimulating discussion during the entire research work.

I acknowledge the cooperation and assistance of my colleagues in the Chemical Energy Research Centre, the Department's Technical Staff responsible for the practical aspects of apparatus construction, and the Physics Department in making available facilities for X-ray analysis etc.

I should like to thank [redacted] for their patience and understanding during the period I have been engrossed in the present project. I also want to thank [redacted] for their encouragement.

I would like to express my gratitude to [redacted] for the typing of this thesis.

Thanks are due to Chloride Alcad, and to the Science and Engineering Research Council for financial support.

Chemical Energy Research Centre,
Department of Chemistry,
The City University,
London E.C.1.

CONTENTS

INDEX FOR FIGURES

INDEX OF TABLES

ABSTRACT

All aqueous secondary battery cells evolve hydrogen and oxygen towards the end of the charging cycle and when being overcharged. This leads to a progressively diminishing volume of electrolyte being present in the battery cell, and a maintenance function involving topping up the electrolyte with distilled water is, therefore, necessary to restore the electrolyte to its original volume. In order to avoid such function, catalyst such as Pd/Al_2O_3 has been used commercially to recombine the H_2/O_2 mixture so that the reformed water is allowed to return to the cell. Unfortunately, as the catalyst ages, it tends to suffer from " start-up " problems and eventually fails to function completely. Although many investigations have been carried out in the past 15 years or so, the problems remain unsolved. Therefore, the life and reliability of the catalysts in a catalytic reaction would be of paramount importance with secondary cell systems.

In the course of these investigations, the concepts of free-space and water condensation on the catalyst surface were discovered. These have led to an understanding of the problems which affect the life and reliability of catalysts in catalytic devices or hydrocaps. Generally, the " start-up " problems were due to flooding by a thin film of water on the catalyst surface. As a result, the catalyst loading and specific surface area of the catalyst were increased significantly, and more active catalysts (e.g. Pt or Pd dispersed on $NiCo_2O_4$) were used. However, all these methods failed to solve the " start-up " problem. On the other hand, the incorporation of a valve system to isolate the catalyst from the free-space during

shut-down period, so that the water arising out of the slow reaction between residual H_2/O_2 on the catalyst surface is kept to minimum. Furthermore, the water droplets lying on the sides of the hydrocap containing the H_2/O_2 recombination catalysts tend to vaporise on standing and the water molecules are finally adsorbed on the packing material and/or catalyst. Such problems were successfully solved using a packing material (NiO) capable of adsorbing water vapour from its surrounding so as to reduce condensation of water on the catalyst, and itself capable of catalysing H_2/O_2 recombination under the temperature conditions attained in use.

The modification of commercial hydrocaps for the ingress of air (and thus oxygen) to the catalyst bed, and the provision of such an external source of oxygen enables substantially complete reaction of all hydrogen evolved in cases where there is a shortage of evolved oxygen, and in situations where substantially only hydrogen is evolved.

The catalytic activities of platinized $NiCo_2O_4$, Co_3O_4 and $La_{0.5}Sr_{0.5}CoO_3$ have been found to be greater than that of platinum dispersed on alumina or glass powder. The mechanisms for the promotional effect of these metal oxides as active support for the reaction of hydrogen with oxygen to form water were studied by means of a differential system. Electrochemical studies and gas chromatography results show that the metal oxides did not absorb hydrogen nor oxide reduction as confirmed by x-ray powder diffraction analysis. However, the kinetic characteristics and specific platinum activity measurements show that the interaction of hydrogen and oxygen over the metal oxides is due to a temperature effect. The mechanism of catalytic oxidation of hydrogen by the oxide catalysts proceeds via alternate reduction and oxidation of the oxide surface, the reduction of the cations takes

place on the oxide surface, which is reoxidised by oxygen.

The information on Co_3O_4 agreed reasonably well with the only published data, whilst the information on $NiCo_2O_4$, $La_{0.5}Sr_{0.5}CoO_3$ and lithiated Co_3O_4 is new.

CHAPTER 1

GENERAL INTRODUCTION.

CHAPTER 1

1 GENERAL INTRODUCTION.

1.1 Introduction to Secondary Battery Cells.

Secondary battery is a useful source of instant energy. It has an important place in industry and in installations serving the public need. The increasing use of energy means that the secondary battery will continue its role as an auxiliary power systems.

Secondary batteries are commonly classified by the nature of the electrolyte, namely, acid and alkaline batteries. The acid batteries use sulphuric acid solutions, generally use lead for the active material and are known as lead-acid batteries. The alkaline batteries utilize potassium hydroxide solutions. It is also customary to classify the alkaline batteries by the principal metallic constituent of the positive and negative active materials, e.g. nickel-cadmium.

The values of the cell voltage [1] for lead-acid, nickel-cadmium, are 2.0 and 1.3 volts per cell respectively.

All secondary aqueous batteries produce hydrogen and oxygen towards the end of the charging cycle and also are being overcharged. Overcharge processes involve electrolyte water decomposition and consequently the loss of the electrolyte by dissociation into hydrogen and oxygen is inevitable.

In acidic media, the reactions are as follows :

Cathode : $4H^+ + 4e \longrightarrow 2H_2$

Anode : $2H_2O \longrightarrow O_2 + 4H^+ + 4e$

Overall process : $2H_2O \longrightarrow 2H_2 + O_2$

In alkaline media, the reactions are as follows :

Cathode : $4H_2O + 4e \longrightarrow 2H_2 + 4OH^-$

Anode : $4OH^- \longrightarrow O_2 + 2H_2O + 4e$

Overall process : $2H_2O \longrightarrow 2H_2 + O_2$

When a secondary cell is charged, the normal discharge electrode processes are reversed, restoring the capacity to the cell plate active materials. For example, in a lead-acid battery[2] the following reactions take place :

Positive electrode : $PbO_2 + 3H^+ + HSO_4^- + 2e \underset{\text{charge}}{\overset{\text{discharge}}{\rightleftharpoons}} PbSO_4 + 2H_2O$

Negative electrode : $Pb + HSO_4^- \underset{\text{charge}}{\overset{\text{discharge}}{\rightleftharpoons}} PbSO_4 + H^+ + 2e$

Overall reaction : $Pb + PbO_2 + 2HSO_4^- + 2H^+ \underset{\text{charge}}{\overset{\text{discharge}}{\rightleftharpoons}} 2PbSO_4 + 2H_2O$

The charge processes will, of course, differ for other secondary accumulator types, e.g. nickel-cadmium[3], nickel-zinc etc., but the overcharge processes are common to all secondary batteries if the state of full charge is required.

All vented aqueous secondary cells, when approaching the end of the charging cycle and when being overcharged evolve hydrogen and oxygen as a result of the excess electrical energy dissociating the water in the electrolyte. Not only is a mixture of hydrogen and oxygen explosive and precautions are necessary to avoid this hazard, but the dissociation of water results in a progressively diminishing volume of electrolyte being present in the battery cell. When the cell is being charged regularly, a maintenance function involving topping up the electrolyte with distilled water is, therefore, necessary to restore the electrolyte to its original volume. This is an essential maintenance function which cannot be ignored or permanent damaged to

the cells will result. This is a time-consuming and inconvenient task.

Various different methods have been used commercially to try to reduce the cost involved in topping up a cell with distilled water. Cells have been designed to accommodate large volumes of electrolyte, thereby extending the periods between maintenance. Also, automatic topping up devices have been designed to eliminate the responsibility of human being from this maintenance function. However, if a catalyst can be used to recombine the hydrogen and oxygen produced when the cell is being charged so that the reformed water is returned to the cell and the volume of the electrolyte does not diminish, thereby eliminating the need for topping up with distilled water. This is a method by which a maintenance free cell can be produced. Therefore, to overcome this problem by providing a H_2/O_2 catalytic recombination device on top of the battery to ensure that all the hydrogen and oxygen evolved during the charging cycle is catalytically recombined to form water which is then returned to the battery.

Sealed secondary batteries which evolve hydrogen and/or oxygen gases especially during the time they are being charged. It has been known that the gases formed in sealed secondary batteries build up pressure within the battery casing, so it is essential to allow at least a portion of these gases to escape. This, in turn, requires that water lost in the decomposition must be periodically replaced in the electrolyte. This has, in turn, limited the use of secondary batteries as power sources, unless the amount of hydrogen and oxygen evolved is catalytically recombined to form water[4] which is then allowed to drip back to the cell, so that the electrolyte volume remains substantially constant. Another method [4] [5] of solving the gassing problem is secondary batteries is to arrange the capacities

of the electrodes.

Sealed cells such as nickel-cadmium or lead acid batteries do not require topping up with water because they are constructed in such a way that only oxygen is evolved when the cell is charged, and this is retained and recombined in the cell which is made with restricted electrolyte being absorbed in a separator between plates of opposite polarity. The electrolyte volume in this type of cell does not change and consequently topping up is unnecessary. Unfortunately, such cells suffer from a performance loss arising from the high internal resistance in the cell due to the presence of an absorbent separator and the restricted electrolyte. Typically, the sealed alkaline nickel-cadmium cells are based on the following design principles :

The negative electrode has an excess (about 40 - 50%) of uncharged active material so that oxygen first evolves at the positive electrode. The cell is operated in the restricted electrolyte condition where the electrolyte does not completely filled the electrode pores and is contained in a partially filled porous plastic separator in the inter-electrode gap. In this way, gas channels are provided for the transport of evolved oxygen from the positive, across the separator, to the negative where it recombines with charged metallic cadmium to form codmium hydroxide. The evolved oxygen at the positive represents an internal short circuit and prevents the negative attaining full capacity, thereby obviating hydrogen evolution and preventing cell pressurisation by reconsuming the oxygen evolved from the positive. The sealed rechargeable nickel-cadmium batteries of such systems tend to have a higher cost and therefore have limited application.

Other accumulator types such as metal-air, e.g. a major problem when the Al-air system[6] is in continuous use for a long time is the reaction products. For example, the slow evolution of hydrogen on discharge should be catalytically consumed for safety reason and the return of reformed water to the cell is not absolutely necessary.

1.2 The Problems.

The best way to avoid topping up of cells with distilled water is to use an effective catalyst to recombine the evolved hydrogen and oxygen to form water which is then allowed to return to the cell. In this way, the electrolyte volume does not change and consequently topping up is unnecessary. Unfortunately, one of the major problems with the current commercial catalysts is that they tend to suffer from " start-up ".

When the catalyst is new, although the start may be delayed, " start-up " will eventually commence and the catalyst will then behave normally but as the catalyst ages, " start-up " becomes more difficult until finally the catalytic recombination reaction will not recommence at all and the catalyst fails. Failure is due to " flooding " of the catalyst by a water film since drying the catalyst in an oven generally restores catalytic activity.

Much effort has been expended over the past 15 years or so to try to overcome this " start-up " problem. Methods such as small heating coils[4] to evaporate the water and hydrophobic materials[5] to repel the water so that the H_2/O_2 recombination reaction will start quickly, also various designs[7] of housing for the catalysts have been commercially developed in order to try to overcome the

" start-up " problem. All these methods have however failed to solve the problems.

Although many investigations have been carried out in U.S.A. and Japan, the " start-up " problems remain unsolved. Therefore, the life and reliability of the catalysts in a catalytic reactor would be of paramount importance with secondary cell systems and major improvements are needed to the catalytic devices or hydrocaps containing H_2/O_2 recombination catalysts.

1.3 Hydrogen and Oxygen Recombination Catalysts.

There are several different types of catalysts can be used to recombine hydrogen and oxygen to form water but the most commonly used are based on precious metals, e.g. platinum or palladium, usually suspended on inert carriers. For example, the commercially available catalytic devices contain Pd/Al_2O_3 for H_2/O_2 recombination. There are cases where precious metals dispersed onto active supports or carriers so that the effective catalyst area is considerably increased compared to catalysts such as Pd/Al_2O_3. The so-called " spillover " catalysts are based on precious metals supported on oxides of tungsten or molybdenum have been studied by Hobbs and Tseung[8][9][10]. In this way the effective reaction zone area is extended onto the support, increasing the net catalytic reaction rate. However, during this investigation, platinized or palladised spinel oxides such as ~~Pt~~/$NiCo_2O_4$ and ~~Pt~~/Co_3O_4 have been shown to be the potential catalysts for H_2/O_2 recombination, where the spinel oxides behave as active supports.

Ladacki[11] et al observed the activity of various metallic catalysts for the H_2/O_2 reaction at ambient and low temperatures down to -196°C . Catalysts like Pd, Pt, Pt-Rh, Pt-Rh-Pb and Pt-Ni suspended on alumina as inert supports; Pd and Pt were shown to possess high catalytic activity towards H_2/O_2 recombination. Earlier work by Boreskov[12] et al and later by Jennings[13] et al also showed that precious metals are the most effective catalysts for H_2/O_2 reaction both at low and high temperatures e.g. -195 to 200°C . Perhaps the studies most relevant to this work are those by Boreskov[14][15] during the period 1952-57, who investigated the effectiveness of Fe, Co, Ni, Cu, Rh, Pd, Pt, Ag and Au as catalysts in the H_2/O_2 reaction. The best catalysts were Pd, Pt and Ni and also some Pt-Au and Pt-Ag alloys. The reactions of H_2/O_2 on Pt under different experimental conditions[16][17] have been studied and such reactions were also investigated by Ostrovskii[18] on silver instead of platinum. The catalytic activity of nickel surface[19] for H_2/O_2 interaction has been considered to take place on clean crystal surfaces.

The reaction between hydrogen and oxygen has been studied over a wide range of oxides, and the catalytic reactions occur at relatively high temperatures than that of precious metals. Lanthanide oxide[20][21][22], for example, the H_2/O_2 recombination takes place in the temperature range 100 - 200°C at pressures from 1 to 10 Torr. The oxides of the rare earth elements[23][24] show catalytic activity at temperature range 300 - 500°C and a total pressure of over 500 Torr. The catalytic reaction of the oxides of first row transition metals[25][26] takes place in a wide range of temperatures, e.g. 100°C for MnO_2 and 470°C for TiO_2 at atmospheric pressure. Ferric oxide[27][28] also shows

catalytic activity towards H_2/O_2 recombination at about 200°C at atmospheric pressure.

Although there are many different types of catalysts capable of catalysing H_2/O_2 to form water, the most suitable and effective are based on precious metals dispersed onto active supports.

1.4 Applications of Hydrogen/Oxygen Recombination Hydrocaps.

The water control devices, commercially available under the tradename of hydrocaps[29], were developed principally for electric vehicle batteries; and hydrocap is required for each cell in a batteries. For successful applications of hydrocaps where maintenance, safety and reliability factors are of paramount importance; for example, the Hydrocap trade literature cites atomic energy plants, mines, hospitals, power plants, on locomotives, boats, submarines and other applications.

In the case of electrical vehicle batteries, particularly for road vehicles such as milk floats, where the battery can be equipped with hydrocap for water control would reduce the relatively high cost of maintenance and increase reliability and extend battery life.

For the newly designed hydrocaps, Tseung[30] et al have successfully modified the devices to accommodate any non-stoichiometric gas composition produced when the charging voltage is less than 1.50V.

1.5 Market Surrey of Hydrocaps.

The catalytic activity of 1.5 mg of precious metal dispersed onto spinel oxides is generally higher than that of the commercial catalyst containing 5 mg of precious metal suspended on alumina per hydrocap. This is because the spinel oxide is an active support whereas

alumina is inert. However, the reduction of precious metal loadings is not of great importance in battery recombination caps, since the catalyst cost represents a small proportion of the overall device cost. For example, each commercially available hydrocap costs about £2 ($3), and each one contains 5 mg Pd which at current prices (£1.61 per g, May 1983) amounts to less than 1p. Fabrication and other materials costs therefore dominate. But, if the life of the device could be prolonged, then its wider adoption should follow and costs could be reduced through mass production.

If we consider the newly designed type of hydrocap and its modifications to fix into the conventional six vented filler caps in battery (ie. One hydrocap per car battery). all these would cost slightly more than the present hydrocap. But, an extra of about £1 for each hydrocap would be expected through mass production. However, with such invention, the most important criterion is to increase the life and reliability of the batteries. Furthermore, the cost of maintaining the cells by regular topping up with distilled water can be eliminated.

The possibility of using the new type of water control devices will undoubtedly have a place in secondary battery technology. Secondary batteries have a wide area of applications (section 1.4), and one would estimate the total number of hydrocaps constantly in service to be approximately 2 - 3 millions in the United Kingdom alone.

CHAPTER 2

LITERATURE SURVEY.

CHAPTER 2

2 LITERATURE SURREY.

2.1 Introduction to Heterogeneous Catalysts.

A catalyst can only increase the rate of a process which is thermodynamically feasible, e.g. one in which there is a decrease in free energy. Heterogeneous catalysts are solids that increase the rates of chemical reactions by the specific properties of their surfaces, and such catalysts are generally not in the same phase[31] as the reacting mixture, e.g. gas reactions catalysed by a solid.

2.1.1 Types of Heterogeneous Catalysts.

Heterogeneous catalysts are normally classified according to the functions they perform and their electrical and thermal conductivity properties. Metals are usually good conductors and their primary catalytic function is hydrogenation and dehydrogenation. In metal oxides, the oxygen ions can sometimes be removed or added to the lattice depending on the experimental conditions. For example, the influence of crystal structure on the activity of $NiCo_2O_4$ and Co_3O_4 has been reported by King and Tseung[32][33], the spinel phase of $NiCo_2O_4$ is metastable and begins to change to cubic phase at about $450^{\circ}C$, and above $900^{\circ}C$ the spinel structure of Co_3O_4 becomes lower oxide CoO of cubic structure with loss of oxygen. The electrochemical studies of lithiated nickel oxide and $La_{0.5}Sr_{0.5}CoO_3$ perovskite oxide by Tseung[34] showed that oxygen molecule is dissociatively chemisorbed on these oxides. Other types of heterogeneous catalysts such as solid salts with their main catalytic function is to effect polymerisation or isomerisation.

2.1.2 The Role of the Surface in Heterogeneous Catalysis.

Bond[35] suggested that there are three principal functions of heterogeneous catalysts :

(a) the catalysts acts as a third body so that the excess energy can be removed.

(b) " activation " of the reactants, e.g. precious metals dissociate hydrogen gas molecules into atoms.

(c) " geometric factor " in which the reactants are brought together in a way that the possibility of a transition state formation is kept to a minimum.

It is therefore quite clear that the surface of catalysts plays a significant role in heterogeneous catalysis.

2.1.3 Theoretical Considerations of Rates of Adsorption and Desorption.

The rates of adsorption and desorption have been discussed by Bond[36] that both the adsorption and desorption rates vary exponentially with their respective activation energies, and the process involving the gas phase A_2 molecule is as follows :

$$A_2 + 2* \longrightarrow 2A_*$$

Where * represents a single adsorption site.

The rate of adsorption (r_a) is given by

$$r_a = -\frac{dPA_2}{dt}$$

$$= \left[* \; *\right] \sigma \; Z \exp\left(\frac{-E_a}{RT}\right)$$

Where PA_2 = the pressure of A_2 in the gas phase.

$\left[* \; *\right]$ = the concentration of pairs of empty sites.

σ = the chance that collision of a molecule of A_2 with a pair of empty sites will result in adsorption.

Z = the number of collisions of A_2 molecules with the total surface per unit time.

E_a = the activation energy of adsorption.

R = gas constant.

T = temperature.

Z is sometimes called the surface collision number, and is given by

$$Z = PA_2 (2\pi mKT)^{-\frac{1}{2}},$$

where m = mass of A_2 molecule.

K = Boltzmann constant.

For the desorption process involving

$$2A^{*} \longrightarrow A_2 + 2^{*}$$

the desorption rate expression (r_d) is as follows :

$$r_d = + \frac{dPA_2}{dt}$$

$$= k_d \theta^2 \exp\left(-\frac{E_a}{RT}\right)$$

where θ = the fraction of sites covered by atoms of A.

E_d = the activation energy of desorption.

k_d = velocity constant.

2.2 Metal Catalysis.

There are several metals that can be used as heterogeneous catalysts for oxidation reaction, e.g. the catalytic oxidation of hydrogen. The noble metals of Groups VIII and IB in the periodic table are very effective catalysts for this reaction. This, highly dispersed platinum and palladium will catalyse the H_2/O_2 recombination at low temperature (e.g. 20°C), and silver and gold exhibit catalytic activity at higher temperature in the region of 100°C [37].

2.2.1 Supported Metal Catalysts.

The three commonly used methods[38][39] for the preparation of supported metals are : (a) impregnation, (b) co-precipitation and (c) deposition.

However, there are substantial differences between catalysts prepared by the three methods. Those prepared by the impregnation and deposition methods will have the catalyst readily available at the surface of the support or carrier. In the case of co-precipitation, some of the catalyst could be embedded within the carrier. These suggestions have been confirmed by the studies of nickel-silica catalyst[40]. In addition, the catalytic activity is also dependent on the chemical nature of the support[41][42]. The support could be catalytically active or inert.

2.2.2 Promoted Metal Catalysts.

The promoted metal catalysts are normally classified according to the way the supports porticipate in a catalytic reaction. Support that increases the exposed catalyst surface area is called a structural promoter, and sometimes the support lowers the area but increases the

specific activity, is generally called an electronic promoter[38].

2.2.3 The Formation of Hydrogen Atoms at Metal Surfaces.

Two possible mechanisms[43] have been proposed for the atomization of molecular hydrogen :

$$H_2 + 2* \longrightarrow \underset{*}{2H} \; ; \; \underset{*}{H} \longrightarrow H^{\bullet} + *$$

and $$H_2 + * \longrightarrow \underset{*}{H} + H^{\bullet}$$

where * represents a single adsorption site.

With tungsten filaments this takes place at temperature up to 1000°C . The temperature for the atomization of hydrogen molecule will of course vary for different metals. Perhaps, the best way is to use precious metals such as Pt and/or Pd for the formation of hydrogen atoms. This normally takes place at lower temperature (e.g. less than 20°C) and atmospheric pressure, those are the important conditions for practical purposes.

2.3 Hydrogen and Oxygen Reaction Kinetics.

The rates of chemical reactions principally form the subject of chemical kinetics. Experimentally, the rate of a chemical reaction is dependent on the temperature, pressure and the concentrations of the species involved. It is apparent that from the study of all these factors, much can be learned about the reaction mechanism regarding the transformation of reactants to products.

There are several important parameters that can be determined experimentally about the H_2/O_2 reaction kinetics. For example, rates, orders and activation energies etc.

The interaction of H_2/O_2 will never take place at ambient

temperature unless a catalyst such as Pt or Pd is present. But, at higher temperature (e.g. 200°C), metal oxides like CuO[25], MnO_2[26] and Fe_3O_4 [27][28] etc. are capable of catalysing H_2/O_2 recombination.

2.3.1 Precious Metals.

Although the interactions between hydrogen and oxygen have been investigated extensively, the kinetics are not well established even for some precious metals. In the earlier work[44][45] showed that the rate of H_2/O_2 reaction over Pt catalyst was proportional to the hydrogen pressure and independent of oxygen pressure. Also, the specific catalytic activities of Pt wire and of silica-supported Pt, for the oxidation of hydrogen have been shown to be similar[15]. In the case of Pd, Stephens[46] observed the rapid reaction of hydrogen with adsorbed oxygen and vice versa, with an activation energy of 1.8 Kcal. $mole^{-1}$.

2.3.2 Metal Oxides.

Using the kinetic method, the catalytic oxidation of hydrogen on various types of metal oxides have been studied by a number of authors[25][26][27][28]. Metal oxides such Fe_3O_4, MnO_2 and ZnO etc, the reaction takes place by alternative reduction and oxidation of the catalyst surface. They measured and compared the principal kinetic characteristics of the catalytic reaction and of the reduction of the catalyst surface and subsequent oxidation by oxygen, with a difficult stage of reaction of hydrogen with the catalyst surface oxygen. The rates, orders and activation energies of the oxidation of hydrogen on ferric oxide [27][28] were determined in a circulation-flow apparatus under conditions of a large excess of oxygen. All

these could be of useful information about the kinetic studies on spinel oxides, e.g. $NiCo_2O_4$ and perovskites. Other oxides[23][24] such as the oxides of Nd, Er, Pr and Tb have also been investigated using a stoichiometric mixture of H_2/O_2 ; the activity of the higher oxides of elements of variable valence is greater than that of the sesquioxides of elements of constant valence. According to Bakumenko[24], it was only possible to observe the differences when small concentrations of H_2 and O_2 were used.

It is therefore possible to elucidate the mechanism of the catalytic oxidation of hydrogen on spinel oxides and perovskites by measuring and comparing the rates, orders and activation energies.

2.4 Thermodynamic Considerations.

A process is said to be thermodynamically feasible if its free energy decreases. The relationship between free energy and entropy is

$$\Delta G = \Delta H - T\Delta S$$

where ΔG = change in Gibbs free energy.

ΔH = change in enthalpy.

ΔS = change in entropy.

and T = temperature.

However, consider the reaction between gaseous H_2 and gaseous O_2 to form liquid water,

$$H_2(g) + \tfrac{1}{2}O_2(g) \longrightarrow H_2O(l) \ ;$$

at 25°C, the values of ΔG, ΔH, and ΔS are -56.70, -68.32 and -0.039 Kcal. respectively[47]. The large negative value of ΔG suggests that H_2 and O_2 could react at this temperature. It is well known, however,

that the two gases can be in contact for years at this temperature without reaction. Although the thermodynamic conditions are favourable, the rate of reaction at 25°C, without a catalyst, is unfavourable. The addition of a small amount of catalyst (e.g. Pt or Pd), makes the kinetic conditions favourable, so that the reaction takes place, perhaps explosively, and a packing material is therefore required to prevent explosion risks.

2.4.1 Enthalpy.

The standard change in enthalpy (ΔH^{o}) in a particular reaction is given by

$$\Delta H^{o} = H^{o} \text{ (products)} - H^{o} \text{ (reactants)} \quad \text{----------(1)}$$

In order to determine the dependence of enthalpy on temperature we differentiate with respect to temperature, also the dependence of enthalpy on pressure is very small, ΔH^{o} can be considered as a function of temperature only[48].

Equation (1) becomes

$$\frac{d\Delta H^{o}}{dT} = \frac{dH^{o}}{dT} \text{ (products)} - \frac{dH^{o}}{dT} \text{ (reactants)}.$$

But, $\frac{dH^{o}}{dT} = C_{p}^{o}$

where C_{p}^{o} = Standard molar heat capacity.

$$\therefore \frac{d\Delta H^{o}}{dT} = \Delta C_{p}^{o}\, dT \quad \text{----------(2)}$$

Integrating between a fixed temperature T_{o} and any other temperature T yields :

$$\int_{T_o}^{T} d\Delta H^{o} = \int_{T_o}^{T} \Delta C_p^{o} \, dT$$

This gives

$$\Delta H_T^{o} = \Delta H_{T_o}^{o} + \int_{T_o}^{T} \Delta C_p^{o} \, dT \qquad \text{----------(3)}$$

Thus, if $\Delta H_{T_o}^{o}$ is known, then ΔH_T^{o} can be calculated at temperature T, provided the heat capacities of all the substances taking part in the reaction are known.

2.4.2 Entropy.

The entropy (S) of a system is defined by the differential equation.

$$dS = \frac{dQ_{rev}}{T} \qquad \text{----------(1)}$$

Where Q_{rev} = heat from the system.

T = temperature.

The entropy change $(\Delta S)^{(49)}$ from state 1 to state 2 is

$$\Delta S = S_2 - S_1$$

$$= \int_1^2 \frac{dQ_{rev}}{T} \qquad \text{----------(2)}$$

Also, the standard entropy change is given by

$$\Delta S^{o} = S^{o} \text{ (products)} - S^{o} \text{ (reactants)} \qquad \text{----------(3)}$$

The entropy change for a constant pressure transformation from temperature T_1 to some temperature T_2 is therefore.

$$\Delta S = S_{T_2} - S_{T_1}$$

$$\Delta S = \int_{T_1}^{T_2} \frac{C_p}{T}\, dT$$

$$\text{or} \quad S_{T_2} = S_{T_1} + \int_{T_1}^{T_2} \frac{C_p}{T}\, dT \text{ ----------(4)}$$

Where C_p = heat capacity at constant pressure.

Thus, the entropy increases with temperature. However, according to the reaction

$$H_2(g) + \tfrac{1}{2} O_2(g) \longrightarrow H_2O\ (l)$$

Since the entropy of gases is greater than the entorpy of condensed phases, there will be a large decrease in entropy in this reaction, simply because H_2 and O_2 are consumed to form condensed water. Since the recombination of H_2/O_2 will be carried out at constant pressure in a circulation-flow apparatus, it would be appropriate to discuss the related data based on experimental conditions. In the synthesis of liquid water from gaseous H_2 and gaseous O_2, Brown[47] revealed that the standard entropy change for the reaction is in fact in agreement with the calculated value.

It is therefore from equation (3) that if the value of $\Delta S^\circ_{T_o}$ for a given reaction at tmeperature T_o is known, the value of ΔS°_T at temperature T can be obtained.

$$\Delta S^\circ = S^\circ \text{ (products)} - S^\circ \text{ (reactants)}$$

Differentiating with respect to temperature at constant pressure yields

$$\left(\frac{\partial \Delta S^\circ}{\partial T}\right)_p = \left(\frac{\partial S^\circ \text{(products)}}{\partial T}\right)_p - \left(\frac{\partial S^\circ \text{ (reactants)}}{\partial T}\right)_p$$

$$\left(\frac{\Delta S^{\circ}}{\delta T}\right)_p = \left(\frac{C_{p(\text{products})}}{T}\right) - \left(\frac{C_{p(\text{reactants})}}{T}\right)$$

$$= \frac{\Delta C_p}{T} \qquad \text{----------(5)}$$

To write equation (5) in differential form and integrating between temperatures T_o and T gives

$$\int_{T_o}^{T} d(\Delta S^{\circ}) = \int_{T_o}^{T} \frac{\Delta C_p}{T} \, dT$$

This yields

$$\Delta S^{\circ}_T = \Delta S^{\circ}_{T_o} - \int_{T_o}^{T} \frac{\Delta C_p}{T} \, dT$$

2.4.3 Free Energy.

Lowry and Cavell[50] revealed the relationship of ΔH, ΔS, and ΔG in the reaction

$$H_2(g) + \tfrac{1}{2}O_2(g) \longrightarrow H_2O(l) .$$

At constant pressure, these changes are related to one another by the equation

$$\Delta G = \Delta H - T\,\Delta S,$$

and the conversion of $H_2(g)$ and $O_2(g)$ to water is spontaneous if there is a decrease in the free energy of the system. It would be useful to consider the application of the above equation to different conditions:

(a) ΔH is positive. In this case, the change is spontaneous if $T\,\Delta S$ is positive and greater than ΔH, so a high temperature is probably needed.

(b) ΔH is zero . T ΔS must be positive in order to give a negative ΔG value.

(c) ΔH is negative and T ΔS small in comparison. The reaction is spontaneous only when ΔG is close to ΔH and is also negative.

Despite favourable thermodynamics, however, in the earlier discussion (section 2.4) showed that $H_2(g)$ and $O_2(g)$ will not form water within any practical length of time. The importance of thermodynamics in H_2/O_2 recombination is that the thermodynamic predictions do not normally specify the time interval required for the transformation. Although there is a free energy difference[47] between the initial state, $H_2(g) + \frac{1}{2}O_2(g)$, and the final state, H_2O (l); such free energy difference has nothing to do with the presence or absence of a catalyst. It is clear that under the normal experimental conditions, a catalyst is required to make the kinetic parameters measurable.

2.5 Transport Properties.

In a transport process, the physical quantity such as mass or energy is transported from one region of a system to another. The amount of a physical quantity transported per unit time through a unit of area perpendicular to the direction of flow, is proportional to the gradient of other physical property such as temperature and pressure. Diffusion is the mass transport which occurs in a mixture if a concentration gradient is present, e.g. if the concentration is not uniform in a mixture of two gases, the gases diffuse into one another until the composition is uniform. Generally, the amount transported per unit time through a unit area depends on the so-called law of transport[51],

$$J_z = - B \frac{\partial Y}{\partial Z}$$

Where J_z = the amount of the quantity transported per unit area per unit time in the direction of z-axis.

$-B$ = a proportionality constant.

$\frac{\partial Y}{\partial Z}$ = the gradient of Y in the direction of flow ; Y could be the quantity of temperature or pressure.

The physical quantities therefore play an important role in the transport phenomenon.

2.5.1 Mass Transfer.

In the case of gases, diffusion is often used to describe the amount of gas transferred.The principles of diffusion have been investigated by Fick[51] and Graham[52]. According to Graham's Law which states that the rate of diffusion of a gas is inversely proportional to the square root of its density. As a result, in a mixture of hydrogen and oxygen, hydrogen being the lighter molecules would expect to travel faster than the oxygen molecules under the same experimental conditions, resulting in a slow H_2/O_2 interaction process. However, the introduction of a constant circulation-flow apparatus[27][28] enables the kinetic conditions measurable. In this way, the influence of mass transfer to the catalyst surface is kept to minimum.

2.5.2 Transport to the Adsorbent.

Langmuir[53][54][55] suggested that for two molecules A and B to react, they should be adsorbed on adjacent sites. Such mechanism is known as Langmuir-Hinshelwood mechanism or adjacent mechanism and the rate of reaction is determined by processes occuring in the adsorbed

layer. These could be the important factors that control the amount of adsorbate being transported to the surface of adsorbent. The rate of transfer is therefore proportional to $\theta_A \theta_B$, Where θ_A is the fraction of sites covered by substance A and θ_B that covered by substance B. In 1906, Bone and Wheeler[44] proposed that, the rate of combination of hydrogen and oxygen on various catalytic surfaces is not governed by diffusion. However, Bodenstein and Fink[56] in 1907 suggested that in a catalytic reaction an adsorbed layer of the reacting substance or substances was formed. This is a slow reaction that determines the rate of transport to the adsorbent which in this case is a catalytic surface.

CHAPTER 3

THE LIFE AND RELIABILITY OF CATALYSTS —— THE FREE-SPACE APPROACH.

CHAPTER 3

3 THE LIFE AND RELIABILITY OF CATALYSTS —— THE FREE - SPACE APPROACH.

3.1 Introduction.

The commercially available hydrocaps [57] contain palladium dispersed onto inert carriers. Such catalysts, although widely used for H_2/O_2 recombination in secondary batteries, they tend to suffer from " start-up " problems. When a battery is being charged, there is a continuous stream of hydrogen and oxygen gas mixture passing over the catalyst, recombination will take place but when the charging is terminated, the catalytic reaction will eventually stop. The catalyst will gradually cool down because the exothermic reaction is no longer taking place and water forms on the surface of the catalyst. On recommencing the flow of H_2/O_2 gas mixture, because of this layer of water it is often difficult to get the catalytic recombination reaction to restart. Thus, a complete loss of catalytic activity is unavoidable due to " flooding ". The concept of catalyst flooding can be explained by the following phenomenon.

When a catalyst in a hydrocap is fixed to a commercial cell there is normally a volume of gas constantly in contact with the catalyst. This volume is alternatively known as free space or gassing space, and could be as large as 1 litre in a medium sized cell. When the cell is being overcharged, hydrogen and oxygen are being evolved through electrolyte water decomposition, this volume will be full of hydrogen and oxygen gas mixture, which passes over the catalyst in the same quantities as it is being evolved. This gas mixture is then

converted to water. When the charging is stopped the volume of gas passing over the catalyst decreased until it finally stops at which point the catalyst will cool down, due to the termination of the exothemic reaction. However, over a period of time the gas mixture remaining in the free space will slowly diffuse through the catalyst bed whereupon H_2/O_2 recombination will slowly take place. The rate of flow will be too slow to generate enough heat to vaporise the water so formed, such water will then lie on the surface of the catalyst which inhibits or even prevents subsequent catalytic action.

This important discovery has led to an understanding of the problem which affects the life and reliability of catalysts in the commercial hydrocaps or catalytic devices.

At about 200°C, several mixed oxides have been found to be active supports for Pt or Pd for H_2/O_2 recombination reactions, attempts will be made to evaluate such promotional catalytic activity in $NiCo_2O_4$ and related oxides for H_2/O_2 interactions.

3.2 The Study of Hydrocaps.

3.2.1 Catalysts and Supports.

The components in the hydrocaps [57] were examined by dismantling a number of commercially available hydrocaps. Each cap contained between 19 and 21 cylindrical catalyst pellets, approximately 3.2 mm in diameter X 3.6 mm long, and the average weight of each pellet was 47.3 mg. The total surface area of the 20 Catalyst pellets was 9.2 cm^2. The pellets consisted of Pd metal suspended on an inert alumina support. Sixty pellets were dissolved in aqua regia and analysis of

the solution for Pd content by atomic absorption showed that hydrocap contained 0.48% of alumina weight. The average Pd content per hydrocap is therefore about 5mg dispersed onto 1g of alumina support.

3.2.2 Packing Materials.

The packing material used in the commercial hydrocaps was confirmed by X-ray powder diffraction to be lead dioxide. The BET surface area was 123 m^2/g. The average weight of PbO_2 per cap was about 5g. All the 20 catalyst pellets were located within the bulk of the packing material, which was in turn housed in a porous cone-shaped ceramic holder so that a maximum degree of efficiency could be attained in directing the reactant gases onto the catalyst. Perhaps, it is worthwhile to mention here that PbO_2 acts as a diffusion barrier to the gases, and to avoid the possibility of initiating a chain reaction and explosion of the H_2/O_2 mixture.

The following information was also obtained :

(a) average weight of reactor unit 28 - 29 g

(b) average weight of ceramic holder 17 - 18 g

3.3 Experimental Techniques for the Determination of Catalytic Activity.

3.3.1 Catalytic Loading.

3.3.1.1 Experimental Assembly.

Standard hydrocaps were used in this experiment, since this would reduce the variable to a minimum. Fig. 1 shows a schematic diagram of test assembly; a water bubbler was attached to the outlet to gauge the effectiveness of the catalyst. The experiments were

carried out for two systems :

(a) with normal hydrocap, the so-called open system and

(b) a closed system where the small outlet hole of the hydrocap was plugged.

3.3.1.2 Experimental.

Before performing the actual experiment in " start-up " time versus catalyst loading, the hydrocap was first evaluated by checking the time taken to cope with 3A electrolyser current. All experiments were done manually by increasing the electrolyser current in steps of 0.2A, making sure that no gas bubbles appeared in the outlet. In order to simulate the worse possible situation, the hydrocap was allowed to cool to room temperature for 2-3 hours before the commencement of the experiment. The subsequent experiments (repeated) were carried out after an overnight 'incubation' so that the hydrocap was cold when the experiments began. All experiments were repeated three times and the average results were then recorded.

In order to check the effect of catalyst loading on the " start-up " time, the hydrocap was carefully opened and a further amount of 0.5 wt % Pd/Al_2O_3 added, making a total weight of catalyst to 2g.

Generally, the above method is suitable for controlling the volume of free space required. After filling the calibrated cylinder with water (Fig. 1), the volume of free space containing a stoichiometric amount of H_2/O_2 in the calibrated cylinder can be controlled by the amount of electricity used in the electrolyser.

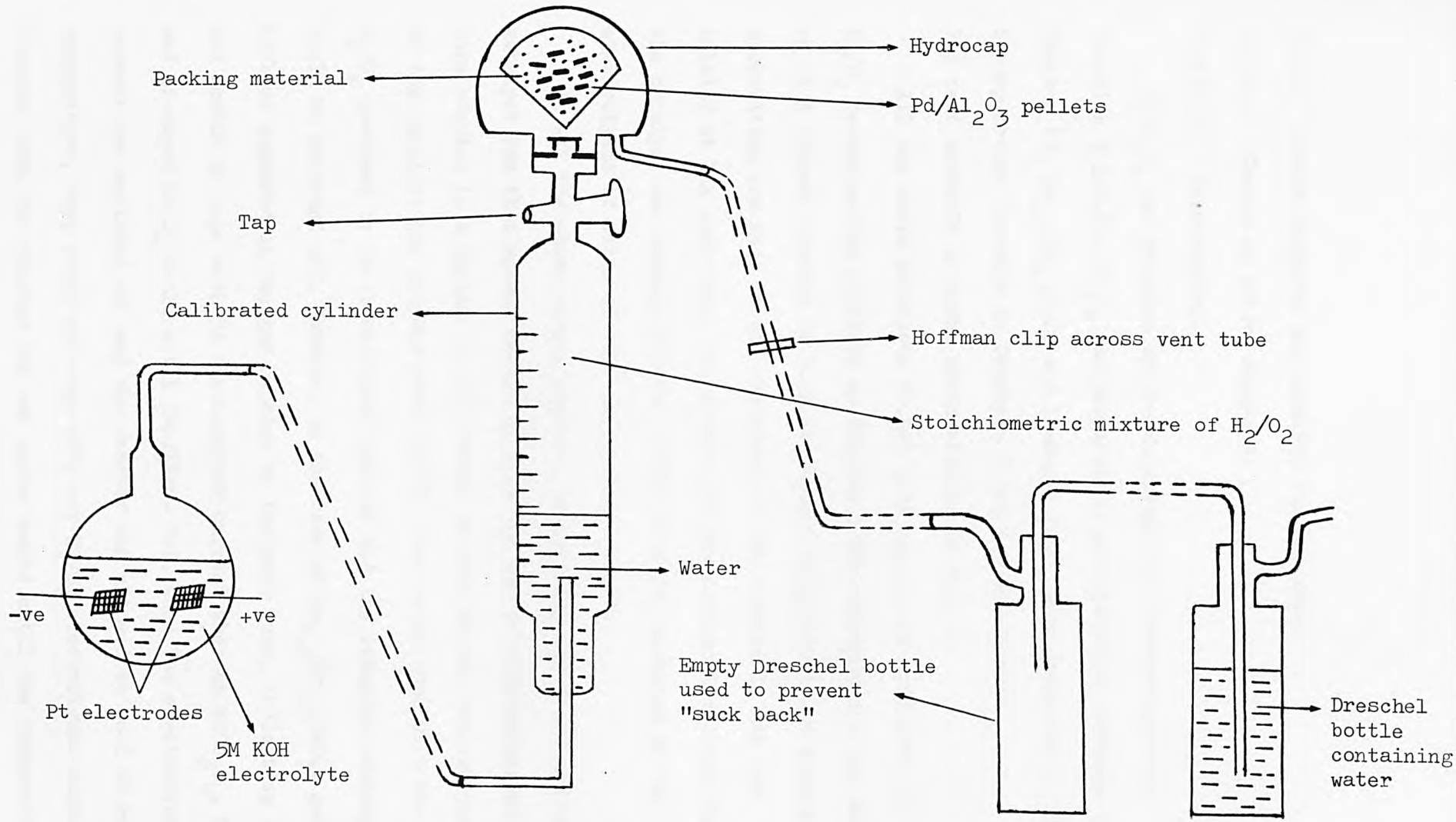

Fig. 1 Free space assembly (Schematic).

3.3.2 Active Supports and Catalyst Surface Area.

3.3.2.1 Choice of Active Supports.

3.3.2.1.1 Experimental.

$NiCo_2O_4$ was prepared by freeze-drying and co-precipitation (section 3.3.2.2). Co_3O_4 was prepared by precipitation (details in Chapter 4). $La_{0.5}Sr_{0.5}CoO_3$ and Li-doped Co_3O_4 were prepared by freeze-drying method (details in Chapters 8 and 9 respectively).
The test assembly is shown schematically in Fig. 2.

All the above catalysts (0.5g) were separately evaluated for H_2/O_2 recombination activity as follows : The electrolyser was switched on at a current density of 0.2A at ambient temperature and visual observation was made on the occurance of gas bubbles in the gas bubbler at the exit tube. The absence of gas bubbles indicated that the catalyst was coping with the amount of H_2/O_2 produced by the electrolysis of water at that particular current.

In all the above cases, however, no activity was found and the catalyst was then slowly heated up with the aid of electrothermal tape coupled to a Variac. In all cases, as soon as the temperature of the catalyst bed reached about 200°C, they could cope with the H_2/O_2 produced by 3A electrolyser current and the external heating could be switched off. However, in the case of $La_{0.5}Sr_{0.5}CoO_3$, gas bubbles appeared in the gas bubbler at the exit tube, indicating it was unable to cope with 3A electrolyser current whereas $NiCo_2O_4$, Co_3O_4 and Li-doped Co_3O_4 could still function. But, when the electrolyser current was switched off and the reactor was allowed to cool to room temperature, they could not cope with any H_2/O_2 electrolyser current. However, when the reactor bed was again heated until the temperature of the reactor bed reached 110°C, they could cope with 3A electrolyser

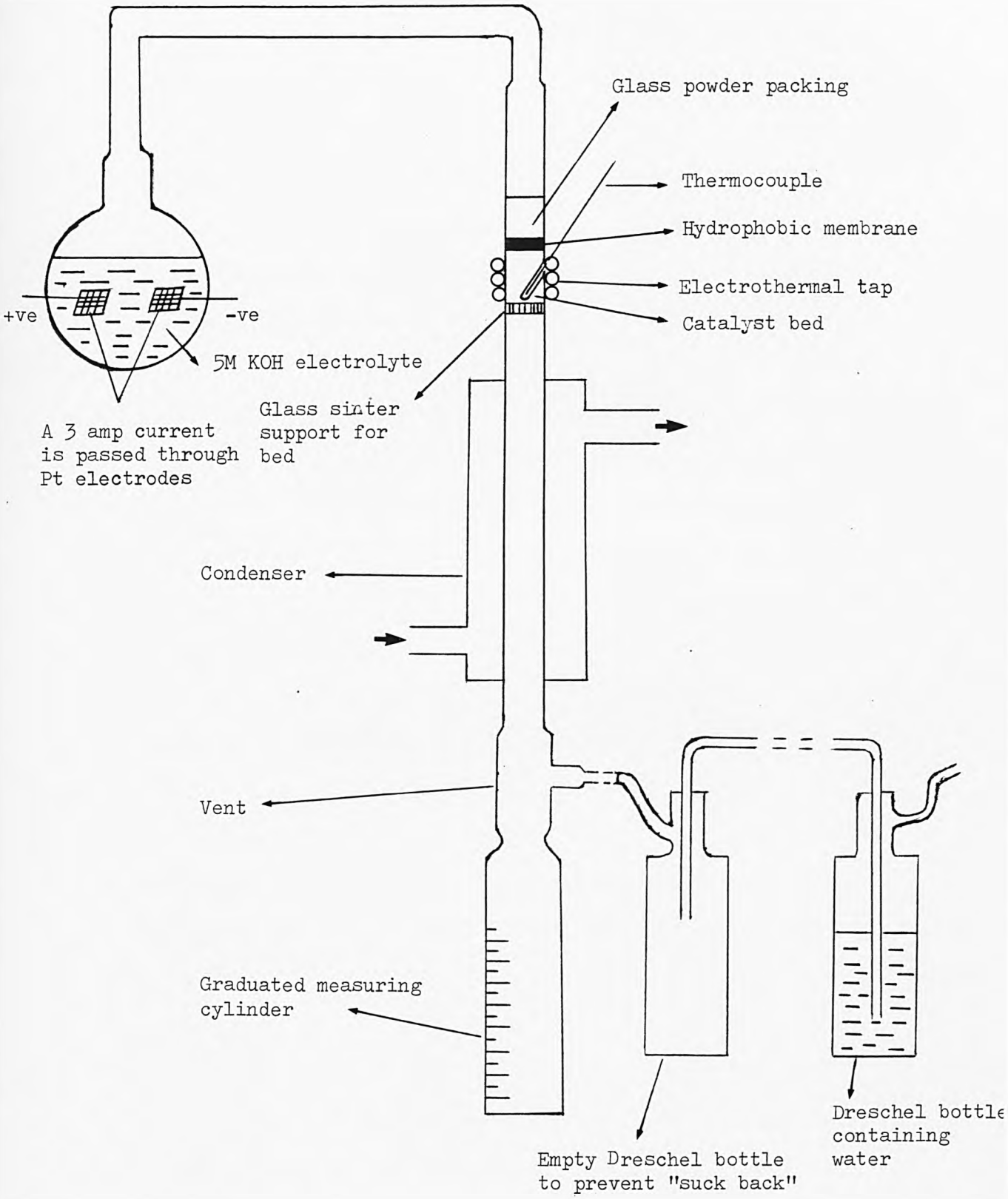

Fig. 2 Catalyst reaction apparatus.

current, and hence $NiCo_2O_4$ was chosen as active support. However, the catalytic activity of all the above oxides will be investigated in the subsequent chapters.

3.3.2.2 $NiCo_2O_4$ as Active Support.

3.3.2.2.1 Preparation of $NiCo_2O_4$.

(a) Freeze Drying Method.

The X-ray powder patterns and the conductivity of freeze-dried $NiCo_2O_4$ have been studied by Tseung and Bevan [58]. Freeze-dried $NiCo_2O_4$ from water has been prepared by Hibbert and Tseung[59] using $Co(NO_3)_2 . 6H_2O$ and $Ni(NO_3)_2 . 6H_2O$ in the ratio of 2 : 1. The sample prepared by this method involving the use ~~of~~ of liquid nitrogen and ~~sublimed~~ dried under vacuum as shown schematically in Fig. 3. The resulting solid was then decomposed under vacuum in the same apparatus at 250°C for 3h and ~~cured~~ heated in air at 400°C for 10h.

(b) Co-precipitation Method.

A mixture of metal salts ($CoCl_2 . 6H_2O$ and $NiCl_2 . 6H_2O$ in the ratio of 2 : 1) was dissolved in distilled water. The mixed chloride solution was then precipitated from freshly prepared 5M KOH solution. The precipitate so formed was thoroughly washed free of KOH and dried. The resulting powder was ~~sintered~~ heated first at 300°C for 5h and then 400°C for 10h.

3.3.2.2.2 Experimental.

The experimental set-up was similar to Fig. 1. The co-precipitation $NiCo_2O_4$ was impregnated with $PdCl_2$ solution, dried at 110°C for 1h and reduced in a flowing stream of H_2 gas at 200°C for a further 1h to form $Pd/NiCo_2O_4$. The Pd concentration was fixed at 2 wt % .

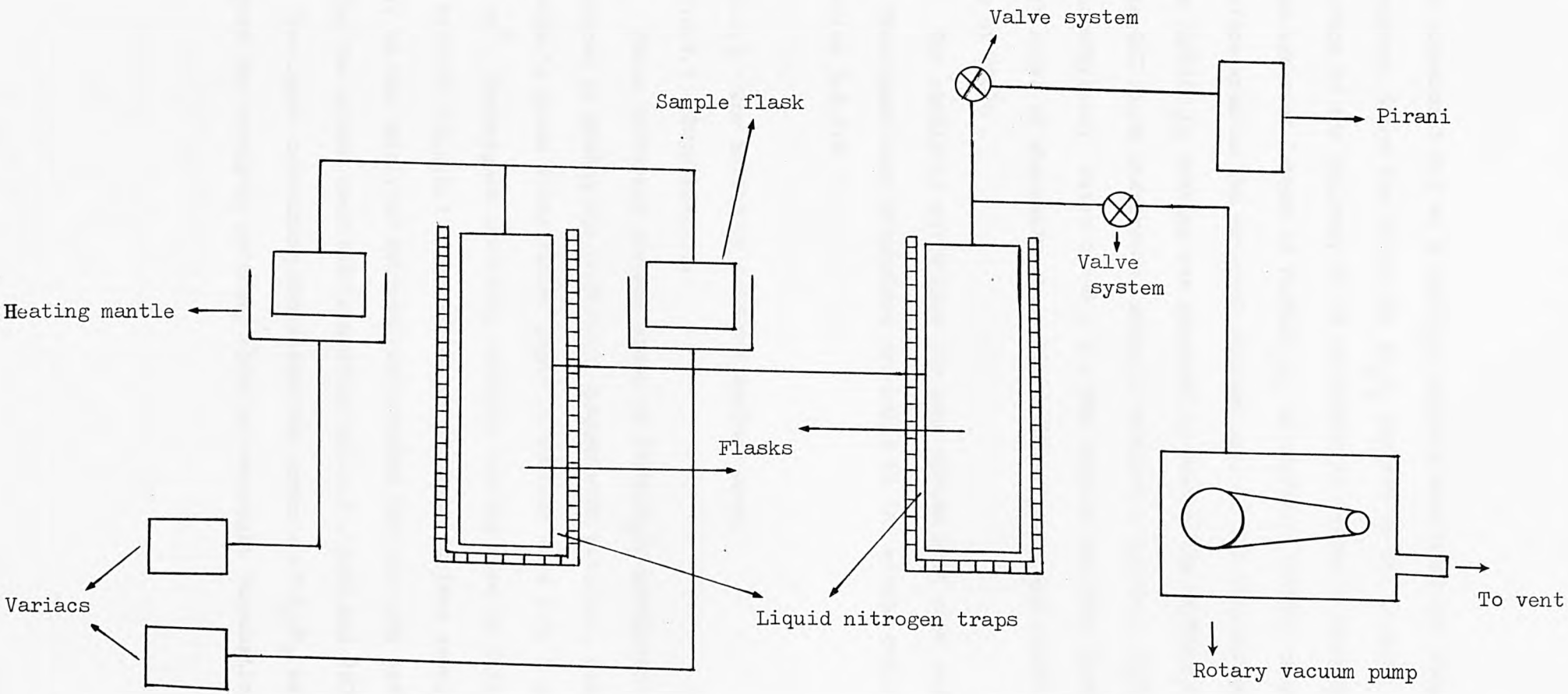

Fig. 3 Schematic freeze-drying apparatus.

The commercial 0.5 wt % Pd/Al_2O_3 pellets were used for comparison purposes. Since the Pd on the Al_2O_3 pellets is all located on the surface of the pellets, it is necessary to devise a technique to form adherent layers of $Pd/NiCo_2O_4$ on surfaces, having comparable surface area as the external surface area of the alumina pellets. The $Pd/NiCo_2O_4$ coating was prepared by mixing the $Pd/NiCo_2O_4$ powder with ICI Fluon Dispersion, using a catalyst : p.t.f.e. (polytetrafluorethylene) ratio of 10 : 3 . The mixture was then brushed onto both sides of Whatman's glass fibre filter paper and cured for 1h in air at 300°C .

The catalytic activities for open system with zero and 100 cc of free space were determined according to the method outlined in section 3.3.1.2 .

3.3.2.3 The Effect of Catalyst Surface Area.

3.3.2.3.1 Experimental.

Three different surface areas of $Pd/NiCo_2O_4$ catalysts were prepared by mixing the $Pd/NiCo_2O_4$ powder with p.t.f.e., using Whatman's glass fibre filter paper of surface area 2.5, 5 and 15 cm^2 . Techniques involving catalyst coating were in fact similar to section 3.3.2.2.1 . The effect of catalyst surface area, if any, on the catalytic activity was studied for the open system using the method decribed in section 3.3.1.2 . Zero and 100 cc of free space containing stoichiometric amounts of H_2/O_2 were tested for catalytic activity after an overnight 'incubation' .

3.3.3 Relationship between Free Space and " Start-Up " Time.

3.3.3.1 Experimental.

All experiments were carried out using the commercially available hydrocaps for closed and open systems. Substantially the same experimental set-up was used as in Fig. 1 . In order to verify the relationship between free space and " start-up " time, several volumes of free space containing stoichiometric amounts of H_2/O_2 were used and the individual average time taken to reach 3A electrolyser current was compared by plotting volume of free space against " start-up " time.

3.4 The Automatic " On-Off " Valve System.

3.4.1 General Considerations.

The results in section 3.3.3.1 showed that if the amount of free space is reduced to zero, the " start-up " time to 3A electrolyser current is extremely rapid. Then, one practical engineering solution is to incorporate an automatic " On-Off" valve assembly in the hydrocap so that the amount of free space could be kept to a minimum.

3.4.2 Experimental.

A ground glass cone and socket joint was used as the shut off valve in the H_2/O_2 recombination assembly (Fig. 4). Two different weight of glass cones were used : 2.1826 and 4.6335g . After the H_2/O_2 assembly (hydrocap) had been tested for activity up to 3A electrolyser current, the glass tap was closed and a 300 cc free space containing stoichiometric amounts of H_2/O_2 produced in the electrolyser to displace water from the graduated cylinder filled

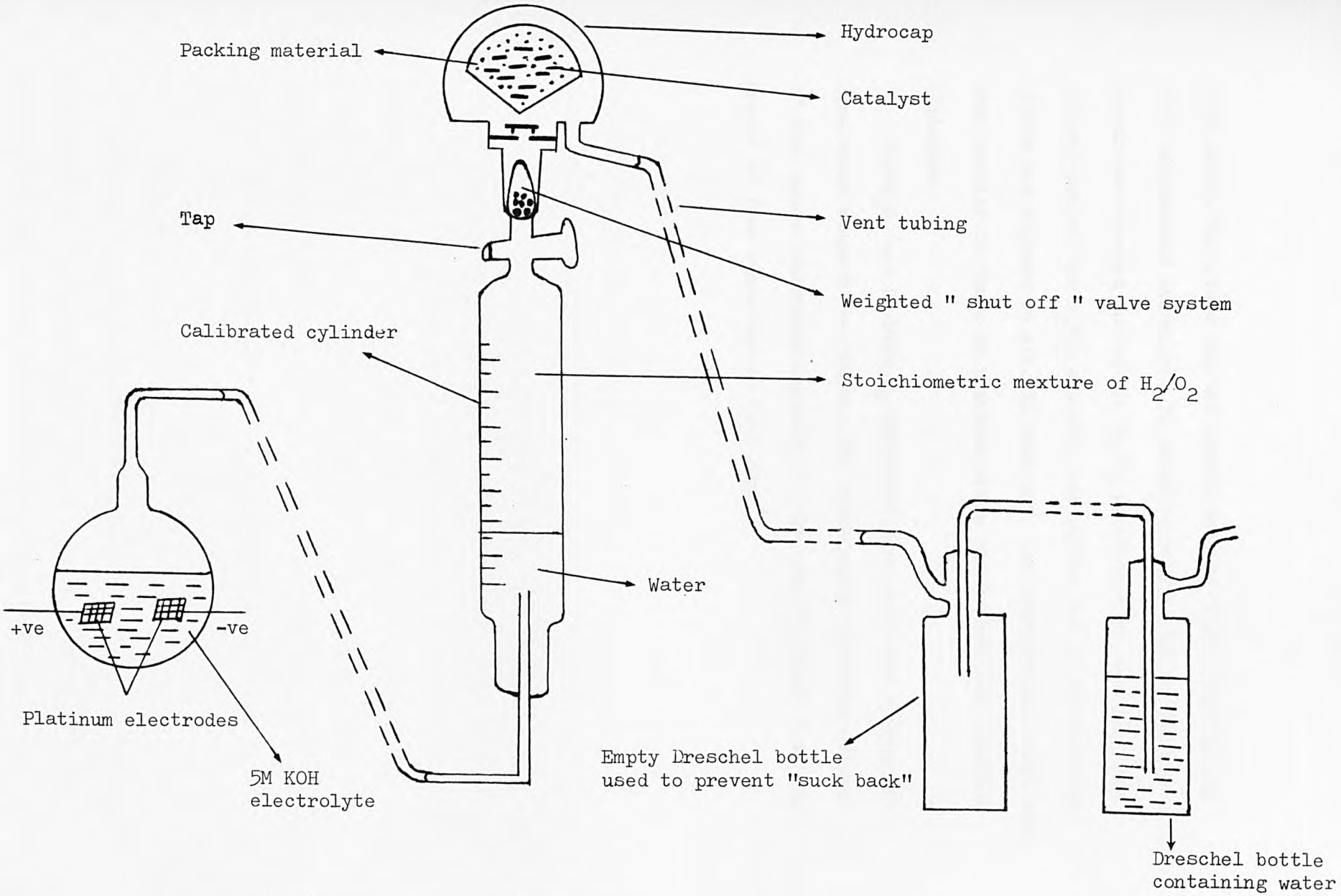

Fig. 4 Valve assembly (Schematic).

with water. The glass tap was opened and the whole assembly was left undisturbed overnight. In order to ensure that no partial vacuum was created inside the H_2/O_2 recombination assembly, the outlet tube of the H_2/O_2 assembly was pulled out of the Dreschel bottle and exposed to air. In this way, the experimental conditions were similar to those in practice where the outlet hole remained unplugged.

Pd/Al_2O_3 and $Pd/NiCo_2O_4$ catalysts were used with volume of free space range 0 —— 300 cc. The experiments involving volume of free space controlled manually by tap were to ensure that the amount of free space was in fact zero.

3.5 Results and Discussion.

3.5.1 Catalyst Loading.

Table 1 shows the " start-up " time to 3A electrolyser current for open and closed systems at zero and 100 cc free space. A maximum humidity was created in a closed system, indicating more water condensing on the catalyst surface than that of the open system, rendering it ineffective during the next recharging cycle. The results clearly suggest that the catalytic activity cannot be restored by increasing catalyst loading even in the normal hydrocap where the outlet hole is always open.

3.5.2 Optimisation of $Pd/NiCo_2O_4$ Catalyst.

The BET surface areas of $NiCo_2O_4$ prepared by freeze-drying and co-precipitation were 50 and 46 m^2/g respectively. X-ray powder diffraction confirmed that the spinel phase had been formed.

Table 2 shows the catalytic ~~active~~ activity of $Pd/NiCo_2O_4$ is higher than Pd/Al_2O_3 of similar Pd loading, indicating $NiCo_2O_4$ is an active support and Al_2O_3 is an inert carrier. This is provided $NiCo_2O_4$ is admixed with Pd or Pt. When the H_2/O_2 recombination reaction is initiated, the heat generated at the precious metal surface will raise the temperature of the $NiCo_2O_4$ to a sufficiently high temperature so that it too can catalyse the H_2/O_2 recombination reaction.

3.5.3 Catalyst Surface Area.

Although $NiCo_2O_4$ exhibited catalytic activity, the " start-up " problem still existed even with larger catalyst surface area to accommodated the amount of water from condensation (Table 3).

3.5.4 The Effect of Free Space.

As the free space was gradually increased (0 → 12.5 cc → 25 cc → 50 cc → 100 cc, Tables 4 and 5), the time required to reach 3A increased proportionally. However, in the case of closed system (Table 5), when the free space was increased to 100 cc, the catalyst in the hydrocap showed no activity for H_2/O_2 interaction. When this is compared to the open system of 100 cc free space, the " start-up " time may be delayed, " start-up " will eventually commence. Fig. 5 illustrates the relationship between " start-up " time and free space. This clearly shows that significant improvements can be obtained by using an open system; in fact, such condition is comparable to hydrocap in normal service. But, further improvements are needed.

3.5.5 Incorporation of Valve System.

Table 6 shows the " start-up " time to 3A by using a glass cone weighing 2.8126g - 60 minutes when the free space was 300 cc; by increasing the weight of the glass cone to 4.6335g, the " start-up " time was reduced to 36 minutes, comparable to the time taken when the free space was zero, (by mechanical closing of glass tap, Tables 7 and 8) —— 37 minutes. Tables 9 and 10 show that the valve assembly (4.6335g) was also effective for $Pd/NiCo_2O_4$. However, without an " on-off " valve system, the catalyst in the hydrocap failed to restart when the free space was 100 cc (Tables 3, 5, 8 and 10).

System	0.5 wt % Pd/Al_2O_3 Loading (g)	Time required to reach 3A electrolyser current (min)	
		Volume of free space (c.c)	
		0	100
open	1	37	228
open	2	24	172
closed	1	38	No activity
closed	2	31	No activity

TABLE 1 Start-up time Vs catalyst loading

System	Volume of free space (c.c)	Time required to reach 3A electrolyser current (min)			
		Pd loading (mg)			
		0.5 wt % Pd/Al_2O_3		2 wt % $Pd/NiCo_2O_4$	
		5	1.3	5	1.3
open	0	37	40	30	33

TABLE 2 Catalytic activities of Pd/Al_2O_3 and $Pd/NiCo_2O_4$

Pd loading (mg)	Surface area of Catalyst layer (cm^2)	Time required to reach 3A electrolyser current (min)	
		Volume of free space (c.c)	
		0	100
5 (2 wt % $Pd/NiCo_2O_4$)	2.5	31	186
5 (2 wt % $Pd/NiCo_2O_4$)	5	30	188
5 (2 wt % $Pd/NiCo_2O_4$)	15	30	185

TABLE 3 Start-up time Vs catalyst surface area (open system)

Current (A)	Time elapsed (min)									
	Free Space in Calibrated Cylinder (c.c)									
	0	12.5	25	50	100	0	12.5	25	50	100
	Close System					Open System				
0.2	0	0	0	0	0	0	0	0	0	0
0.4	1	2	67	127	205	1	1	1	5	143
0.6	2	20	72	146	-	2	2	2	47	160
0.8	3	29	76	150	-	3	15	29	49	180
1.0	10	32	78	155	-	13	23	44	58	185
1.2	14	39	82	157	-	19	26	51	68	200
1.4	19	44	84	159	-	22	29	57	73	205
1.6	22	47	86	160	-	24	31	60	76	210
1.8	25	48	87	161	-	26	34	64	82	215
2.0	28	51	89	162	-	28	36	66	86	218
2.2	30	52	90	164	-	30	39	70	91	220
2.4	32	58	94	166	-	31	42	72	94	222
2.6	34	61	95	168	-	32	45	74	96	225
2.8	36	63	96	171	-	34	48	76	97	226
3.0	38	65	98	176	-	37	54	79	101	228

TABLE 4 Start-up time for 5mg Pd/1000 mg Al_2O_3

System	0.5 wt % Pd/Al_2O_3 (g)	Time required to reach 3A electrolyser current (min)				
		Volume of free space (c.c)				
		0	12.5	25	50	100
open	1	37	54	79	101	228
closed	1	38	65	98	176	No activity

TABLE 5 Start-up time Vs volume of free space

Wt of Valve (g)	Volume of free space (c.c)	0.5 wt % Pd/Al_2O_3 (g)	Time required to 3A electrolyser current (min)
2.8126	300	1	60
4.6335	300	1	36

TABLE 6 Relationship between weight of valve and start-up time (open system)

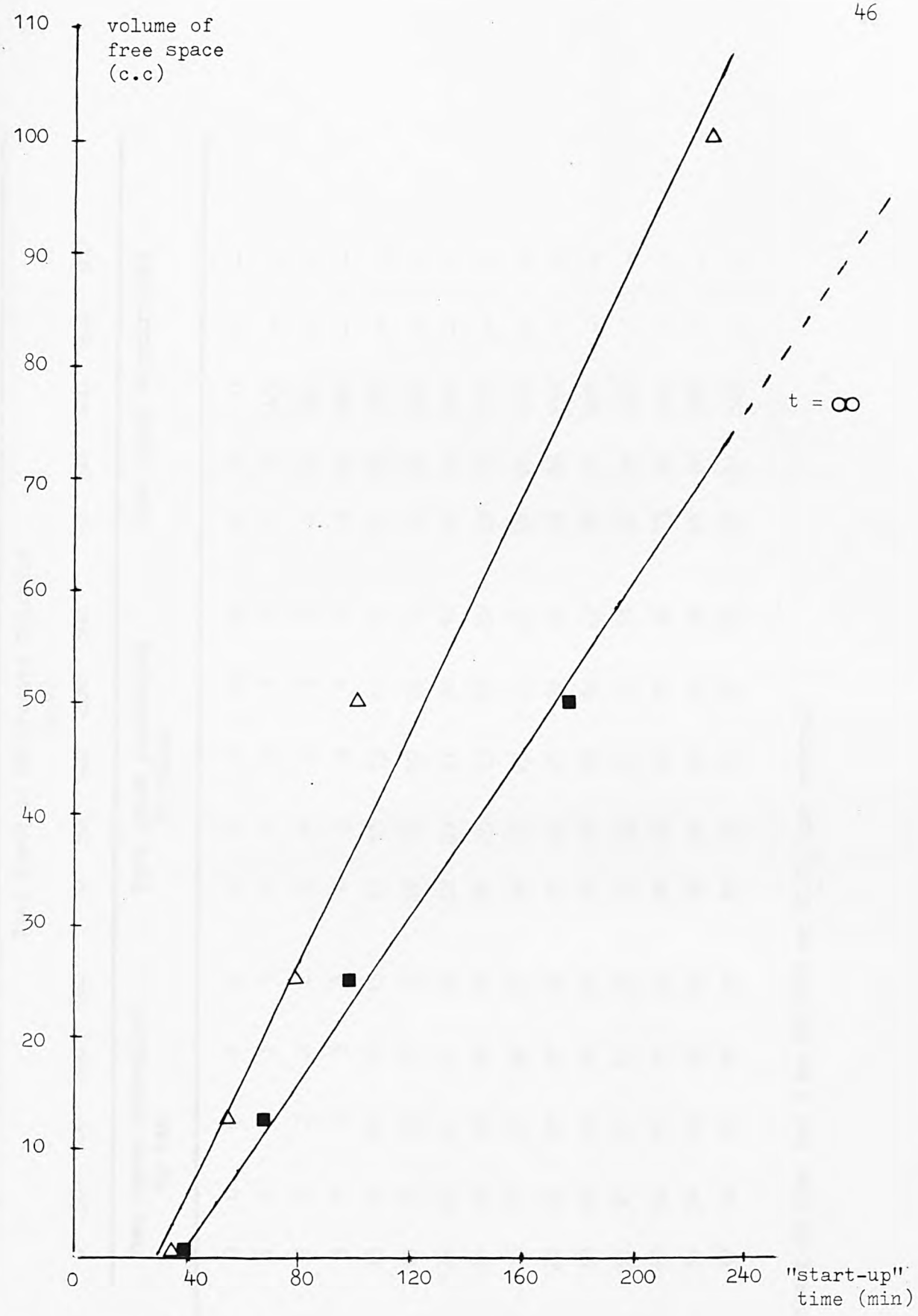

Fig. 5 Volume of free space Vs "start-up" time.

△ open system

■ closed system

Current (A)	*Time elapsed (min)*															
	Free Space in Calibrated Cylinder (c.c)															
	0	50	100	200	300	0	50	100	200	300	0	50	100	200	300	
	Free space controlled by tap					Free space controlled by valve					Free space uncontrolled					
0.2	0	0	0	0	0	0	0	0	0	0	0	0	0	-	-	
0.4	1	1	1	1	1	1	1	1	1	2	1	5	143	-	-	
0.6	2	2	2	2	2	2	2	2	3	3	2	47	160	-	-	
0.8	3	3	3	3	4	4	3	3	4	5	3	49	180	-	-	
1.0	13	12	13	10	13	11	13	13	12	10	14	58	185	-	-	
1.2	19	18	19	18	18	18	18	17	18	15	19	68	200	-	-	
1.4	22	20	21	21	20	22	21	21	20	18	21	73	205	-	-	
1.6	24	23	23	24	23	24	25	23	23	20	23	76	210	-	-	
1.8	26	25	25	26	27	26	27	25	25	24	26	82	215	-	-	
2.0	28	27	27	27	28	27	28	27	28	27	28	86	218	-	-	
2.2	30	28	29	30	30	30	31	30	30	29	30	91	220	-	-	
2.4	31	30	31	31	32	32	33	31	31	31	32	94	222	-	-	
2.6	32	32	33	33	34	34	34	33	33	32	33	96	225	-	-	
2.8	34	34	35	35	35	36	36	35	35	34	36	97	226	-	-	
3.0	37	36	37	37	37	37	37	36	37	36	37	101	228	-	-	

TABLE 7 Start-up time for 5 mg Pd/1000 mg Al_2O_3 (open system)

Volume of free space (c.c)	Time required to reach 3A electrolyser current (min)		
	Free space controlled by tap	Free space controlled by valve	Free space uncontrolled
0	37	37	37
50	36	37	101
100	37	36	228
200	37	37	No activity
300	37	36	No activity

TABLE 8 Start-up time for 5 mg Pd/1000 mg Al_2O_3 (open system, summary)

Current (A)	Time elapsed (min)															
	Free Space in Calibrated Cylinder (c.c)															
	0	50	100	200	300	0	50	100	200	300	0	50	100	200	300	
	Free space controlled by tap					Free space controlled by valve					Free space uncontrolled					
0.2	0	0	0	0	0	0	0	0	0	0	0	0	0	-	-	
0.4	1	1	1	2	1	1	1	1	1	1	1	8	69	-	-	
0.6	2	3	2	3	2	3	3	2	2	2	2	30	119	-	-	
0.8	3	4	3	4	3	4	4	4	3	3	3	42	128	-	-	
1.0	4	6	4	5	5	5	6	6	5	4	5	50	142	-	-	
1.2	10	11	8	10	9	8	10	8	9	10	9	58	150	-	-	
1.4	13	14	12	12	13	12	13	14	13	12	11	63	156	-	-	
1.6	15	16	14	13	15	14	15	15	14	13	14	72	163	-	-	
1.8	16	18	17	16	17	17	18	17	18	17	17	78	169	-	-	
2.0	19	20	18	19	18	19	20	20	20	19	18	81	174	-	-	
2.2	20	21	20	21	22	21	22	23	21	21	21	84	177	-	-	
2.4	23	24	22	23	23	22	24	25	24	23	22	86	179	-	-	
2.6	26	27	25	26	25	24	27	27	26	25	25	88	181	-	-	
2.8	28	29	28	29	28	27	28	29	29	28	28	92	183	-	-	
3.0	30	30	31	31	30	30	30	30	31	30	30	95	185	-	-	

TABLE 9 Start-up time for 5 mg Pd/1000 mg $NiCo_2O_4$ (open system)

Volume of free space (c.c.)	Time required to reach 3A electrolyser current (min)		
	Free space controlled by tap	Free space controlled by valve	Free space uncontrolled
0	30	30	30
50	30	30	95
100	31	30	185
200	31	31	No activity
300	30	30	No activity

TABLE 10 Start-up time for 5 mg $Pd/NiCo_2O_4$ (open system, summary)

3.6 Conclusions.

The results, therefore, show conclusively that the provision of an automatic " on-off " valve used in a H_2/O_2 recombination device that " start-up " problems due to flooding by a thin film of water arising out of the slow reaction between H_2/O_2 on the surface of the catalyst can be completely eliminated. The incorporation of the valve system is to ensure that the free space is kept to a minimum during " shut down" period, regardless of the size of battery. When the cell is being charged, the H_2/O_2 gas mixture arising from the water electrolyte decomposition will trigger the valve to open when the gas pressure is greater than 0.3 Psi, so that the H_2/O_2 gas mixture can pass over the catalyst whereupon H_2/O_2 recombination takes place. In this way, the condensed water drips back to the cell while the valve is opening. Therefore, after each charging cycle, not only the life and reliability of catalyst in the hydrocap can be restored, but the condensed water is then returned to the cell so that the volume of electrolyte does not diminish.

CHAPTER 4

THE LIFE AND RELIABILITY OF CATALYSTS —— THE CAPILLARY CONDENSATION APPROACH.

CHAPTER 4

4 THE LIFE AND RELIABILITY OF CATALYSTS —— THH CAPILLARY CONDENSATION APPROACH.

4.1 Introduction.

The solution to " start-up " time for H_2/O_2 recombination catalysts in commercial hydrocaps has been mentioned (Chapter 3) in connection with free space, where all the experiments were performed in a time interval of overnight ' incubation '. However, when a catalyst in a hydrocap or catalytic device is fixed to a commercial cell which is periodically charged (e.g. 1 - 2 weeks interval) ; further problems arise regarding the life and reliability of the catalyst. This is due to water condensation on the surface of the catalyst via a different principle from Chapter 3, and further investigations are needed so that the " start-up " problems can be successfully solved, regardless of the time interval between charge.

When an aqueous secondary cell is charged towards the end of the charging cycle and also when being overcharged, the H_2/O_2 gas mixture generated passes over the catalyst in the hydrocap in the same quantity as it is evolved. This gas mixture is catalytically converted to water which is then allowed to return to the cell. However, after each charging cycle, when the hydrocap was thoroughly examined by carefully opening the top of the catalytic device showed that several water droplets were found lying on the sides of the device. This water, although present in ~~samll~~ small amount, tends to vaporise on standing and the water molecules from the gas phase are eventually adsorbed on the packing material and/or catalyst. On commencing the flow of H_2/O_2 gas mixture, because of this layer of water it is often difficult to

get the catalyst to behave normally. Although the start may be delayed , " start-up " will finally commence, but as more water condenses on the surface of the catalyst, " start-up " becomes increasingly difficult and loss of H_2/O_2 gas mixture resulted. This will in turn decrease the volume of electrolyte being present in the cell.

In order to ~~effectively~~ achieve " start-up " , the amount of water condenses on the surface of the catalyst must be ~~avoided~~ eliminated and this is ~~accompanied~~ achieved by introducing a packing material that possesses a greater tendency of adsorbing water vapour from its surrounding than the catalyst. In this way, the small amount of water, if any, that condenses on the catalyst would have no influence on catalytic activity.

Various proposals[4][5][7] have previously been made in attempts to solve the " start-up " problem, or at least to reduce it, but none has hitherto proved especially successful.

4.2 Theoretical Considerations.

4.2.1 General Theory of Adsorption

The phenomenon of adsorption is generally classified as monolayer and multilayer adsorption with mutual interaction of the adsorbed particles. However, if adsorption takes place in pores[60], the radius of which is big enough to allow multimolecular adsorbed layers to be slowly built up, a very different situation occurs, especially when the relative pressure increases from zero to unity. For example, the relative pressure of a vapour which is in contact with a porous adsorbent or a pore in the form of an interstices[61] between closed-

packed and equal-sized spherical particles. A monomolecular layer is initially formed on the surfaces of wider pores and on the non-porous part of the surface. However, multimolecular adsorption will commence as soon as the relative pressure increases. When the relative pressure reaches a value of 0.2 - 0.3 , say, ~~the rate of~~ adsorption increases more rapidly than that corresponding to multimolecular adsorption[62]. This is provided the adsorbent contains pores and/or interstices, the width of which is equal to several times the diameter of the molecules being adsorbed. This is caused by the so-called capillary condensation of the vapour discussed.

4.2.2 The Principle of Capillary Condensation.

The increase in the thickness of the multimolecular adsorbed layer on reaching a certain relative pressure could cause the layers on opposite sides of the narrowest part of the pore to join together, forming a concave meniscus. Thus, adsorbate molecules in the meniscus surface are attracted into the adsorbed phase with an intermolecular force greater than into the plane surface of the same liquid, simply due to the influence of the larger number of surrounding molecules. The vapour pressure above this curved surface is then less than that over a plane surface of the same temperature. The vapour condensation takes place preferentially on this meniscus until the entire volume of the pore is slowly filled with condensate[63].

It is therefore from this mechanism that even wider pores will be filled if the pressure rises. The relationship between the vapour pressure P and the radius of curvature r of the meniscus in a pore filled with condensed vapour is defined by the Kelvin equation[62][63] as shown below for a spherical concave meniscus.

$$RT \ln \frac{P}{P^o} = - \frac{2 \gamma Vm}{r_m} = - \frac{2 \gamma Vm}{(r_p - t)}$$

Where $\frac{P}{P^o}$ = relative vapour pressure.

r_m = radius of meniscus.

γ = surface tension of condensate.

Vm = molar volume of the condensate.

r_p = pore radius.

t = meniscus thickness

T = Temperature

R = Universal gas constant.

In addition, below the critical temperature of the adsorbate[64], adsorption is usually multilayer but the presence of pores or interstices will introduce the capillary condensation phenomena.

4.2.3 Pore Size Measurement.

The pore size distribution can be determined by a technique called mercury porosimetry[65][66]. The idea of using mercury intrusion to measure pore size was first suggested by Washburn[67][68] and often called Washburn equation :

$$r_p = - \frac{2 \gamma \cos \theta}{p}$$

Where r_p = the radius of pore.

γ = surface tension.

θ = angle of contact.

P = the pressure exerted on the mercury to force it into a pore of radius r_p .

Generally, the technique of mercury porosimetry consists essentially in measuring the extent of mercury penetration into an evacuated solid

as a function of the applied hydrostatic pressure. Another method of measuring pore size is by capillary condensation [62][63]. In recent years, automatic porosimeters are frequently used to determine the pore structure of catalysts and other porous materials.

4.2.4 Water Vapour Sorption Isotherm of Solid.

In the Langmuir sorption isotherm it is assumed that there is a uniform solid surface upon which molecules from the gas phase are adsorbed [69]. Example of Langmuir model :

Rate of evaporation = $k_1\theta$

Rate of condensation = $k_2P(1 - \theta)$,

at equilibrium,

$$\theta = \frac{k_2P}{k_2P + k_1}$$

$$= \frac{bP}{bP + 1} \quad \text{---------- (1)}$$

Where θ = the fraction of the surface covered by a monolayer.

k_1, k_2 = rate constants.

$$b = \frac{k_2}{k_1}$$

P = gas pressure.

Since θ is a fraction, it can be expressed in terms of the monolayer

$$\theta = \frac{V}{Vm} \quad \text{----------(2)}$$

Where V = volume of gas adsorbed at equilibrium.

Vm = volume of gas in a completed monolayer.

Hence, equations (1) and (2) become :

$$\frac{1}{bVm} + \frac{P}{Vm} = \frac{P}{V}$$

which is called the Langmuir equation and the slope of the line is equal to the reciprocal of the monolayer.

The amount of gas adsorbed can be determined by gravimetric measurement and vapour pressure drop method. According to Langmuir, the multilayer coverage is an operative model up to moderate relative vapour pressure, $\frac{P}{P_o} = 0.3 - 0.6$ (69), where P_o is the vapour pressure, if the pure gas at the temperature of the isotherm and P is the equilibrium pressure. Above this range, capillary condensation will take place.

4.3 Packing Materials.

The PbO_2 packing material in the commercial hydrocap, together with three different surface areas of NiO samples and Co_3O_4 powder were examined for their ability to adsorb water vapour from their surrounding by capillary condensation. Their catalytic activity towards H_2/O_2 combination/recombination at elevated temperature was also considered.

4.4 Preparation.

4.4.1 Nickel Oxide.

$NiCl_2\ 6H_2O$ was dissolved in distilled water and the solution was added to a freshly prepared 5M KOH solution. The resultant precipitate was oven-dried at 80°C for 1h and then sintered at 300°C in air for 5h to form high surface area of NiO (section 4.5.2). The low surface area sample was obtained by sintering at higher temperatures (e.g. 400 - 500°C).

4.4.2 Cobalto - Cobaltic Oxide.

Co_3O_4 was prepared by precipitation method by mixing a solution of $Co(NO_3)_2.6H_2O$ with 5M KOH solution. The precipitated $Co(OH)_2$ was decomposed in air at 200°C for 10h to give the spinel phase of Co_3O_4 (section 4.5.1).

4.5 Characterization.

4.5.1 X-ray Diffraction.

The materials were finely powdered in a mortar and then carefully packed into thin wall Lindemann glass tubes. X-ray powder diffraction photographs were obtained for the materials prepared using radiation from a Mo or Cu cathode. In general, the information on those materials agreed reasonably well with the published data.

4.5.2 BET Surface Area and Particle Size.

The specific surface area of all the samples were determined by the so-called BET technique, as illustrated in the work of Brunauer, Emmett & Teller, together with their co-workers[70] -[73]. Lack of facilities (section 4.2.3) precluded the measurement of particle size for the materials prepared, but it is resonable, at least in theory that a satisfactory indication of particle size can be made, assuming spherical particles of equal size, the following relationship applies[74]

$$\text{Surface area} = \frac{6}{\rho \times d}$$

where ρ = density.

d = diameter of the particle.

4.6 Hydrogen/Oxygen Recombination Temperature.

4.6.1 Experimental.

The steady state temperatures for H_2/O_2 recombination at various electrolyser currents (e.g. 0.5 - 3.0 A) were determined using a thermocouple inserted into a commercially available hydrocap. The temperatures at the catalyst sites and packing material were then separately measured. However, at a particular electrolyser current, sufficient time (2h) was allowed before the temperature was recorded. The procedure was repeated three more times to ensure that all temperatures were correctly taken.

4.7 Experimental Techniques for the Determination of Capillary Condensation Phenomenon.

4.7.1 Water Adsorption.

The Co_3O_4 powder was initially oven-dried at 120°C until a constant weight was obtained. The powder was then exposed to small amount (e.g. 3 cc) of water environment in a sealed jar and a second sample was similarly exposed to air only. Gravimetric measurement of the amount of water vapour adsorbed by Co_3O_4 was made for the first three weeks. The sample that exposed to water environment was then allowed to stand undisturbed for another five more weeks at room temperature, and the total amount of water adsorbed was 229 mg per 1 g of Co_3O_4

4.7.2 Water Desorption.

The Co_3O_4 samples from section 4.7.1 were exposed to air and dried NiO of different surface areas in a closed jar. The amount of water evaporated or transferred from Co_3O_4 to NiO was determined as a function of time at room temperature. In this way, the relationship

between the rate of water desorbed from Co_3O_4 and the surface area and/or particle size of NiO (as adsorbent) can be thoroughly examined.

4.7.3 Low and High Surface Area of Packing Materials.

Three different surface areas of NiO (0.5g) were used as packing materials and Co_3O_4(0.5g) as H_2/O_2 combination/recombination catalyst. The experimental set-up is shown schematically in Fig. 6 . All samples were oven- dried at 120°C for 1h before the commencement of the experiment.

Gravimetric measurement of the water vapour adsorption on Co_3O_4 was carried out by periodically checking the weight change. In order to simulate the worse possible situation, sufficient exposure time (about 700h) was allowed for water vapour adsorption to take place on Co_3O_4 at room temperature. Thereafter, 0.3g of Co_3O_4 was evaluated by measuring the rate of H_2/O_2 recombination (Chapter 7) at 85°C. However, if the adsorbed water on Co_3O_4 has affected its catalytic activity, then such activity should be restored when it is dried.

4.7.4 The Life and Reliability of Catalyst in Hydrocap.

The H_2/O_2 recombination activity of catalyst in hydrocap was determined using the apparatus shown schematically in Fig. 3 according to the method briefly outlined in section 3.3.1.2, except the time between charge had been prolonged (e.g. 2 weeks).

The PbO_2 packing powder in the commercial hydrocap was successively replaced by three different surface areas of NiO while the 0.5 wt % Pd/Al_2O_3 catalyst remained unchanged. Likewise, a 3mg Pt/100mg Co_3O_4 catalyst was also tested.

The catalytic activities of PbO_2 and NiO were separately determined at elevated temperatures using the method described in

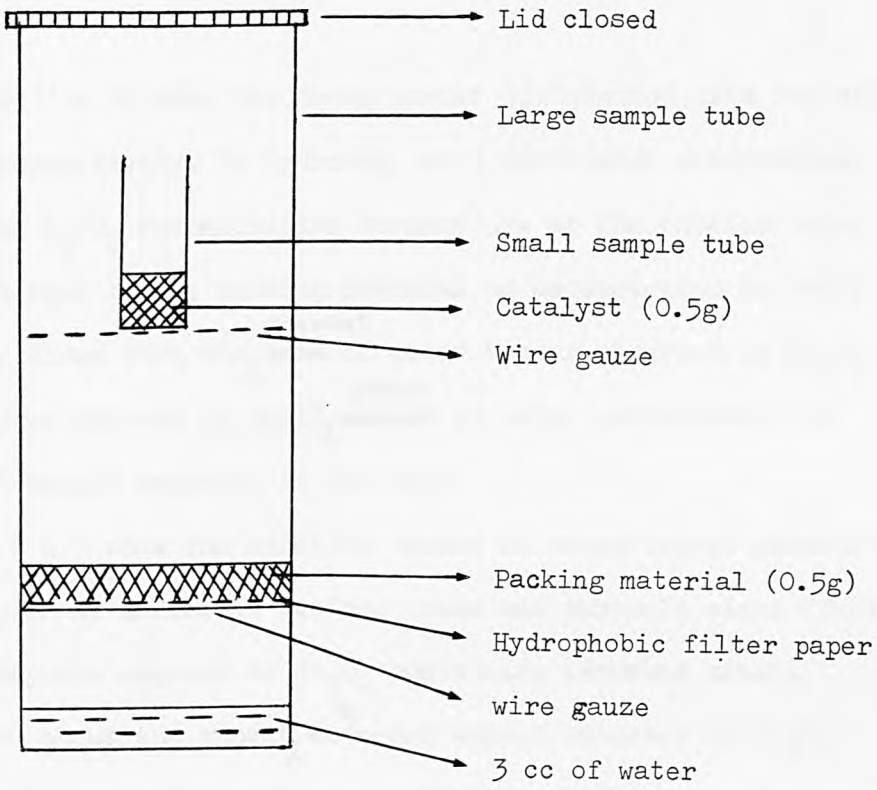

Fig. 6 Water vapour adsorption experiment.

Chapter 7 . 0.3 g each of the oxide was gradually heated to a temperature in which H_2/O_2 recombination took place with a measurable rate. MnO_2 and Co_3O_4 were also evaluated for potential packing materials.

4.8 Results.

Tables 11 & 12 show the X-ray powder diffraction data for NiO and Co_3O_4 respectively. In hydrocap, at a particular electrolyser current, the H_2/O_2 recombination temperature at the catalyst site is higher than that of the packing material as demonstrated in Table 14.

Fig. 7 shows that the ~~rate~~ amount of water vapour adsorbed by Co_3O_4 increases when exposed to small ~~amount~~ volume of water environment, as compared to sample exposing to air only.

Figs. 8 & 9 show the relative amount of water vapour adsorbed by NiO samples of different surface areas and particle sizes (Table 13) when they are exposed to Co_3O_4 containing adsorbed water.

Fig. 10 shows the amount ~~fo~~ of water vapour adsorbed by Co_3O_4 (as catalyst) is significantly reduced when a high surface area with small particle size of NiO (as packing material) is present as shown in Fig. 6 .

Fig. 11 illustrates that the catalytic activity of Co_3O_4 is affected by condensation of water vapour, but such activity is restored after the catalyst has been dried.

Fig. 12 shows the H_2/O_2 combination/recombination activities for NiO , PbO_2 , MnO_2 or Co_3O_4 as alternative packing materials.

Table 15 shows the " start-up " times for different catalysts and packing materials.

ASTM d-value (Å)	Intensity (I/I_o)	Experimental d-value (Å)	Intensity (I/I_o)
2.09	100	2.09	VS
2.41	60	2.41	S
1.48	40	1.48	M
1.26	20	1.26	W
1.21	20	1.21	W
0.94	10	0.95	VW
0.93	10	0.93	VW

TABLE 11 X-ray powder diffraction data for NiO

VS = very strong

S = strong

M = medium

W = weak

VW = very weak

ASTM d-value (Å)	Intensity (I/I_o)	Experimental d-value (Å)	Intensity (I/I_o)
4.67	20	4.63	W
2.86	40	2.87	S
2.44	100	2.44	VS
2.33	11	2.33	W
2.02	25	2.03	W
1.65	11	1.65	W
1.56	35	1.56	M
1.43	45	1.43	S
1.28	5	1.27	VW
1.23	11	1.23	W
1.22	7	1.22	VW
1.16	3	1.17	VW
1.13	3	1.13	VW
1.08	7	1.07	VW
1.05	15	1.05	W
1.01	7	1.00	VW
0.95	5	0.96	VW
0.93	15	0.93	W
0.92	5	0.91	VW

TABLE 12 X-ray powder diffraction data for Co_3O_4

VS = very strong

S = strong

M = medium

W = weak

VW = very weak

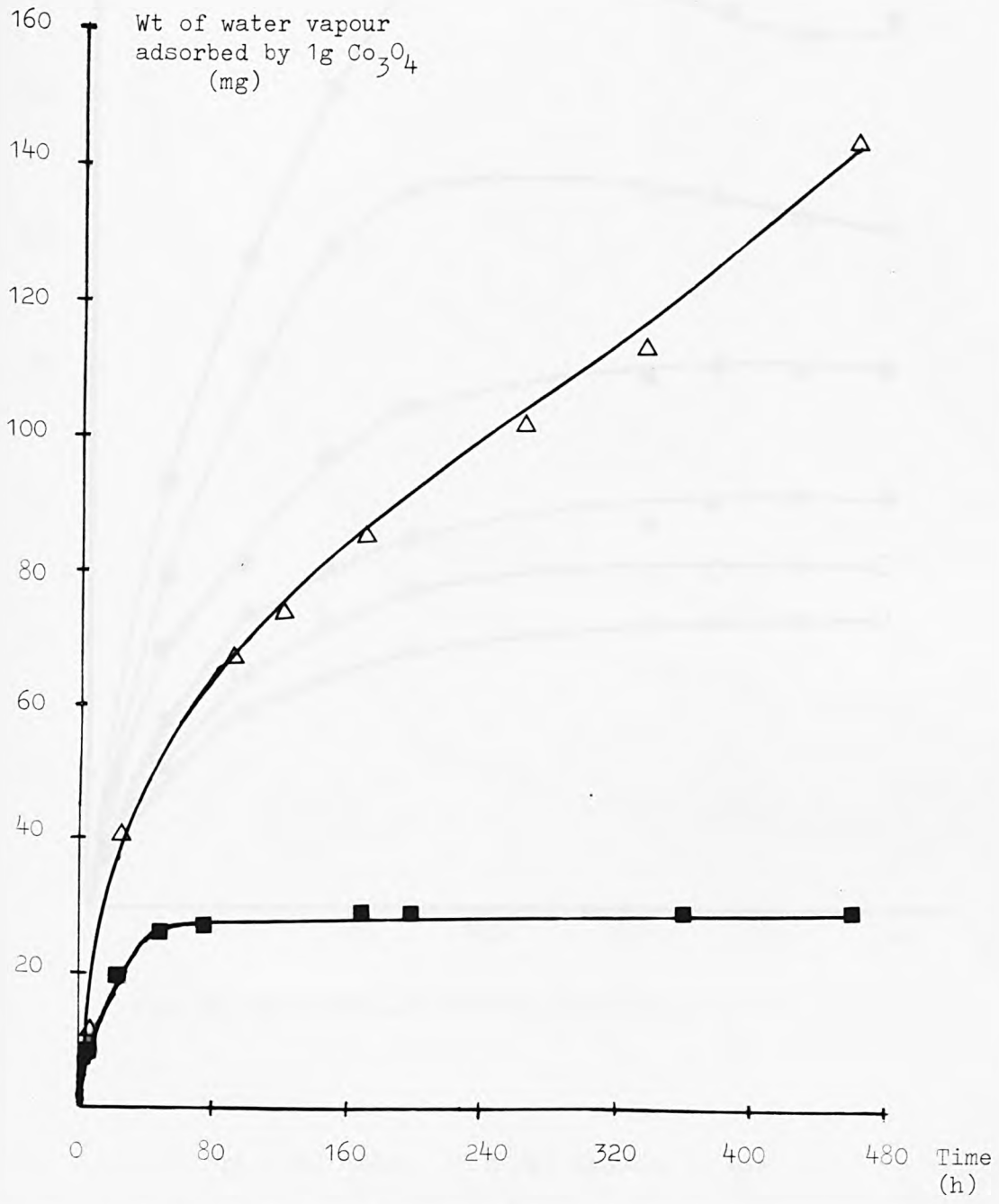

Fig, 7 Water vapour adsorption by Co_3O_4 .

■ Co_3O_4 powder exposed to air

△ Co_3O_4 powder exposed to air & water environment

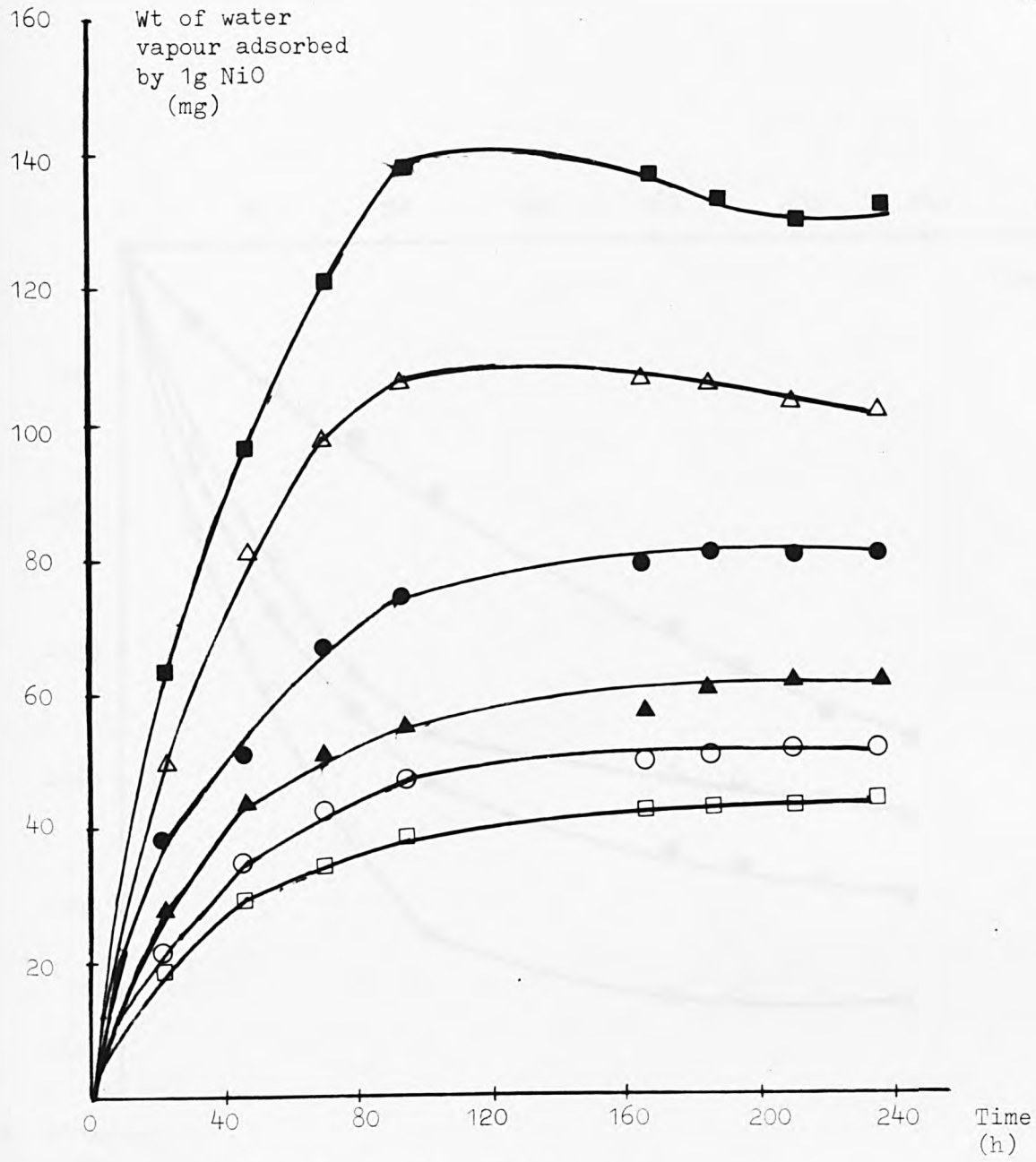

Fig. 8 Water vapour adsorbed by NiO.

□ NiO (SSA = 23 m^2/g) exposed to air

● NiO (SSA = 23 m^2/g) exposed to air and Co_3O_4*

○ NiO (SSA = 125 m^2/g) exposed to air

△ NiO (SSA = 125 m^2/g) exposed to air and Co_3O_4*

▲ NiO (SSA = 168 m^2/g) exposed to air

■ NiO (SSA = 168 m^2/g) exposed to air and Co_3O_4*

* 1g of Co_3O_4 containing 147 mg of water

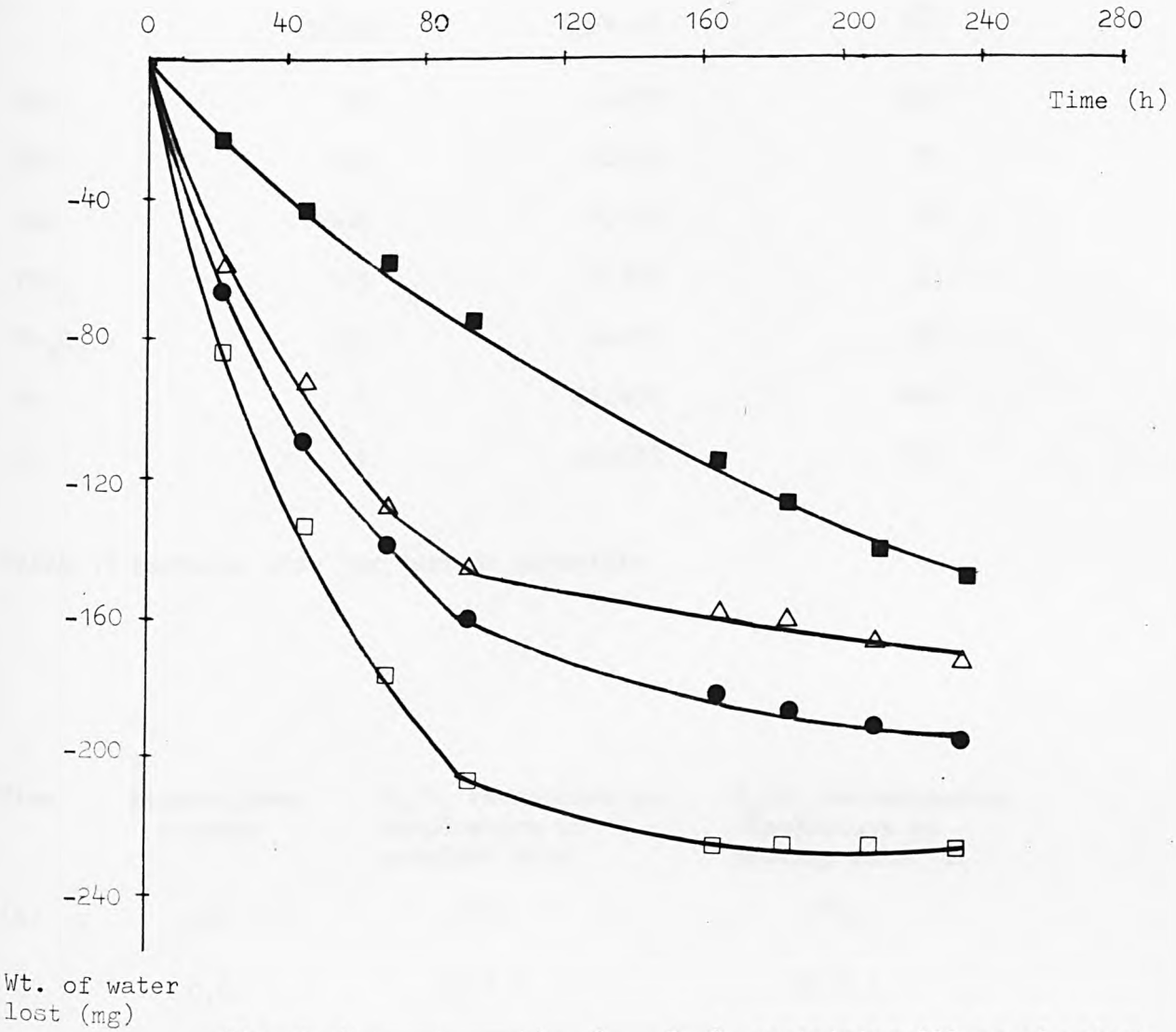

Fig. 9 Water desorption from Co_3O_4 containing 229 mg of water.

■ water vapour lost to air

△ water vapour lost to air and dried NiO (SSA = 23 m^2/g)

● water vapour lost to air and dried NiO (SSA = 125 m^2/g)

□ water vapour lost to air and dried NiO (SSA = 168 m^2/g)

Material	Surface area (m^2/g)	Density (g/c.c)	Average Particle diameter (Å)
NiO	23	6.670	391
NiO	125	6.670	72
NiO	168	6.670	54
PbO_2	123	9.375	52
Co_3O_4	103	6.070	96
Pt	6	21.452	466
Pd	11	12.022	453

TABLE 13 Particle size for various materials

Time (h)	Electrolyser current (A)	H_2/O_2 recombination temperature at catalyst site (^oC)	H_2/O_2 recombination temperature at packing material (^oC)
2	0.6	45 ± 1	40 ± 1
2	1.0	59 ± 1	53 ± 1
2	1.5	70 ± 1	60 ± 1
2	2.0	86 ± 1	77 ± 1
2	3.0	112 ± 1	100 ± 1

TABLE 14 H_2/O_2 recombination temperatures

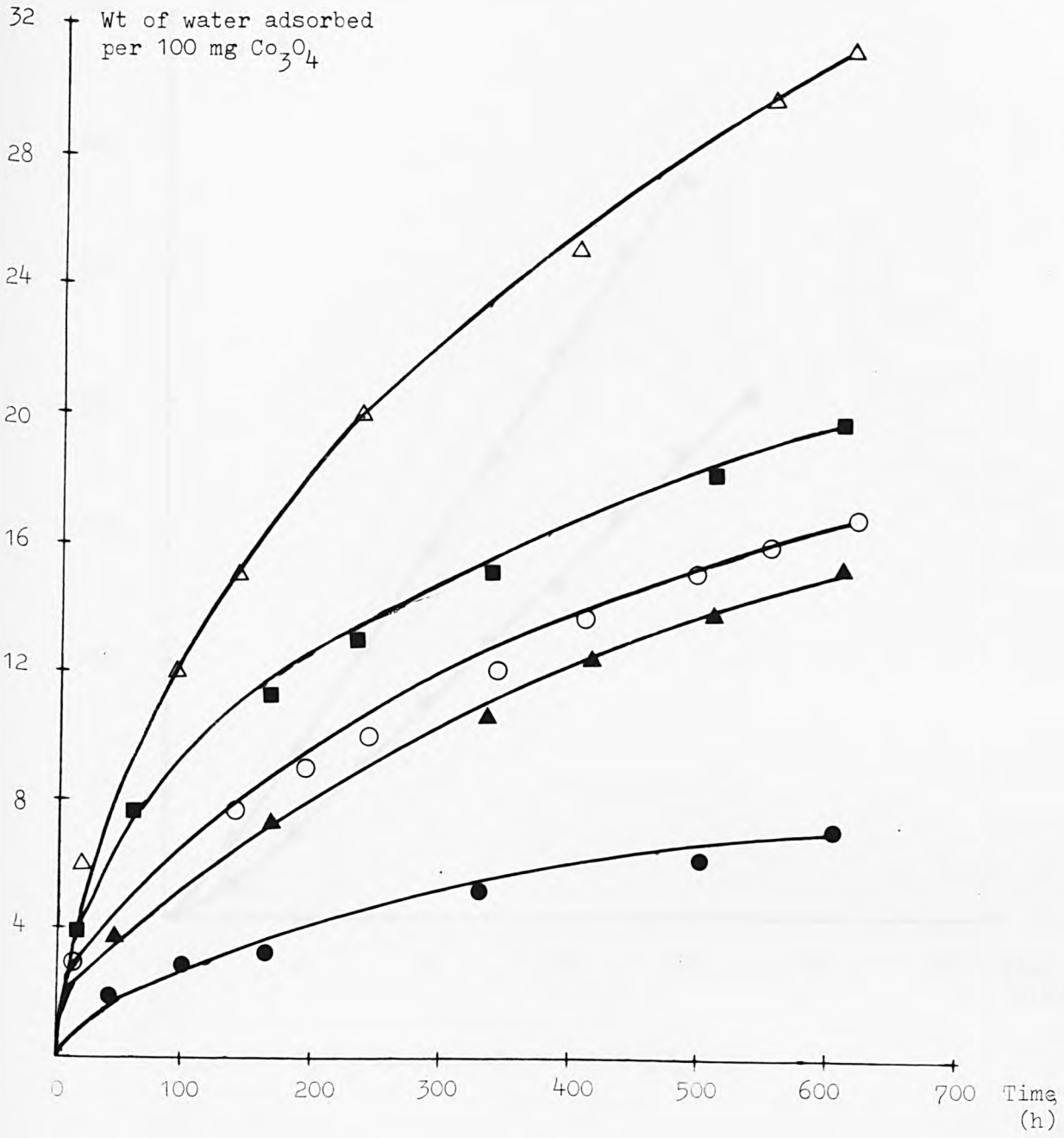

Fig. 10 Weight of water adsorbed by 100 mg Co_3O_4 in the presence of packing materials.

△ Blank

▲ PbO_2 (SSA = 123 m^2/g)

■ NiO (SSA = 23 m^2/g)

○ NiO (SSA = 125 m^2/g)

● NiO (SSA = 168 m^2/g)

Temp = 22 - 23°C

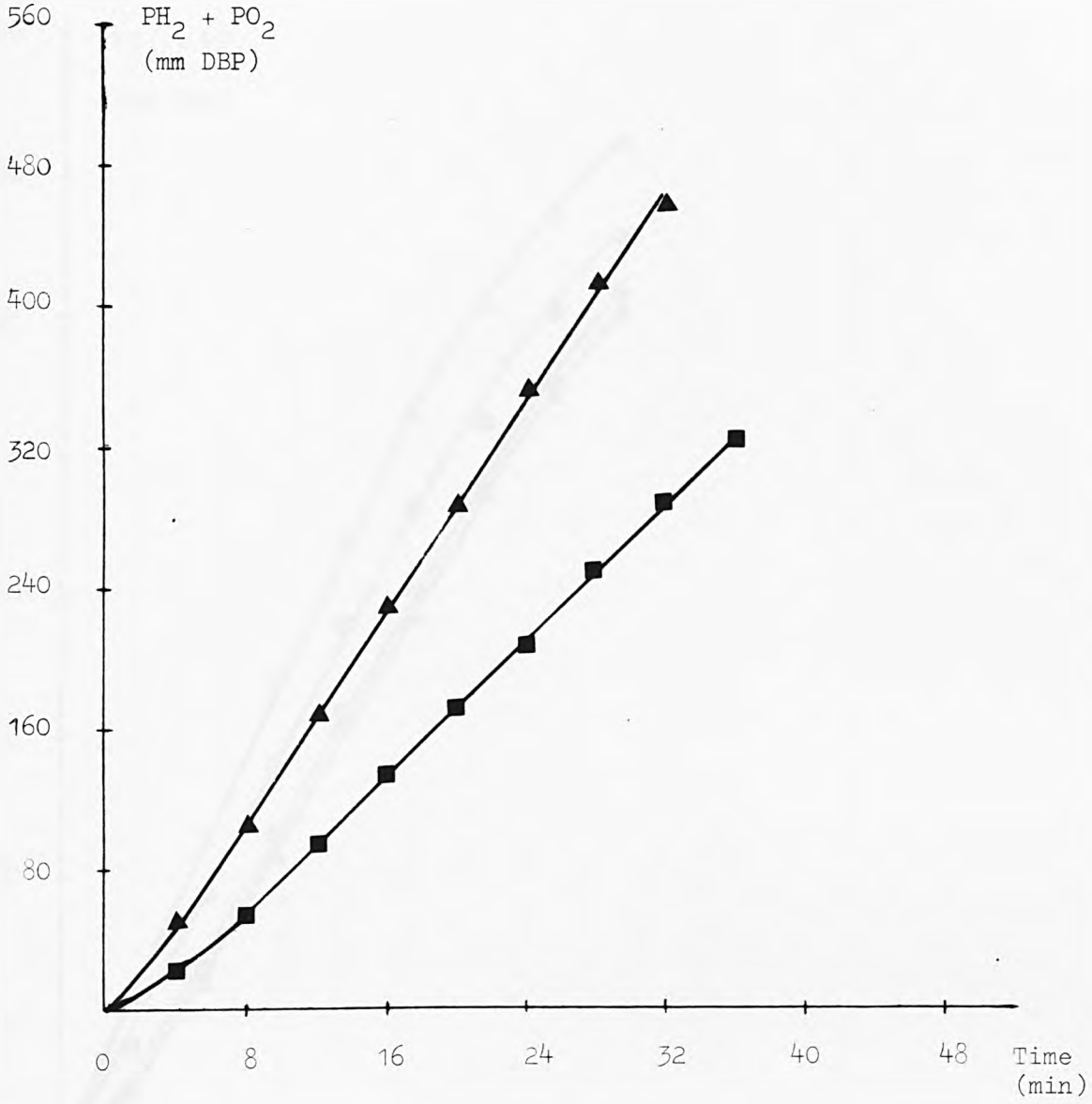

Fig. 11 H_2/O_2 recombination for Co_3O_4 .

▲ Co_3O_4 after oven-dried at 120°C

■ Co_3O_4 (0.3g) containing 34 mg of water

PH_2 = 467 mm DBP

PO_2 = 200 mm Hg

Temp = 85°C

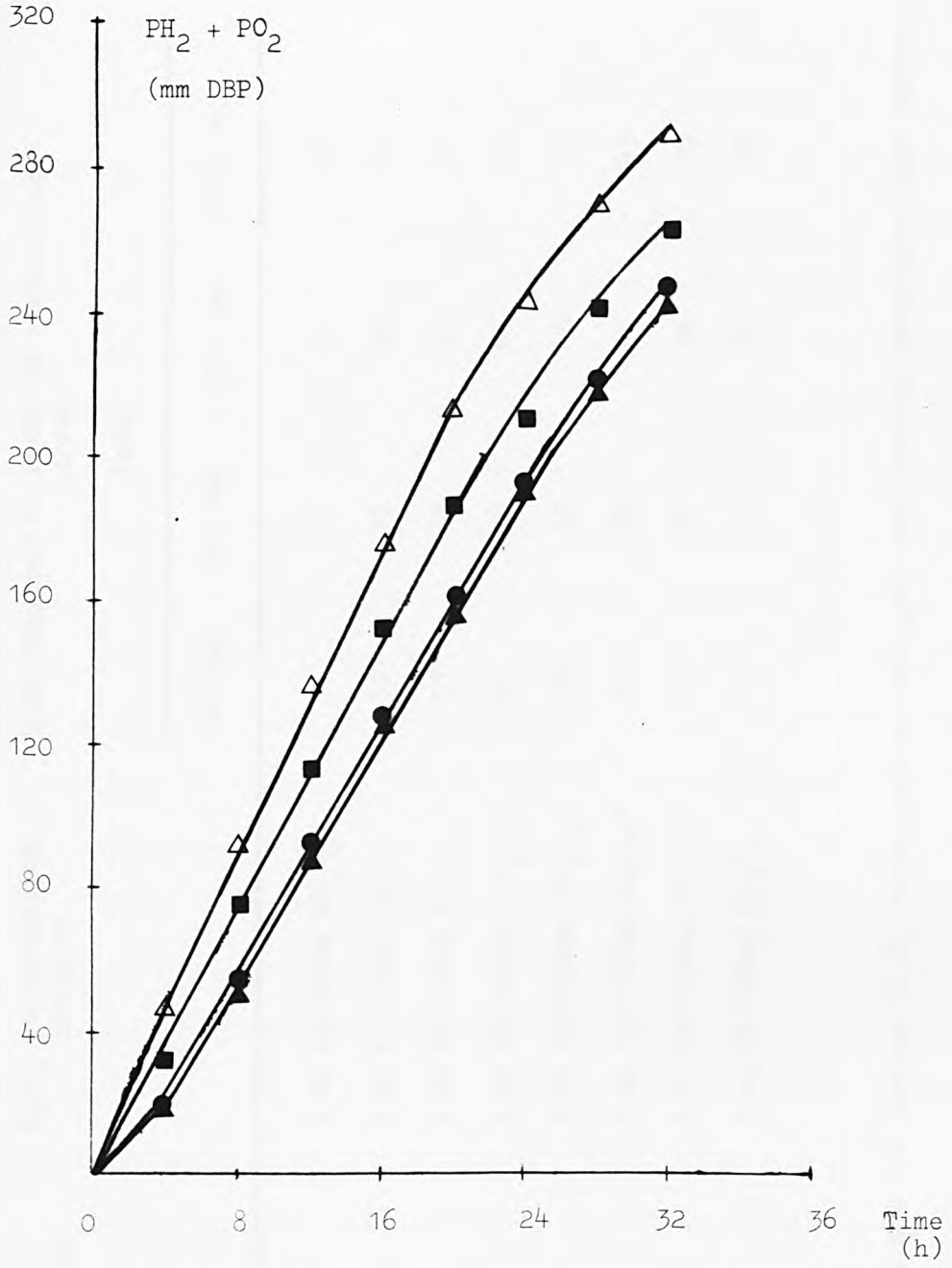

Fig. 12 H_2/O_2 recombination for various packing materials, P^oH_2 = 467 mm DBP, P^oO_2 = 200 mm Hg.

■ MnO_2 at 85°C

△ Co_3O_4 at 60°C

▲ NiO at 54°C

● PbO_2 at 123°C

Packing material (5g)	Surface area of packing material (m^2/g)	H_2/O_2 recombination catalyst	Time required to reach 3A electrolyser current (min)			
			1st day	6th day	15th day	28th day
NiO	23	3 mg Pt/100mg Co_3O_4	31	37	41	46
NiO	125	3 mg Pt/100mg Co_3O_4	31	33	35	37
NiO	168	3 mg Pt/100mg Co_3O_4	31	32	31	31
PbO_2*	123	5 mg Pd/1000mg Al_2O_3*	37	39	43	45
NiO	23	5 mg Pd/1000mg Al_2O_3*	37	42	46	51
NiO	125	5 mg Pd/1000mg Al_2O_3*	36	39	41	43
NiO	168	5 mg Pd/1000mg Al_2O_3*	37	37	36	37
PbO_2*	123	3 mg Pt/100mg Co_3O_4	31	33	35	38

TABLE 15 The " start-up " times for various H_2/O_2 recombination catalysts and packing materials (open system)

* materials from commercial hydrocap

4.9 Discussion.

The results show that the " start-up " problems can be solved when the catalytic device contains a H_2/O_2 recombination catalyst which is located within the bulk of the packing material. The packing material is to be (a) capable of adsorbing water vapour from its environment by capillary condensation so as to reduce condensation of water on the catalyst (Fig. 10), and (b) itself capable of catalysing H_2/O_2 recombination under the temperature conditions attained in use. For example, NiO (Fig. 12) catalyses H_2/O_2 reaction at temperatures as low as 40 - 50°C so that any condensed water present will be evaporated faster than in PbO_2 , since NiO at 54°C and PbO_2 at 136°C under the same experimental conditions give almost the same H_2/O_2 recombination rate (Fig. 12) , indicating NiO is more active than PbO_2 at low temperature.

Table 14 shows conclusively that PbO_2 does not participate in H_2/O_2 recombination at electrolyser current less than 3A. Although there are other possible packing materials such as MnO_2 and/or Co_3O_4, attention has been drawn to NiO and PbO_2 because of the large difference in H_2/O_2 recombination temperature between them.

Other important considerations on packing materials are as follows :

(a) the surface area of the packing material in the H_2/O_2 recombination device should be larger than that of the catalyst (Table 13).

(b) the pore size or the size of the interstices between its individual particles of the packing material should be smaller than that of the catalyst so as to promote preferential capillary adsorption by the packing material . Generally, the size of the interstices varies proportionally with particle size[61] .

(c) for the same reasons, the pore size of the packing material should be smaller than that of the catalyst support (Table 13).

The important relationship of pore size is therefore:

Catalyst > Catalyst support > packing material.

This is to ensure, by appropriate preferential adsorption, that the catalyst itself is kept as dry as possible, so that the catalyst will behave normally as shown in Table 15.

As mentioned earlier, the packing material must itself be capable of catalysing H_2/O_2 recombination under the temperature conditions attained in the device when in operation. As a result, some H_2/O_2 reaction takes place with the packing material itself serving as a secondary catalyst, and the consequent heat energy produced served to vaporise at least part of the moisture that would otherwise accumulate in the pores of the packing material. If the moisture accumulating in the packing material were not to be removed in this way, the efficiency of the packing material in adsorbing water would progressively decline, and this would in turn lead to increased water retention. The efficiency of the packing material for perferentially adsorbing moisture will therefore be impaired, and H_2/O_2 recombination at the catalyst sites can not function efficiently since it would have adsorbed too much moisture during the shut-down period of the previous cycle.

This low-temperature (Fig. 12) catalytic function of the packing material in hydrocaps is therefore a very important factor contributing to the life and reliability of the catalysts in the devices as measured by " start-up " time. This is provided the free space is also kept to a minimum as described in Chapter 3.

CHAPTER 5

THE MODIFICATION OF HYDROCAPS FOR THE INGRESS OF AIR.

CHAPTER 5

5 THE MODIFICATION OF HYDROCAPS FOR THE INGRESS OF AIR.

5.1 Introduction.

The aim of modifying the conventional hydrocaps is to effect the recombination of hydrogen and oxygen. The invention provides a device having inlet means for admitting air from the surrounding atmosphere (and thus oxygen) to the catalyst bed. The provision of such an external source of oxygen enables substantially complete reaction of all hydrogen evolved not only in cases where there is a shortage of evolved oxygen as a result of non-stoichiometric H_2/O_2 evolution from an electric storage cell or other source, but also for use in situations where substantially only hydrogen is evolved. For example, certain metal/air batteries, such as aluminium/air, magnesium/air and zinc/air , which tend to evolve hydrogen slowly on discharge (section 1.1) , or where hydrogen is to be removed from a gas stream.

The removal of hydrogen is essential especially ~~working~~ in an enclosed environment.

5.2 Design of Hydrocaps.

The modified hydrocap is shown diagrammatically in Fig. 13 . The air inlet means consisted of small apertures of circular cross-section. There were five or six apertures each of internal diameter in the range of 2 - 3 mm . All apertures were spaced uniformly across the housing of the device, with some of them located on the top of the housing and the remainder at the sides. In addition, a valve

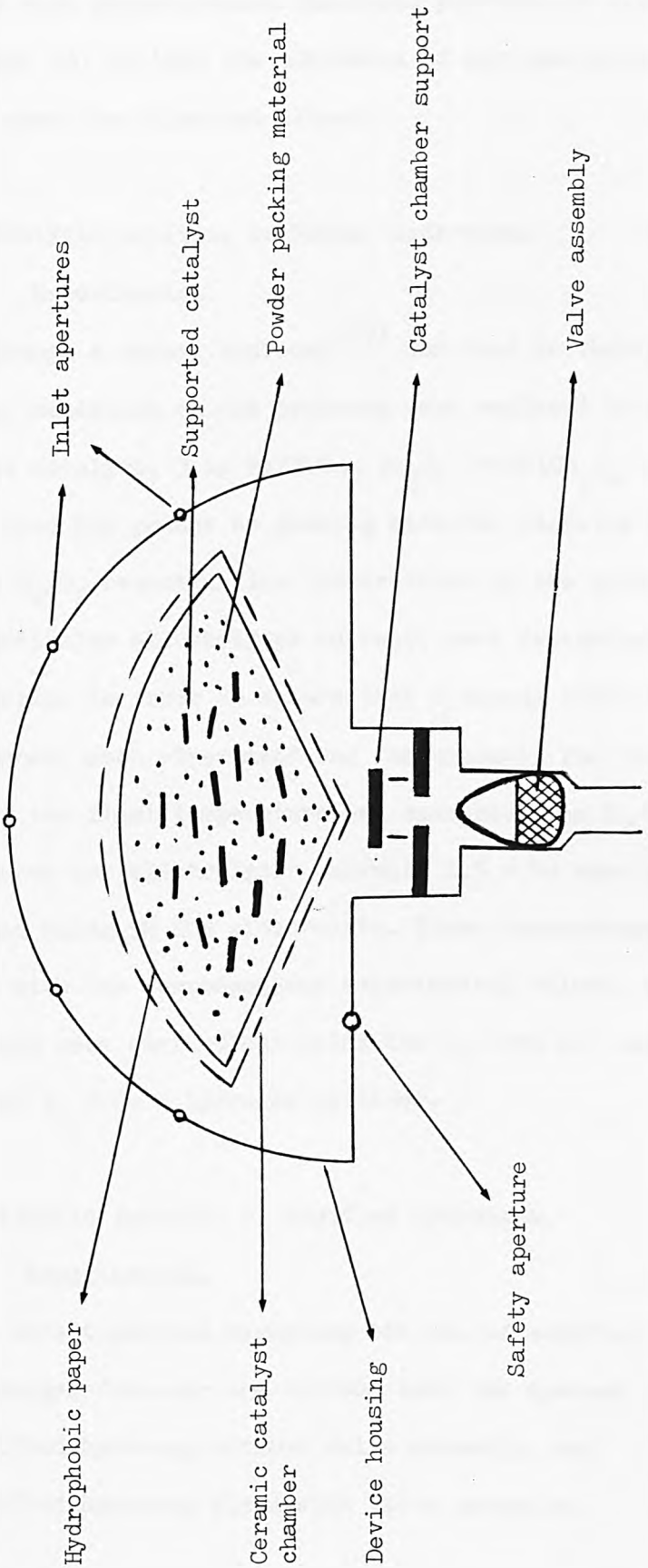

Fig. 13 Diagram showing a modified hydrocap.

assembly with predetermined threshold pressure of 0.31 Psi was also used (Fig. 13) so that the admission of air was increased during periods when the valve was closed.

5.3 The Catalytic Activity of Normal Hydrocaps.

5.3.1 Experimental

Although a normal hydrocap[57] was used in this experiment, the catalytic materials in the hydrocap were replaced by an active supported catalyst, 3 mg Pt/100mg Co_3O_4 ($Pt/NiCo_2O_4$ could also be used), high surface area NiO powder as packing material (details in Chapter 4).

The H_2/O_2 recombination temperatures at the packing material, for a particular electrolyser current, were determined using a thermocouple. In order to ensure that a steady state temperature had been reached, each experiment was continuously run for a period of 2h before the final temperature was measured. The H_2/O_2 reaction temperatures for electrolyser currents 0.5 - 4A were similarly determined using 5M KOH electrolyte. These temperatures were then compared with the corresponding experimental values, where the experiments were carried out using the O_2 from air and the controlled amounts of H_2 from a hydrogen cylinder.

5.4 The Catalytic Activity of Modified Hydrocaps.

5.4.1 Experimental.

The investigations regarding the use of modified hydrocaps to extract oxygen from air are divided into two systems :

(a) modified hydrocap without valve assembly, and

(b) modified hydrocap fixed with valve assembly.

In both cases, a calculated amount of H_2 gas was carefully controlled by a special gas flowmeter from a hydrogen cylinder and then fed to the catalyst housing. In this way, at a particular electrolyser current, for example, the equivalent amount of H_2 passed over the catalyst bed whereupon H_2/O_2 recombination took place using the O_2 from air. In order to ensure that sufficient O_2 was available for complete reaction with the supplied H_2 , the H_2/O_2 recombination temperatures were measured by the method outlined in section 5.3.1 .

Time (min)	Hydrogen/oxygen recombination temperature at various electrolyser currents (°C)					
	0.6A	1.0A	1.5A	2.0A	3.0A	4.0A
0	22 ± 1	22 ± 0	22 ± 0	22 ± 1	22 ± 1	22 ± 0
4	25 ± 0	27 ± 1	30 ± 1	32 ± 1	37 ± 0	40 ± 0
8	30 ± 1	34 ± 1	37 ± 1	46 ± 1	52 ± 1	55 ± 0
12	34 ± 1	40 ± 1	42 ± 0	50 ± 0	72 ± 1	76 ± 1
16	38 ± 1	44 ± 1	50 ± 1	58 ± 1	82 ± 1	98 ± 1
30	40 ± 1	53 ± 1	61 ± 1	78 ± 0	100 ± 1	122 ± 1
120	40 ± 0	54 ± 0	62 ± 1	78 ± 0	100 ± 0	123 ± 1

TABLE 16 H_2/O_2 recombination temperatures in normal hydrocap

Time (min)	Hydrogen/oxygen recombination Temperature at various equivalent electrolyser currents (^{o}C)					
	0.6A	1.0A	1.5A	2.0A	3.0A	4.0A
0	22 ± 0	22 ± 0	22 ± 0	22 ± 0	22 ± 0	22 ± 1
4	25 ± 1	27 ± 0	29 ± 2	31 ± 1	37 ± 0	39 ± 1
8	30 ± 1	34 ± 1	36 ± 1	46 ± 1	51 ± 1	51 ± 2
12	34 ± 1	39 ± 1	41 ± 1	50 ± 0	71 ± 1	71 ± 1
16	38 ± 0	42 ± 1	49 ± 1	57 ± 1	82 ± 1	81 ± 2
30	40 ± 1	53 ± 1	62 ± 1	77 ± 1	99 ± 1	99 ± 2
120	40 ± 0	53 ± 0	62 ± 1	77 ± 0	100 ± 0	102 ± 1

TABLE 17 H_2/O_2 recombination temperatures in modified hydrocap without a valve system

Time (min)	Hydrogen/oxygen recombination temperature at various equivalent electrolyser currents (^{o}C)					
	0.6A	1.0A	1.5A	2.0A	3.0A	4.0A
0	22 ± 1	22 ± 0	22 ± 0	22 ± 0	22 ± 1	22 ± 0
4	25 ± 2	27 ± 1	30 ± 1	31 ± 1	37 ± 1	39 ± 1
8	30 ± 0	34 ± 1	37 ± 1	45 ± 1	52 ± 1	55 ± 1
12	35 ± 1	39 ± 2	42 ± 1	50 ± 1	70 ± 1	75 ± 1
16	38 ± 1	44 ± 1	50 ± 1	57 ± 2	82 ± 1	98 ± 1
30	40 ± 0	53 ± 1	62 ± 1	77 ± 1	100 ± 1	120 ± 1
120	40 ± 0	53 ± 0	62 ± 2	78 ± 1	100 ± 0	122 ± 0

TABLE 18 H_2/O_2 recombination temperatures in modified hydrocap with a valve system

5.5 Results and Discussion.

Table 16 shows the H_2/O_2 recombination temperatures at the packing material sites in normal hydrocap.

The H_2/O_2 recombination temperatures at the packing materials for modified hydrocaps without and with a valve system are shown in Table 17 & 18 respectively.

The results show that the provision of an air inlet means is especially advantageous in combination with a valve assembly (Tables 16, 17 & 18). This becomes obvious when the flow rate of H_2 is large (e.g. $\sim$ 4A equivalent of electrolyser currents). Thus, the admission of air is increased during periods when the valve is closed. This arises principally from the absence of the excess pressure within the device housing (as compared with atmosphere) that would otherwise be established as a result of the continual flow of evolved H_2 from a cell or other source.

In operation, the device is connected, for example, to a battery cell and the " shut-off " valve will open once the pressure of evolved gas(es) in the cell exceeds the predetermined threshold value (set by the weight of the valve) , typically valve opening in response to a pressure differential of greater than 0.3 Psi. Gas is thereby admitted to the catalyst bed. If the evolved gas contains more hydrogen than oxygen, or if it contains hydrogen only, atmospheric oxygen will by admitted through the inlet apertures (Fig. 13) and an appropriate amount will react catalytically with the hydrogen to form water. In the case of a sealed secondary battery, the condensed water drips back to the cell through valve opening. However, in metal/air systems, (Chapter 1, section 1.1) the return of water to the cells is not necessary.

When the pressure differential falls below the predetermined value, the valve assembly (Fig. 13) will return to its closed position under the action of gravity. The " on-off " sequence will be repeated periodically in response to the rate of gas evolution.

The modification of the commercial hydrocaps has therefore effectively consumed all the hydrogen evolved from a cell by reacting catalytically with atmospheric oxygen.

CHAPTER 6

MECHANISTIC STUDIES ON SPINEL OXIDES FOR HYDROGEN AND OXYGEN RECOMBINATION.

CHAPTER 6

6 MECHANISTIC STUDIES ON SPINEL OXIDES FOR HYDROGEN AND OXYGEN RECOMBINATION.

6.1 Spinel Oxide.

Spinels have the general formula AB_2O_4 where A and B are cations in the +2 and +3 oxidation states respectively. The oxide ions form a close-packed cubic lattice with eight tetrahedral sites and four octahedral sites per molecule of AB_2O_4 [75][76]. In a so-called normal spinel oxide such as $MgAl_2O_4$, one-eighth of the tetrahedral sites are occupied by Mg^{2+} ions and the Al^{3+} ions occupy half the octahedral sites. Other mixed oxides possessing normal spinel structure are Co_3O_4, $ZnFe_2O_4$ and $FeCr_2O_4$ etc. However, if half of the B^{3+} species are in tetrahedral sites, with the other half and the A^{2+} species in octahedral; this structure is often written as $B[AB]O_4$, is called the inverse spinel structure, e.g. $NiCo_2O_4$ and $CoFe_2O_4$.

In general, the two common types of cation distributions are as follows :

Normal spinel $\quad \left[A^{2+}\right]_t \left[B^{3+}\ B^{3+}\right]_o\ O_4^{2-}$

Inverse spinel $\quad \left[B^{3+}\right]_t \left[A^{2+}\ B^{3+}\right]_o\ O_4^{2-}$

Where the subscripts t and o represent the tetrahedral and octahedral sites respectively.

The possible combination of charges of A and B are 2 : 3 , 4 : 2 , 6 : 1 and 1 : 3 , but the most common spinel types are 2 : 3 or 4 : 2 .

6.2 Hydrogen Gas Absorbers.

Platinum or palladium-catalysed[77][78][79] and silver-catalysed[80][81] manganese dioxide have been reported to be a good hydrogen absorber, and the hydrogen gas absorption is a reaction between MnO_2 and the H_2 gas. Kozawa[82] investigated the mechanism of the reaction between H_2 gas and oxides such as MnO_2, Mn_3O_4, CuO, PbO_2, RuO_2, HgO and Ag_2O showed that PbO_2, HgO and CuO were poor hydrogen absorbers compared to MnO_2 and RuO_2. According to Kozawa [82] the good hydrogen absorption capability of MnO_2 and RuO_2 was attributed to the nature of the unique oxide system, which is reduced by accepting protons without changing the essential structure. The electrochemical studies on various oxides[82][83][84][85] suggested that MnO_2 and RuO_2 are one phase solid redox system whereas PbO_2, Ag_2O and HgO are two phase solid redox system.

6.3 Spinel Oxides as Hydrogen Gas Absorbers.

According to Kozawa[77], at room temperature a catalyst is required to dissociate H_2 gas into atoms before the atomic hydrogen is injected into the oxide lattice, e.g. MnO_2[77][80][82]. For the same reasons, platinized spinel oxides were tested for H_2 gas absorption at room temperature and atmospheric pressure.

6.4 Sample Preparation.

1g of each platinised Co_3O_4 and $NiCo_2O_4$ was mixed with 60 mg of platinum black and 0.3 - 0.5 cc of water. The mixture was thoroughly blended and oven-dried at 70 -80°C for 2h to remove most of the added water. The dried material was crushed in a mortar. The water treatment[82] was to provide good contact between the spinel oxide and the catalyst.

The unplatinized oxide samples were similarly dried before the test. In addition, platinized Co_3O_4 electrodes were also prepared (section 6.6.1) for H_2 gas absorption experiments.

6.5 Experimental.

6.5.1 Hydrogen Gas Absorption.

The air in the tube was expelled by purging with N_2 gas as shown diagrammatically in Fig. 14. The oil level was slowly raised to a known volume (below sample level) in the graduated measuring cylinder by removing the N_2 gas through the vacuum line. Hydrogen gas was then introduced to lower the oil level inside the measuring cylinder to a known volume. The system was allowed to stand undisturbed at room temperature and the increase in the oil level was recorded as a function of time. The amount of hydrogen gas in the graduated measuring cylinder was pre-calibrated.

6.5.1.1 X-ray Studies for Oxide Reduction.

X-ray powder diffraction patterns were obtained for all spinel oxide samples before and after hydrogen absorption. In this way, the X-ray method (section 4.5.1) could provide information regarding oxide reduction.

6.5.2 Hydrogen Gas Desorption.

Platinized $NiCo_2O_4$ and Co_3O_4 were used in this investigation. The experimental set-up is shown schematically in Fig. 15. After expelling the air in the system by purging with N_2 gas, a slow flow rate (8 - 10 cc/min) of H_2 gas was introduced continuously for 70h

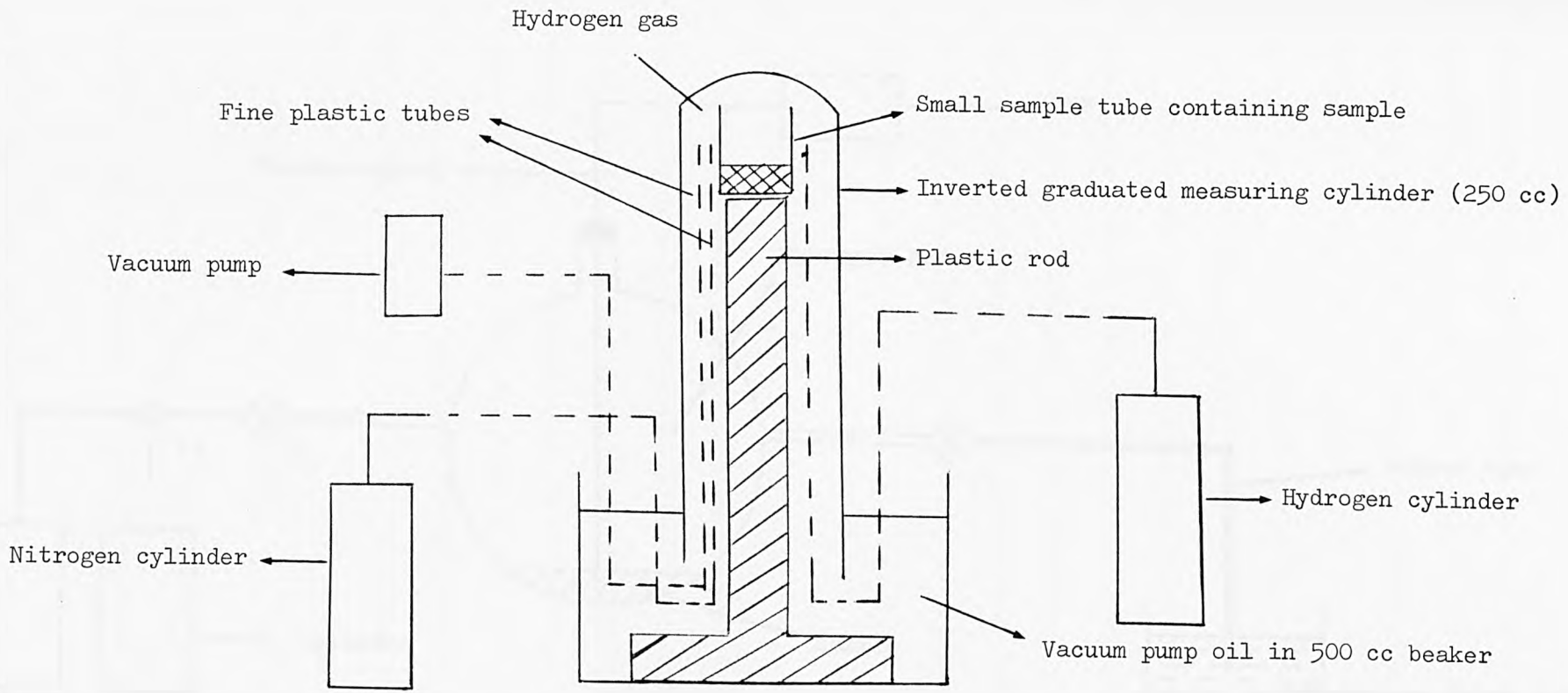

Fig. 14 Apparatus for measuring hydrogen gas absorption.

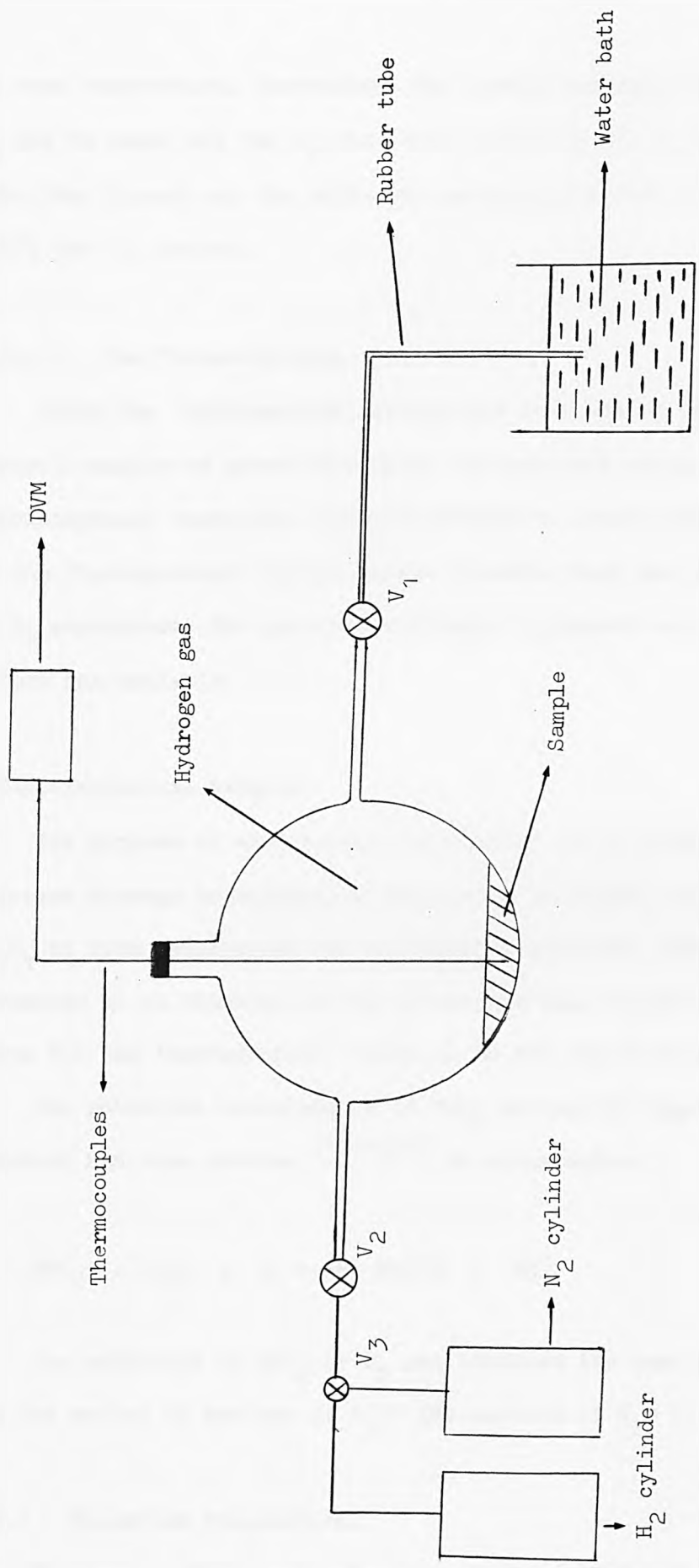

Fig. 15 Apparatus for measuring hydrogen gas desorption.

at room temperature. Thereafter, the system was again purged with N_2 gas to expel all the H_2 gas. Both valves V_1 and V_2 (Fig. 15) were then closed and the oxide was gradually heated to about 200 - 300°C for 15 minutes.

6.5.2.1 Gas Chromatography.

After the 'hydrogenated' oxides had been heated (section 6.5.2), several samples of gases were taken for analysis using the gas chromatography technique. Thermal desorption should yield hydrogen if the 'hydrogenated' spinel oxides absorbed such gas after exposing to H_2 atmosphere. The gas chromatography equipment was pre-calibrated before gas analysis.

6.6 Electrochemical Studies.

The purpose of electrochemical studies is to establish the hydrogen storage or absorption properties in spinel oxides such as Co_3O_4 at room temperature and atmospheric pressure. The important parameter to be examined is the anodic hydrogen oxidation polarization curve for the 'hydrogenated' oxide in 5M KOH electrolyte.

The potential measurements of MnO_2 during the discharge in KOH solution has been studied [85]-[90] as shown below:

$$MnO_2 + H_2O + e \longrightarrow MnOOH + OH^-$$

The reduction of MnO_2 by H_2 gas involved the same mechanism[86], and the source of protons is H_2(= 2H) instead of H_2O (= $H^+ + OH^-$).

6.6.1 Electrode Preparation.

Electrodes of the polytetrafluorethylene (P.T.F.E.) bonded type

were prepared by ultra-sonically mixing a 60% P.T.F.E. dispersion with the catalyst in the ratio 3 : 10 by weight [91]. Using the method by Tseung and Wong[92], weighed quantities of impregnated catalysts were mixed with aqueous P.T.F.E. dispersion and then painted onto 1 cm^2 100 mesh nickel screens. The electrodes were 'cured' at 300°C for 1h.

Generally, complete transfer of the entire mixture to the nickel screen was impossible and the catalyst loadings were estimated from the screen weight change before and after fabrication, assuming the components of the catalyst/PTFE to be transferred in the same ratio as the original mixture. Catalyst (7 wt % Pt/Co_3O_4) loadings were typically 90 - 100 mg cm^{-2}.

6.6.2 Electrochemical Cell Testing.

The electrochemical measurements were made as follows :

After expelling the air in the assembly by purging with N_2 gas as shown schematically in Fig. 16, hydrogen gas was then introduced continuously for 48h. Thereafter, the assembly was again purged with N_2 gas for 6h before the commencement of the experiment.

The electrode was immersed in 5M KOH at room temperature, against a dynamic hydrogen electrode (DHE), and a platinum counterelectrode was used. Galvanostatic polarization curves were obtained for anodic hydrogen oxidation by discharge.

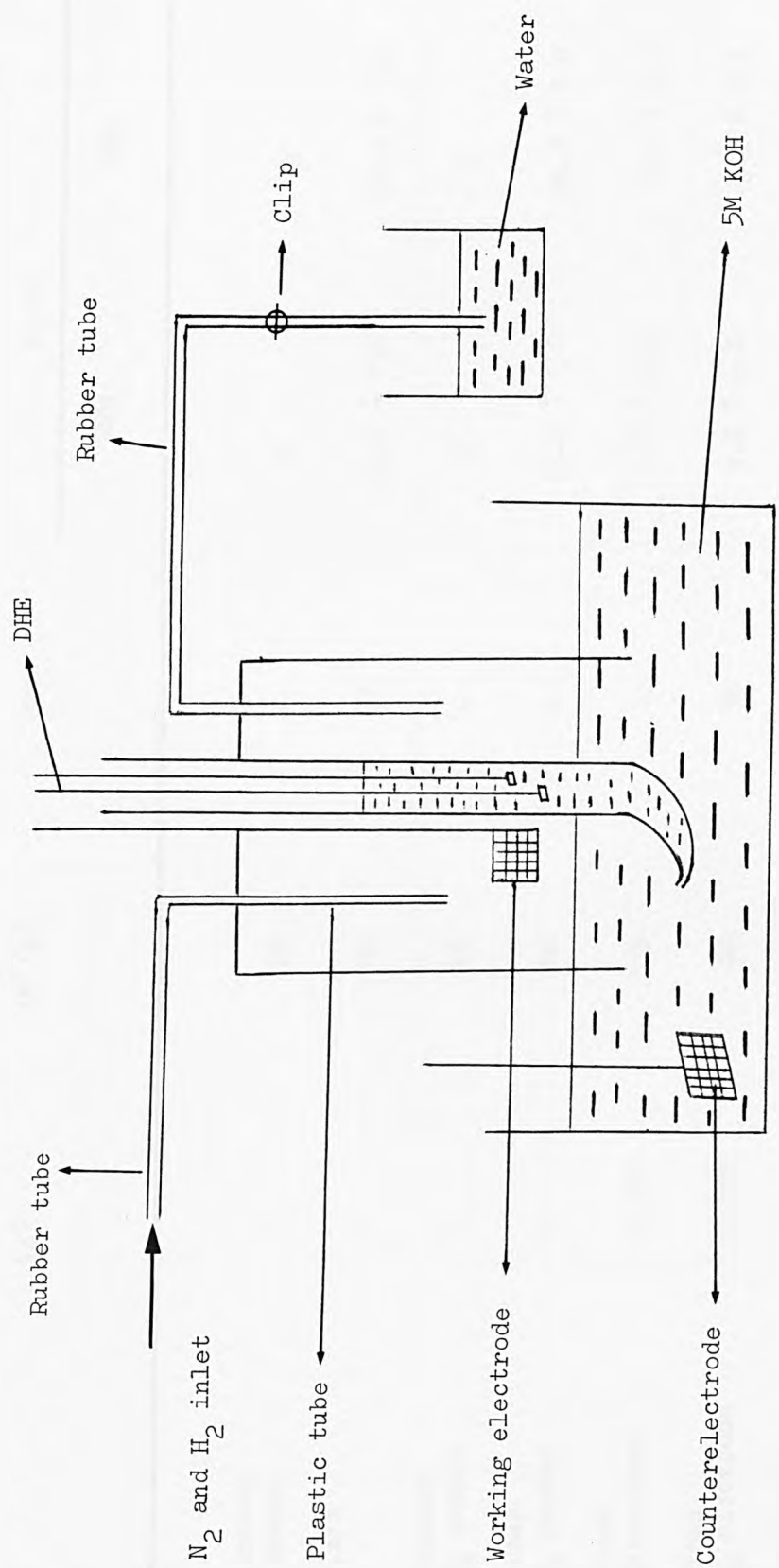

Fig. 16 Electrode cell assembly.

Sample	Weight of spinel oxide (g)	Surface area of spinel oxide (m^2/g)	Pt loading (mg)	Volume of hydrogen gas absorbed (c.c)	
				22h	60h
Unplatinized Co_3O_4 powder	1	103	-	2	3
Platinized Co_3O_4	1	103	60	24.6 ± 1.0	34.2 ± 1.0
Unplatinized $NiCo_2O_4$ powder	1	46	-	2	2
Platinized $NiCo_2O_4$ powder	1	46	60	18.8 ± 1.0	26.3 ± 1.0
Platinized Co_3O_4 electrode	0.150	103	10	4.8 ± 0.3	7.4 ± 0.5
Platinized $NiCo_2O_4$ electrode	0.140	46	10	4.2 ± 0.3	5.7 ± 0.5
Platinium black powder	-	-	60	5.7 ± 0.3	8.6 ± 0.4

TABLE 19 Hydrogen gas absorption by spinel oxides at N.T.P.

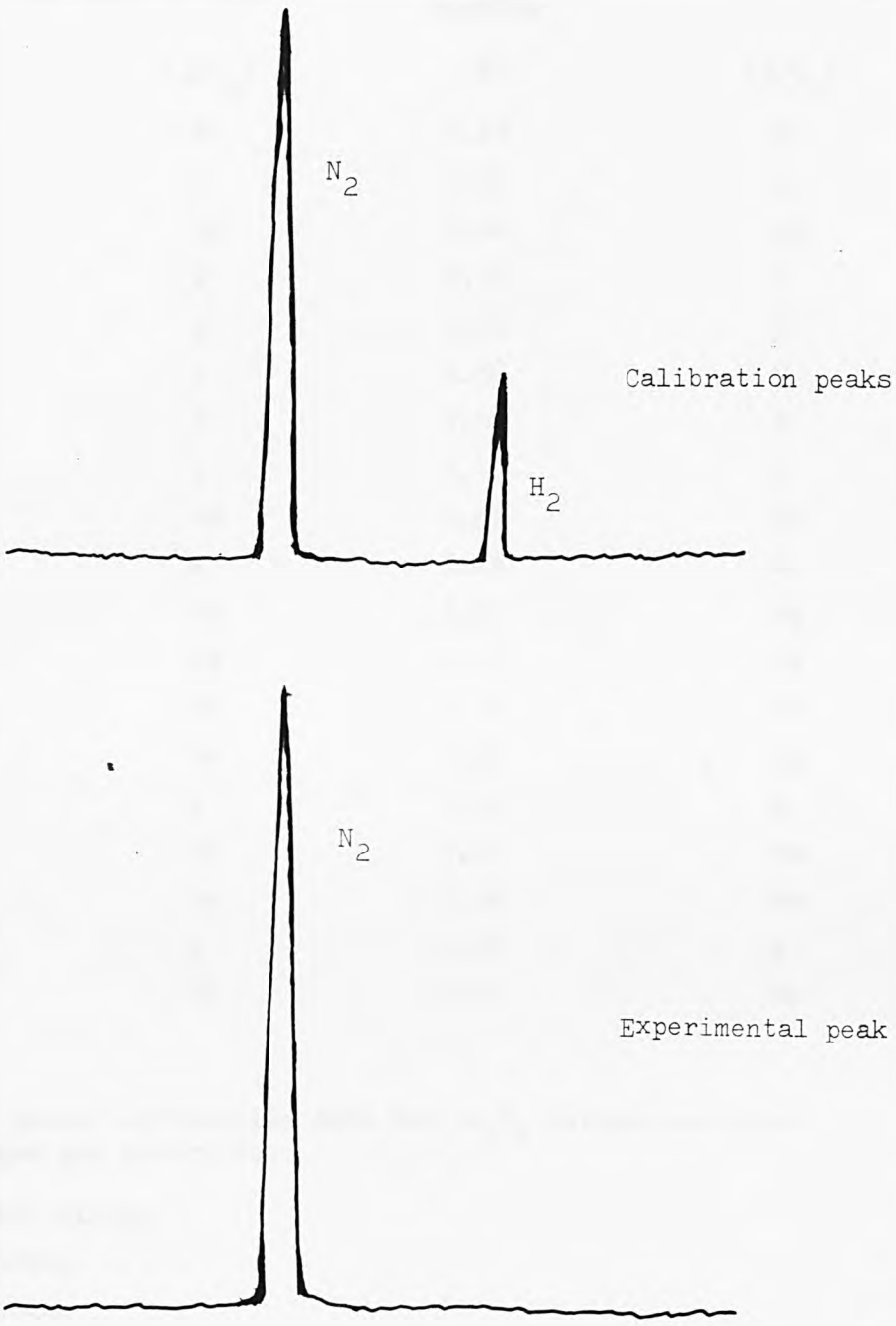

Fig. 17 Hydrogen gas analysis using gas chromatography.

Unhydrogenated Co_3O_4* d-value (Å)	Intensity (I/I_o)	Hydrogenated Co_3O_4 d-value (Å)	Intensity (I/I_o)
4.63	W	4.63	W
2.87	S	2.87	S
2.44	VS	2.44	VS
2.33	W	2.33	W
2.03	W	2.03	W
1.65	W	1.66	W
1.56	M	1.56	M
1.43	S	1.43	S
1.27	VW	1.27	VW
1.23	W	1.23	W
1.22	VW	1.22	VW
1.17	VW	1.17	VW
1.13	VW	1.12	VW
1.07	VW	1.07	VW
1.05	W	1.05	W
1.00	VW	1.01	VW
0.96	VW	0.96	VW
0.93	W	0.93	W
0.91	VW	0.91	VW

TABLE 20 X-ray powder diffraction data for Co_3O_4 before and after hydrogen gas absorption

VS = Very strong
S = Strong
M = Medium
W = Weak
VW = Very weak

* this data is reproduced in Table 12

Unhydrogenated $NiCo_2O_4$ d-value (Å)	Intensity (I/I_o)	Hydrogenated $NiCo_2O_4$ d-value (Å)	Intensity (I/I_o)
4.69	VW	4.69	VW
2.87	M	2.87	M
2.45	VS	2.45	VS
2.03	M	2.03	M
1.58	M	1.57	M
1.43	S	1.43	S
1.23	W	1.23	W
1.05	M	1.05	M

TABLE 21 X-ray powder diffraction data for $NiCo_2O_4$ before and after hydrogen gas absorption

VS = very strong

S = strong

M = medium

W = weak

VW = very weak

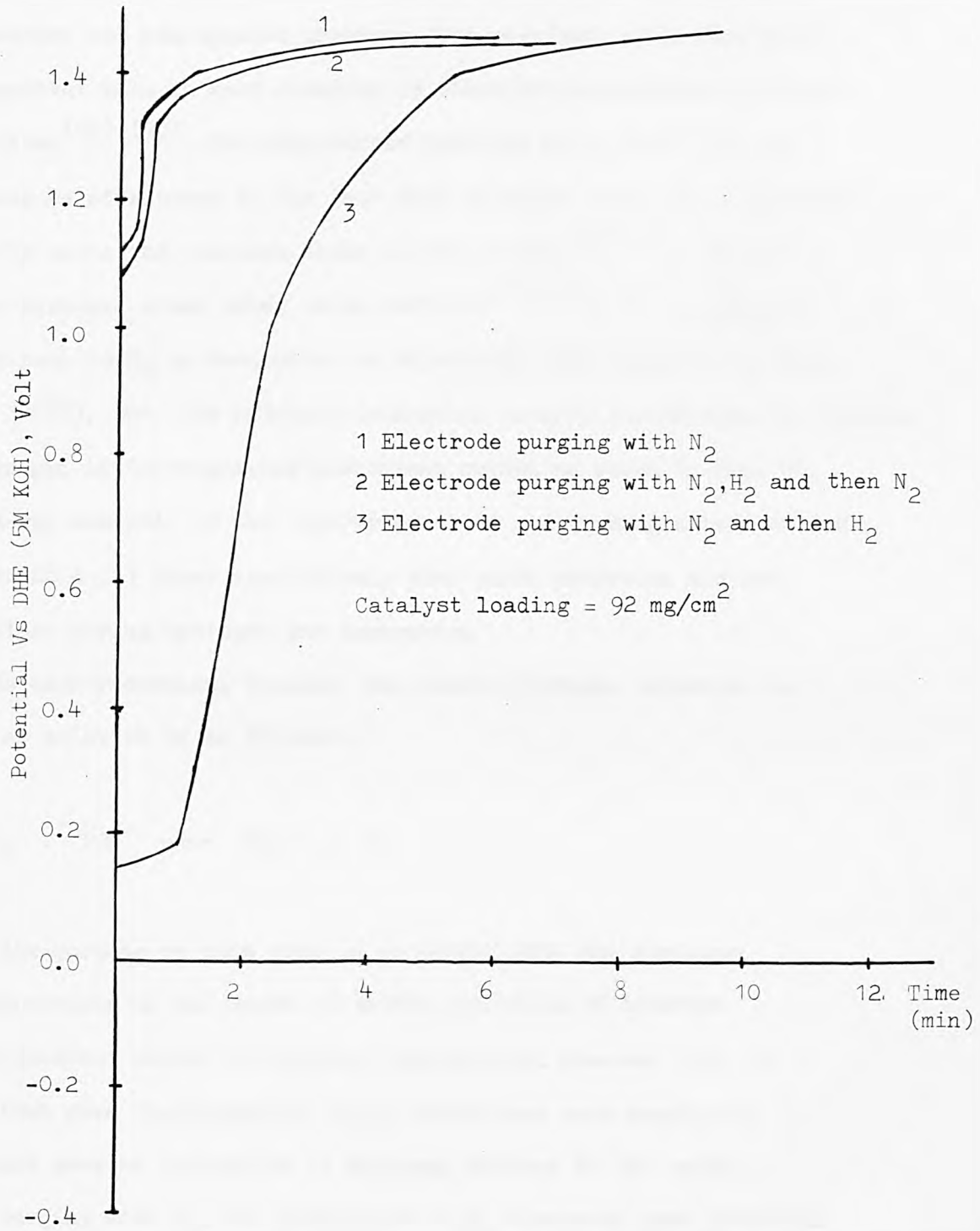

Fig. 18 Anodic polarization curves for platinized Co_3O_4 after purging with H_2.
(i = 10 mA/cm^2, Temp = 21-22°C).

6.7 Results and Discussion.

Table 19 shows that small amount of hydrogen absorption and/or adsorption takes place only in platinized spinel oxides at room temperature and atmospheric pressure. The precious metal thus plays an important role in such reaction by dissociating hydrogen molecules into atoms[93]-[97]. The chemisorbed hydrogen gives Pt-H bond and it could be attributed to the fact that hydrogen atoms are positioned directly above the platinum atoms in the surface[98][99]. However, if the hydrogen atoms enter oxide lattices[80][82], it is possible to get back to H_2 by desorption at relatively high temperature (e.g. 200 - 300°C). But, the hydrogen desorption results demonstrate the absence of hydrogen in 'hydrogenated' platinized oxides as shown in Fig. 17.

X-ray analysis of the 'unhydrogenated' and 'hydrogenated' oxides (Tables 20 & 21) shows conclusively that oxide reduction did not take place during hydrogen gas absorption.

In electrochemical studies, the anodic hydrogen oxidation in alkaline solution is as follows :

$$H_2 + 2OH^- \longrightarrow 2H_2O + 2e$$

Thus, the purpose of this work is to investigate the discharge characteristics in the course of anodic oxidation of hydrogen ('hydrogenated' oxide) in alkaline electrolyte. However, Fig. 18 shows that when 'hydrogenated' Co_3O_4 electrodes were anodically polarized gave no indication of hydrogen storage in the oxide. After purging with H_2, the platinized Co_3O_4 electrode rest potential was about 150 mV Vs DHE. However, if the electrode was successively

purged with H_2 and N_2, the rest potential was about 1.10V Vs DHE. The results suggest that small amount of H_2 adsorption takes place on platinum surfaces.

Generally, the results show that there is no hydrogen storage in spinel oxide lattices or oxide reduction. A possible explanation for the H_2 gas up-take (Table 19) in platinized spinel oxides is as follows :

$$2\,Pt + H_2 \longrightarrow 2\,Pt - H \quad \text{and}$$

$$Pt - H \longrightarrow H - Co_3O_4 + Pt$$

The adsorption of hydrogen on the Pt surface has been studied by several authors[100-104]. In addition, the hydrogen is dissociatively adsorbed to give atoms of hydrogen attached at the metal surface[105][106][107] (e.g. Co and Ni metal surfaces). The role of Pt and spinel oxide surface interaction will be discussed in Chapter 7.

CHAPTER 7

MECHANISTIC STUDIES FOR THE PROMOTIONAL EFFECT ON SPINEL OXIDES FOR HYDROGEN AND OXYGEN RECOMBINATION.

CHAPTER 7

7 MECHANISTIC STUDIES FOR THE PROMOTIONAL EFFECT ON SPINEL OXIDES FOR HYDROGEN AND OXYGEN RECOMBINATION.

7.1 Introduction.

Spinel oxides such as $NiCo_2O_4$ and Co_3O_4 are capable of catalysing H_2/O_2 recombination at relatively high temperatures and atmospheric pressure (Chapter 3). The mechanism for such reaction is to be investigated by chemical kinetics. Generally, the studies of chemical kinetics are related to the development of an understanding of reaction mechanisms.[108].

In certain metal oxides, the reaction between hydrogen and oxygen has been studied by a number of authors (section 2.3.2) . In many cases, the order with respect to oxygen is zero. For example, an overall order of zero has been postulated by Gray and Darby[109] with excess oxygen over nickel oxide and by Read[110] et al over neodymium sulphide. An order greater than zero but less than one in hydrogen has been observed by Bulgakov[27] et al over iron (III) oxide, and by Mamedov[25][26][28] et al with an excess of oxygen over iron (III) oxide, chromium (III) oxide, vanadium (V) oxide, copper (II) oxide, cobalt (II) oxide, cobalt (III) oxide, manganese (IV) oxide, titanium (IV) oxide and zine oxide. In addition, a first-order dependence has been reported by Bakumenko and Chashechnikova[24] over neodymium oxide, and Antoshin[111] et al observed a first-order dependence on the hydrogen pressure over doped lanthanum oxide.

7.2 Reaction Kinetics.

7.2.1 Order of Reaction.

A mathematical definition of the reaction order with respect to the concentration of one particular substance i, C_i, is

$$\text{Order with respect to reagent i} = \left(\frac{\partial \log \text{rate}}{\partial \log C_i} \right)_{C_j}$$

Where the reaction rate is evaluated under the conditions such that the concentration of the other substances, C_j , are constant[112].

7.2.1.1 Zero-order Reactions.

Generally the zero-order equation is $(C_o - C_t) = kt$,

Where C_o = initial concentration of reactant

C_t = concentration of reactant consumed at time t

K = rate constant

t = time

and the total change in concentration is directly proportional to the elapsed time[113].

7.2.1.2 First-order Reactions.

In a first-order reaction such as A $\longrightarrow$ products, the rate is proportional to the concentration of A[114][115]. Plotting $\ln \frac{a}{(a-x)}$ against t will give a straight line for a first-order reaction, where a is the initial concentration of A at zero time and (a-x) is the concentration of A at time t.

7.2.1.3 Second-order Reactions.

Consider a typical second-order reaction, e.g. A ⟶ Products, and if c is the concentration of A at any time, then the rate law is [116]

$$-\frac{dc}{dt} = kc^2$$

Integrating yields

$$\frac{1}{c} = kt + C$$

where the constant C is evaluated by assuming that at t = 0, c = a, so that

$$\frac{1}{c} - \frac{1}{a} = kt$$

where a = initial concentration of A at zero time

c = concentration of A at time t

k = rate constant

t = time

Thus, plotting the reciprocal of the concentration of A against t will give a straight line if the reaction is second-order.

7.2.2 Half-life.

The half-life ($T_{\frac{1}{2}}$) for a given reaction is normally determined according to the order of reaction. For examples, the half-life for a first-order reaction is independent of the initial concentration[114][116], e.g. $T_{\frac{1}{2}} = \frac{\ln 2}{k}$ and k is the rate constant. For a second-order reaction it is inversely proportional to the initial concentration.

7.2.3 Activation Energy.

In 1889, Arrhenius[117] suggested that a molecule would only react on collision if it had higher than the average energy, e.g. if it was activated, the necessary energy for reaction to occur being known as the activation energy. The Arrhenius equation for the dependence of the rate constant (k) on the absolute temperature (T) is as follows :

$$k = A \exp - \frac{E_a}{RT}$$

where E_a = activation energy.

A = preexponential factor.

R = gas constant.

Generally, if the Arrhenius equation is operative, rate constants obtained at several different temperatures are sufficient to determine E_a and A by plotting ln k against $\frac{1}{T}$[118]. A straight line indicates that the Arrhenius relationship is applicable to the reaction investigated. Then from the slope the E_a and from the intercept the preexponential factor may be obtained.

7.3 Specific Platinum Activity.

The extent of support participation in the H_2/O_2 interation can be determined by examining the relationship between catalytic activity and Pt loading, the support loading being held constant. Thus, assuming the rate of H_2/O_2 combination/recombination at a given temperature originates from the Pt ; the Pt activity, j(P) , can be expressed as follows :

$$j(P) = \frac{\text{rate of } H_2/O_2 \text{ recombination (R)}}{\text{Pt loading in mg per 300 mg oxide}}$$

According to Hobbs and Tseung[8] that j(P) should remain independent of variations in the Pt loading. In this case, j(P) represents the true Pt activity. However, if the support also contributes to the rate of reaction, j(P) will apparently increase as the Pt loading decreases.

7.4 Experimental.

7.4.1 Kinetic Studies.

Using the kinetic method, the rates, orders and activation energies of the oxidation of hydrogen on spinel oxides (e.g. $NiCo_2O_4$ and Co_3O_4) were determined in a constant circulation-flow apparatus (Fig. 19) with a flow rate of about 38 cc min^{-1}, under conditions of a large excess of oxygen[25-28] at atmospheric pressure. Reduction and oxidation of the catalysts by the components of the gas mixture were studied in an inert gas (N_2). Special experiments revealed that the nature of the diluent gas (N_2) or glass powder has no effect on reduction or reoxidation. A small amount (2-3g) of drying agent such as silica gel was placed next to the catalyst bed (Fig. 19) to ensure the catalyst was absolutely dry.

The reaction product (water vapour) was condensed in a trap. Reduction and oxidation of the spinel oxides were monitored from the pressure drop in the system consisting of a reactor, heated by an electrothermal tape coupled to a Variac and an electromagnetic circulation pump. A differential manometer[28] filled with dibutyl phthalate (DBP) was used to determine the amount of H_2/O_2 recombination as a function of time. The DBP and Hg manometers were pre-calibrated,

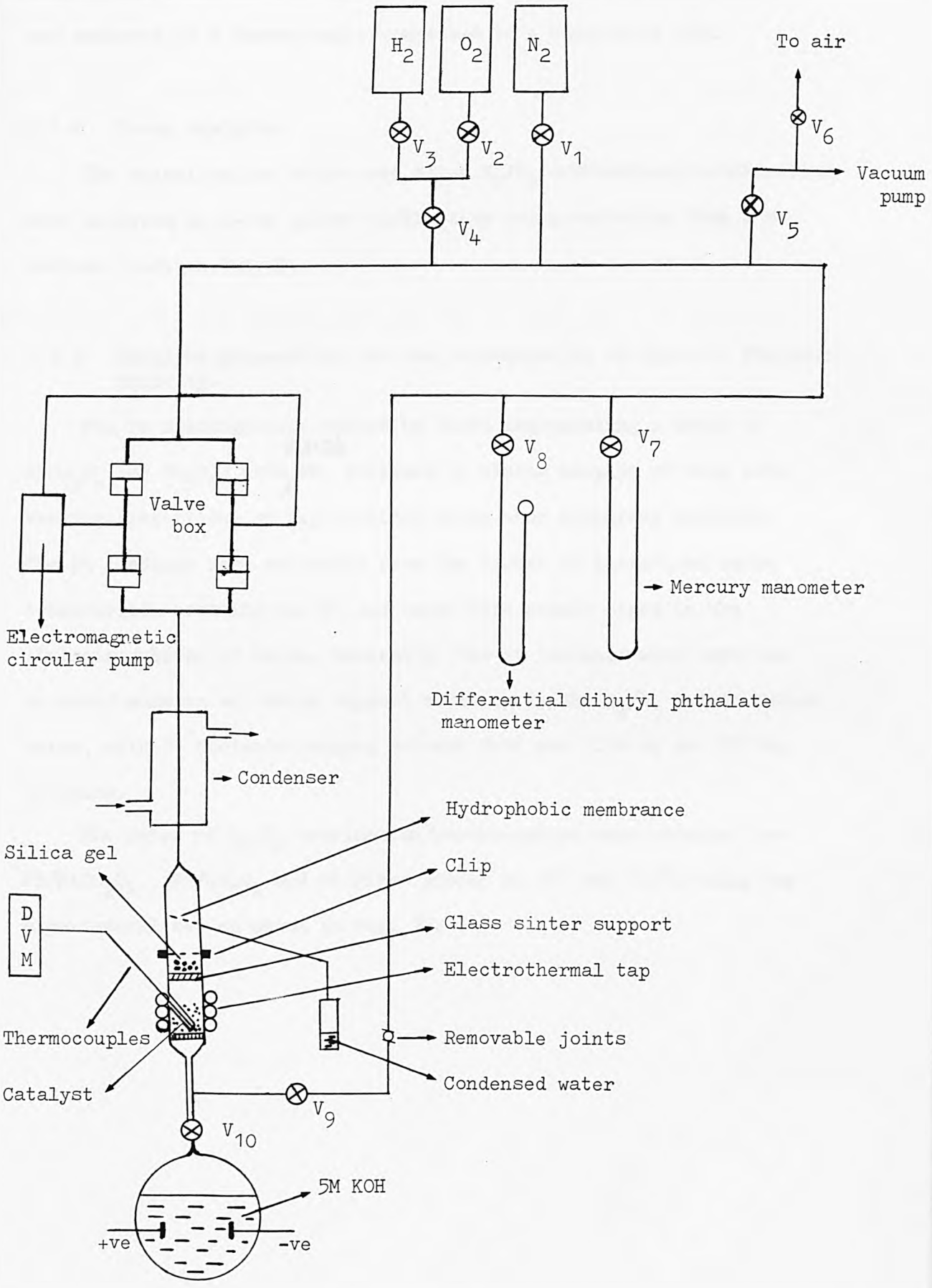

Fig. 19 Scheme of circulation apparatus.

with 10 mm DBP equivalent to 0.42 cc. The catalyst bed temperature was measured by a thermocouple connected to a calibrated DVM.

7.4.2 X-ray Analysis.

The spinel oxides before and after H_2/O_2 combination/recombination were analysed by X-ray powder diffraction using radiation from a Mo cathode (section 4.5.1).

7.4.3 Catalyst Preparation for the Determination of Specific Platinum Activity.

The Pt loadings were varied by first impregnating a batch of $NiCo_2O_4$ (or Co_3O_4) with H_2PtCl_6, followed by mixing samples of this with varying proportions of unplatinized oxide when preparing catalyst. The Pt loadings were estimated from the amount of platinized oxide transferred, assuming the Pt and oxide were evenly mixed in the platinized batch of oxide. Generally, the Pt loadings were kept low to avoid masking any oxide support activity in the H_2/O_2 recombination rates, with Pt contents ranging between 0.04 and 0.14 mg per 300 mg of oxide.

The rates of H_2/O_2 combination/recombination were obtained for $Pt/NiCo_2O_4$, Pt/Co_3O_4 and Pt/glass powder at 25° and 100°C using the experimental set-up shown in Fig. 19.

$P^{o}H_2$ (mm DBP)	log $P^{o}H_2$	Rate ($\times 10^{-2}$ cc s^{-1})	log Rate
467	2.6693	1.60 ± 0.02	- 1.7958 ± 0.0053
600	2.7782	2.00 ± 0.03	- 1.6990 ± 0.0065
734	2.8657	2.63 ± 0.03	- 1.5800 ± 0.0049
867	2.9380	3.28 ± 0.03	- 1.4841 ± 0.0039

TABLE 22 log $P^{o}H_2$ and log rate for hydrogen in H_2/O_2 recombination at 418 K , $P^{o}O_2$ = 200 mm Hg, and 0.3g $NiCo_2O_4$ catalyst

T (K)	$\frac{1}{T}$ ($\times 10^{-3}$ K^{-1})	k ($\times 10^{-3}$ S^{-1})	log k
349	2.8653	0.777 ± 0.004	- 3.1096 ± 0.0023
355	2.8169	1.116 ± 0.001	- 2.9523 ± 0.0003
357	2.8011	1.318 ± 0.002	- 2.8801 ± 0.0007
360	2.7777	1.454 ± 0.001	- 2.8374 ± 0.0003

TABLE 23 log k at various temperatures for catalytic oxidation of hydrogen using 0.3g $NiCo_2O_4$ catalyst

$P^{o}H_2$ = 467 mm DBP

$P^{o}O_2$ = 200 mm Hg

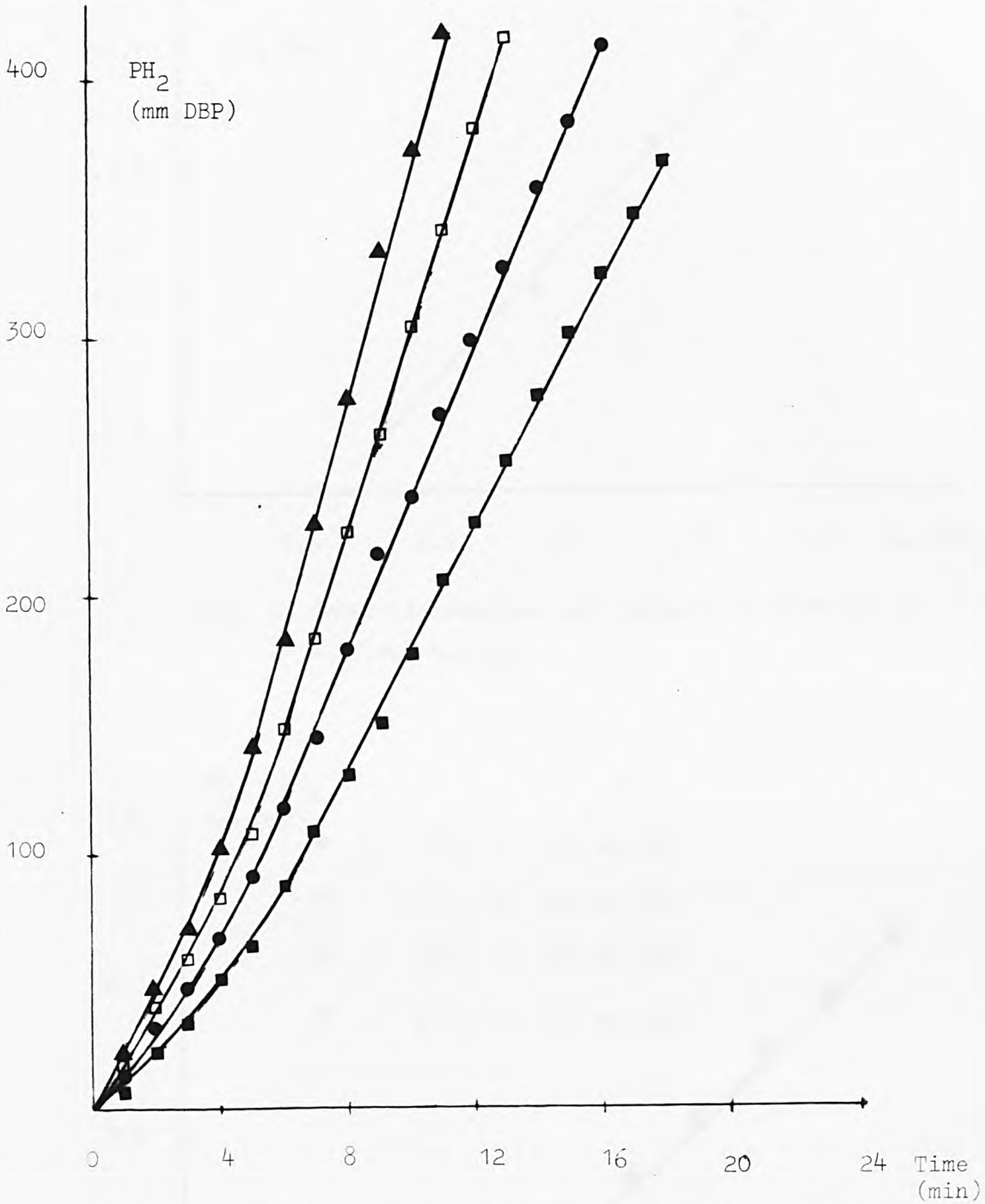

Fig. 20 Rates of reaction for hydrogen in H_2/O_2 recombination at 418K using $NiCo_2O_4$ (0.3g), P^oO_2 = 200 mm Hg.

- ■ 467 mm DBP P^oH_2
- ● 600 mm DBP P^oH_2
- □ 734 mm DBP P^oH_2
- ▲ 867 mm DBP P^oH_2

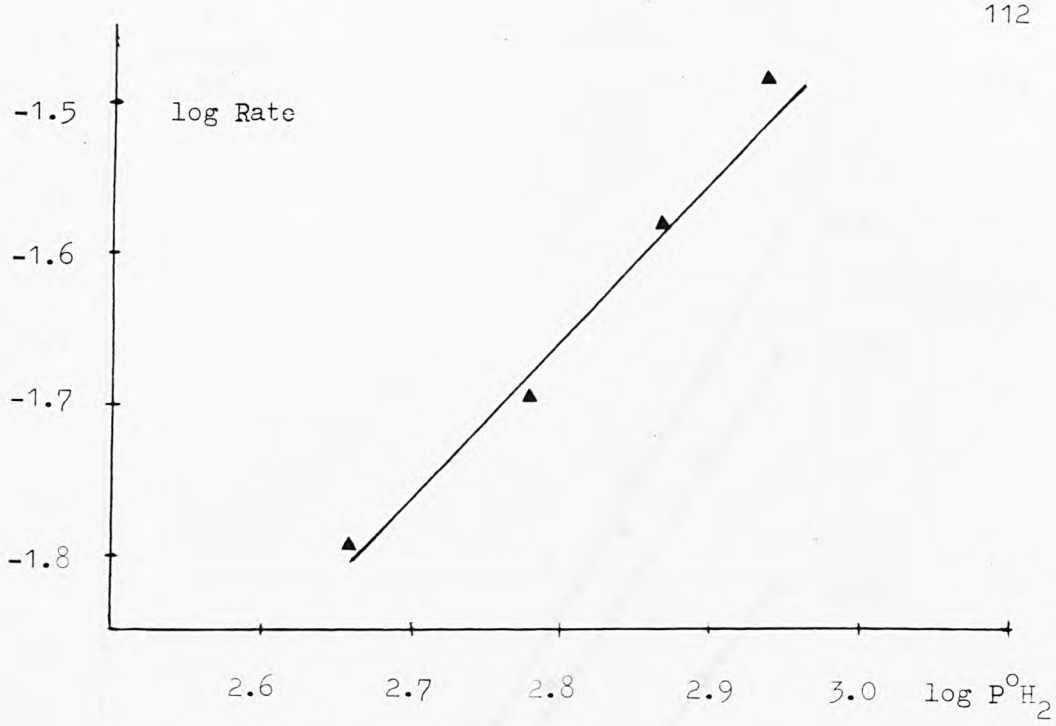

Fig. 21 Order of reaction with respect to hydrogen at 418K for $NiCo_2O_4$.

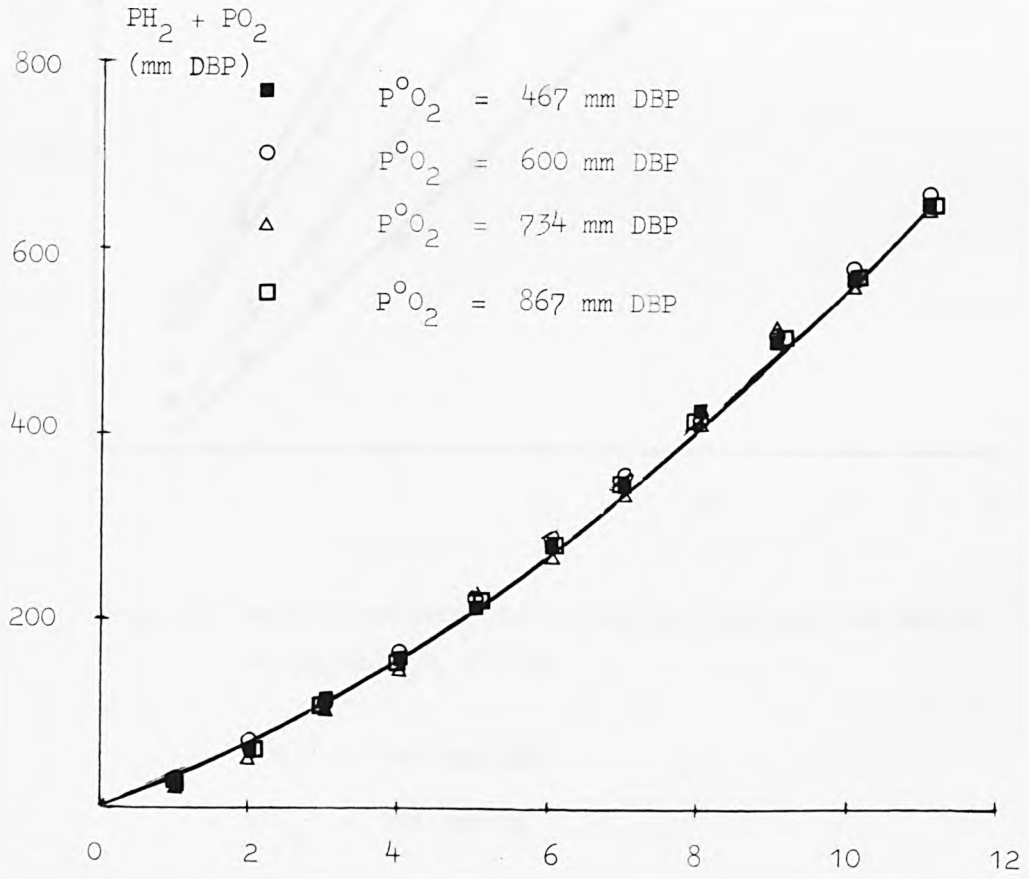

Fig. 22 Rates of H_2/O_2 recombination for $NiCo_2O_4$ at 418K, $P^{\circ}H_2$ = 130 mm Hg.

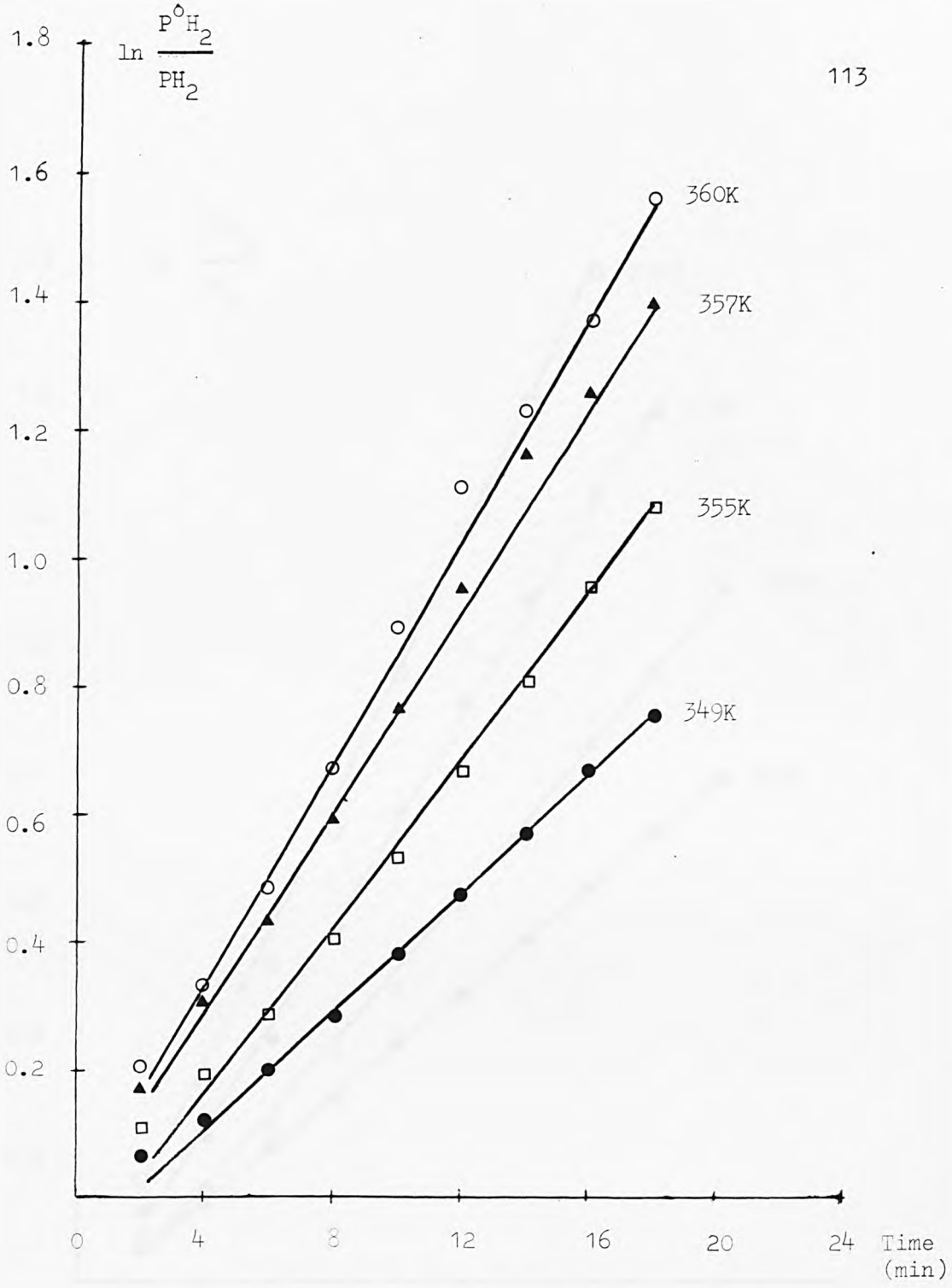

Fig. 23 Rate constants for catalytic hydrogen oxidation using $NiCo_2O_4$ (0.3g)

$P^{\circ}H_2$ = 467 mm DBP

$P^{\circ}O_2$ = 200 mm Hg

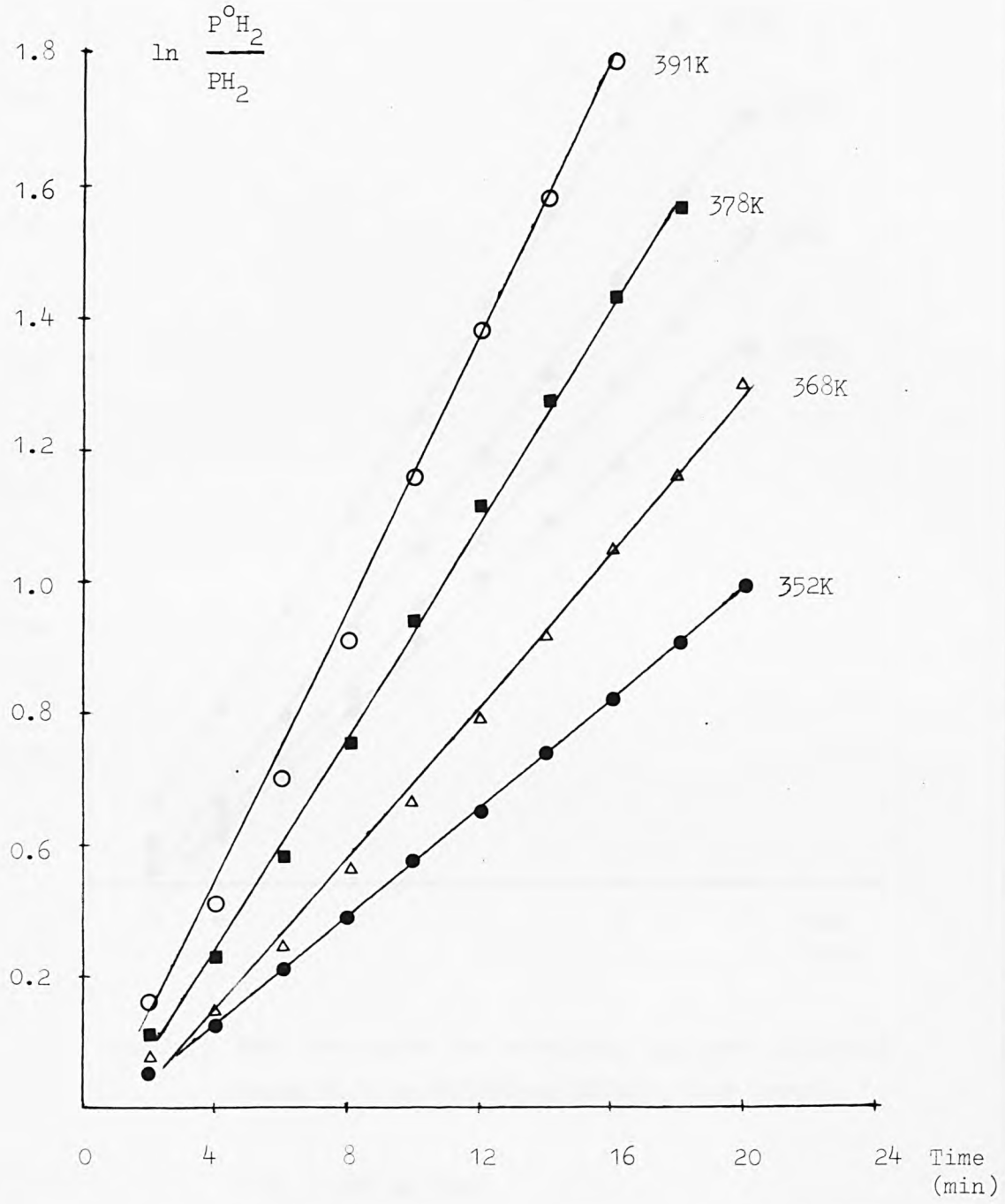

Fig. 24 Rate constants for catalytic hydrogen oxidation using 0.08 mg Pt/300 mg $NiCo_2O_4$ (high temp).

$P^{o}H_2$ = 467 mm DBP

$P^{o}O_2$ = 200 mm Hg

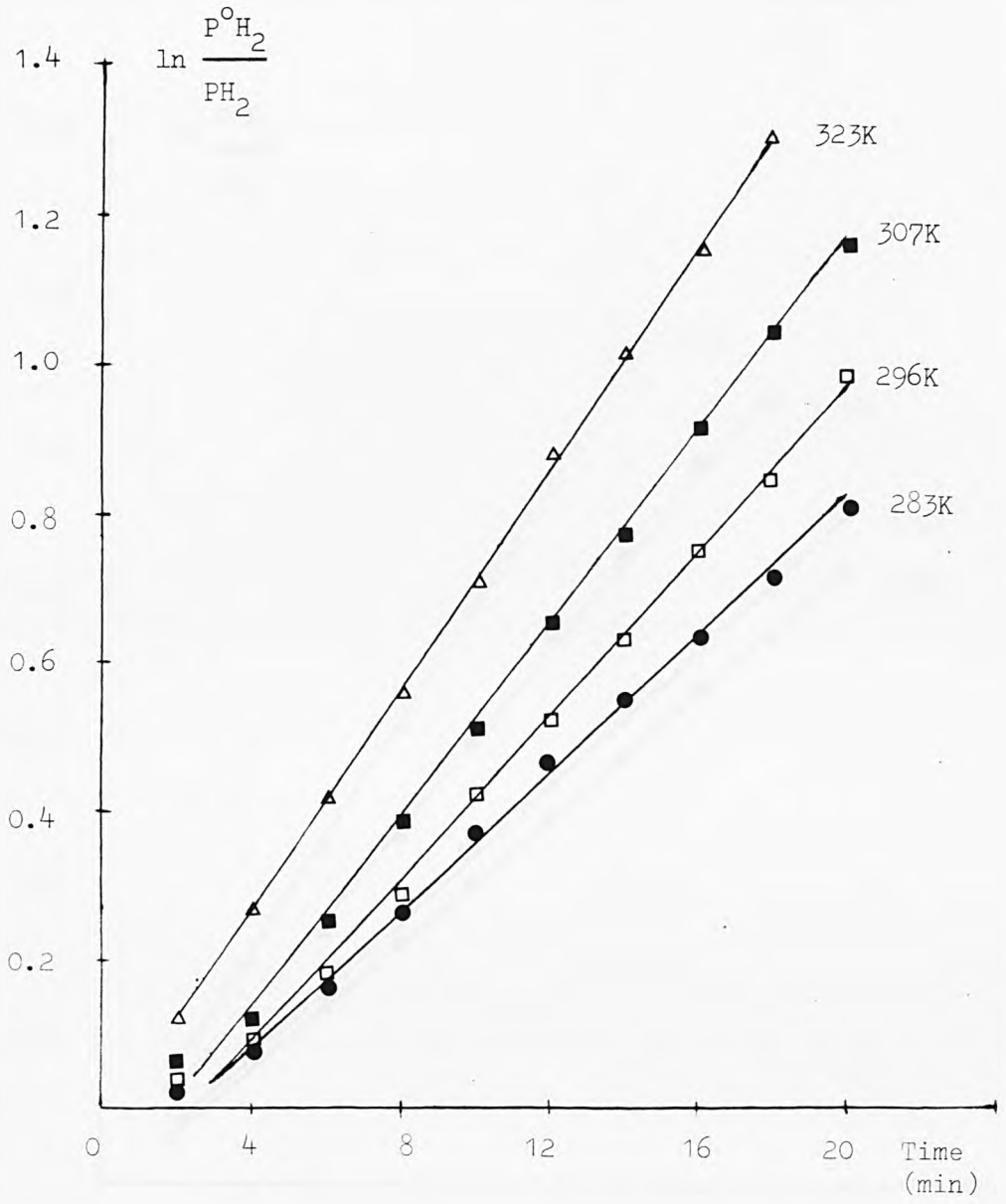

Fig. 25 Rate constants for catalytic hydrogen oxidation using 0.12 mg Pt/300 mg $NiCo_2O_4$ (low temp).

$P^{o}H_2$ = 467 mm DBP

$P^{o}O_2$ = 200 mm Hg

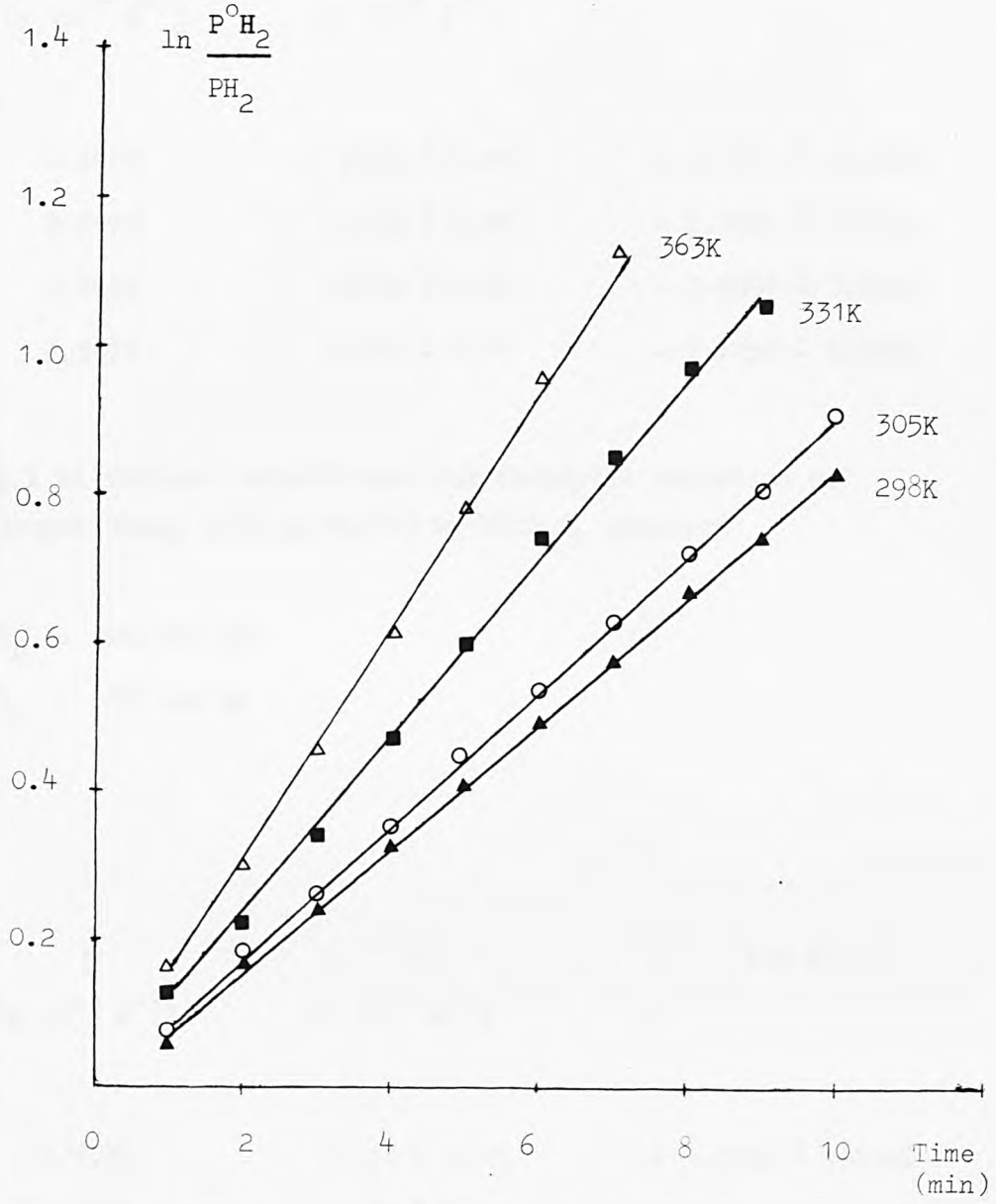

Fig. 26 Rate constants for hydrogen oxidation using Pt catalyst.

$P^{\circ}H_2$ = 467 mm DBP

$P^{\circ}O_2$ = 200 mm Hg

T (K)	$\frac{1}{T}$ ($\times 10^{-3}$ K^{-1})	k ($\times 10^{-3}$ s^{-1})	log k
352	2.8409	6.90 ± 0.01	- 3.1611 ± 0.0006
368	2.7173	10.30 ± 0.01	- 2.9872 ± 0.0005
378	2.6455	13.50 ± 0.01	- 2.8697 ± 0.0004
391	2.5575	18.80 ± 0.01	- 2.7258 ± 0.0002

TABLE 24 log k at various temperatures for catalytic oxidation of hydrogen using 0.08 mg Pt/300 mg $NiCo_2O_4$ catalyst

P^oH_2 = 467 mm DBP

P^oO_2 = 200 mm Hg

T (K)	$\frac{1}{T}$ ($\times 10^{-3}$ K^{-1})	k ($\times 10^{-3}$ s^{-1})	log k
283	3.5335	7.53 ± 0.01	- 3.1232 ± 0.0006
296	3.3783	9.15 ± 0.01	- 2.9108 ± 0.0004
307	3.2573	10.60 ± 0.01	- 2.9746 ± 0.0003
323	3.0959	12.28 ± 0.02	- 2.9108 ± 0.0007

TABLE 25 log k at various temperatures for catalytic oxidation of hydrogen using 0.12 mg Pt/300 mg $NiCo_2O_4$ catalyst

P^oH_2 = 467 mm DBP

P^oO_2 = 200 mm Hg

T (K)	$\frac{1}{T}$ ($\times 10^{-3}$ K^{-1})	k ($\times 10^{-3}$ s^{-1})	log k
298	3.3557	1.395 ± 0.003	- 2.8554 ± 0.0009
305	3.2786	1.486 ± 0.003	- 2.8280 ± 0.0009
331	3.0211	2.011 ± 0.002	- 2.6965 ± 0.0003
363	2.7548	2.642 ± 0.004	- 2.5780 ± 0.0006

TABLE 26 log k at various temperatures for catalytic oxidation of hydrogen using 1.8 mg Pt catalyst

$P^{o}H_2$ = 467 mm DBP

$P^{o}O_2$ = 200 mm Hg

Catalyst	Temp. range (K)	Pt loading (mg)	$NiCo_2O_4$ (mg)	Activation energy (K cal. mol^{-1})
Pt/glass powder	298 - 363	1.8	-	2.18 ± 0.05
$Pt/NiCo_2O_4$	283 - 323	0.12	300	2.11 ± 0.15
$Pt/NiCo_2O_4$	352 - 391	0.08	300	6.69 ± 0.12
$NiCo_2O_4$	349 - 360	-	300	14.38 ± 0.10

TABLE 27 Activation energies for the catalytic oxidation of hydrogen

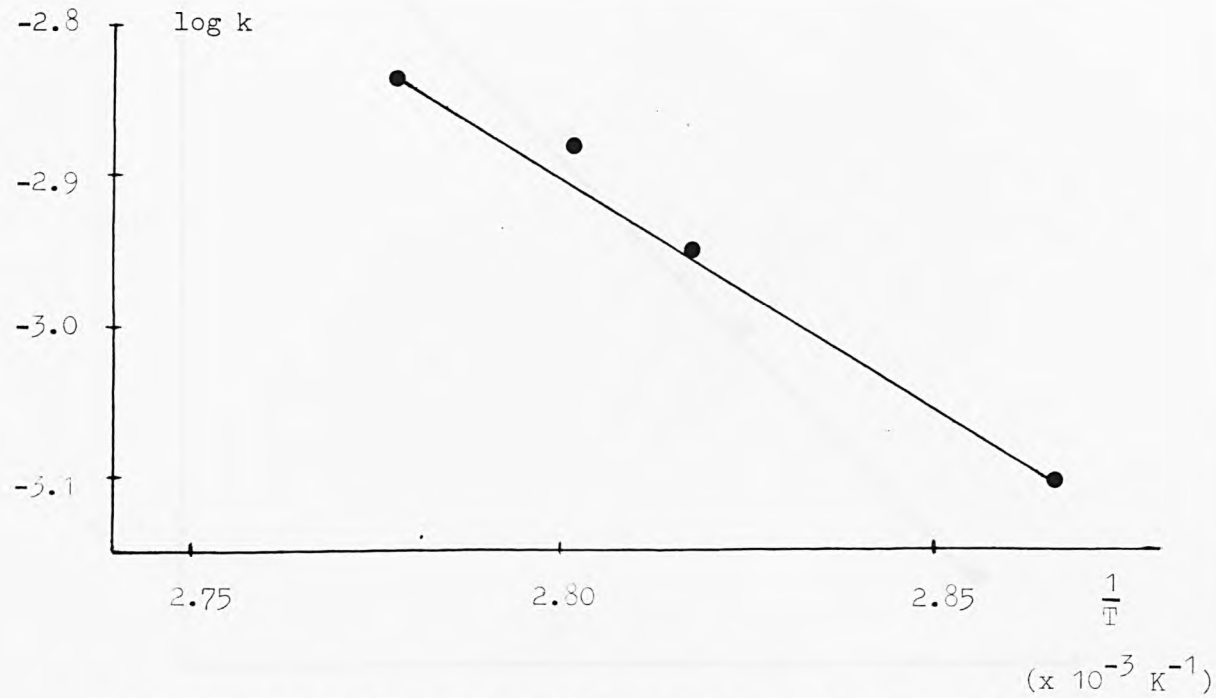

Fig. 27 Activation energy for catalytic oxidation of hydrogen using $NiCo_2O_4$.

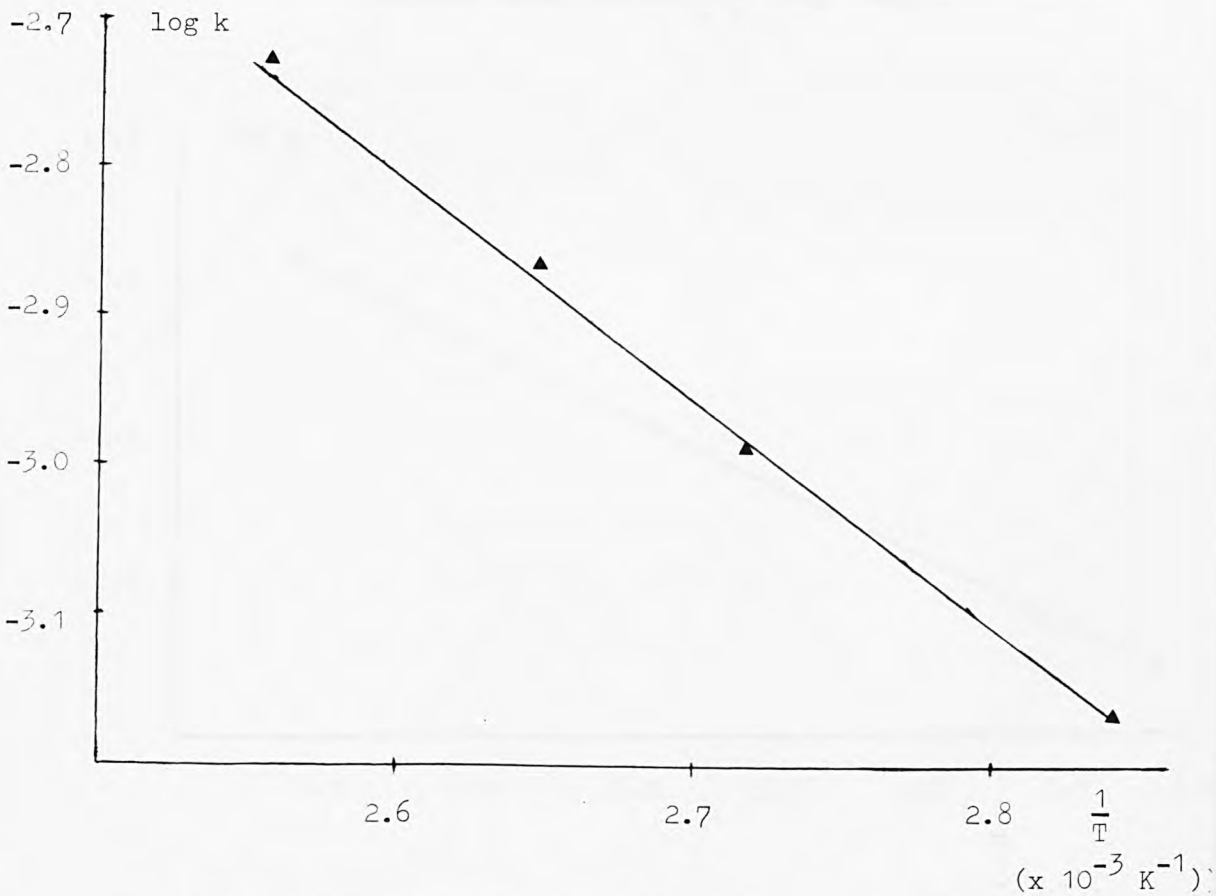

Fig. 28 Activation energy for catalytic oxidation of hydrogen using $Pt/NiCo_2O_4$ (high temp).

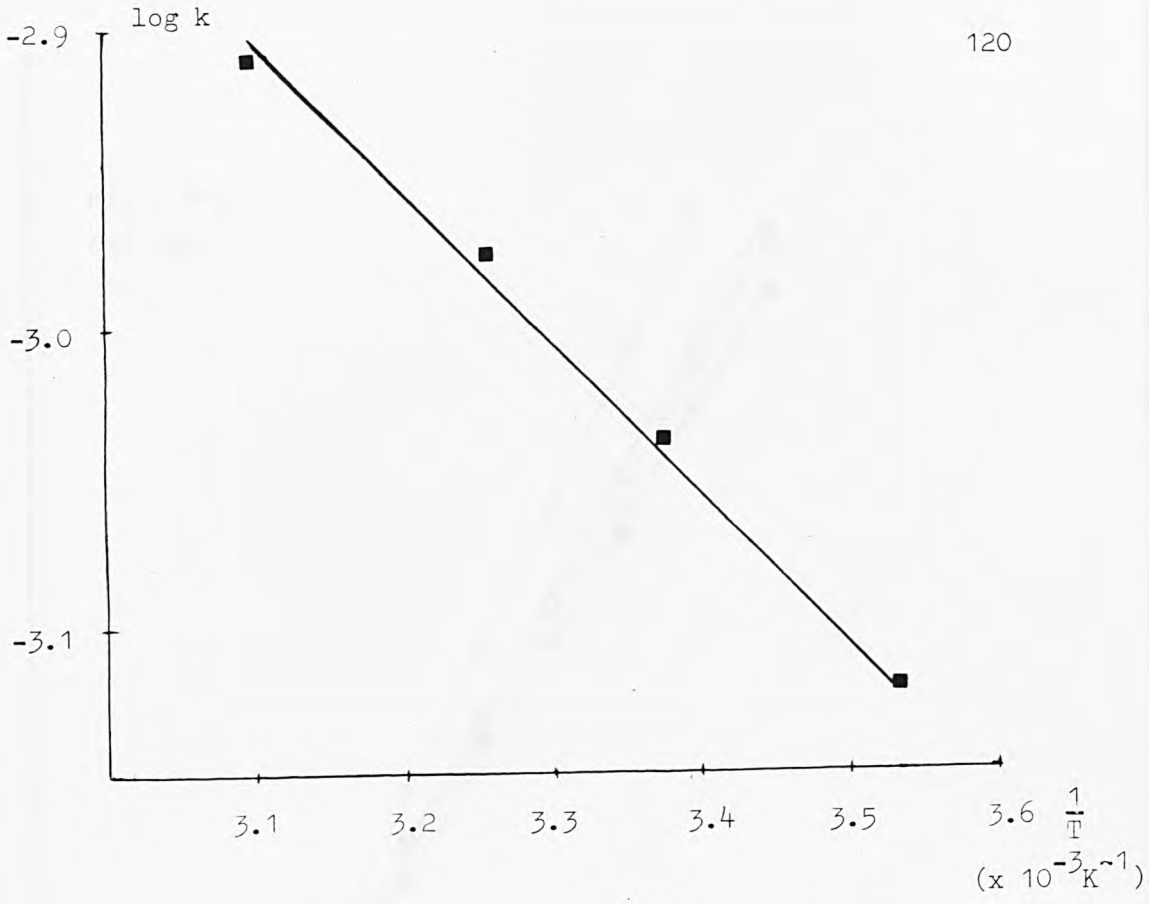

Fig. 29 Activation energy for catalytic oxidation of hydrogen using $Pt/NiCo_2O_4$ (high temp).

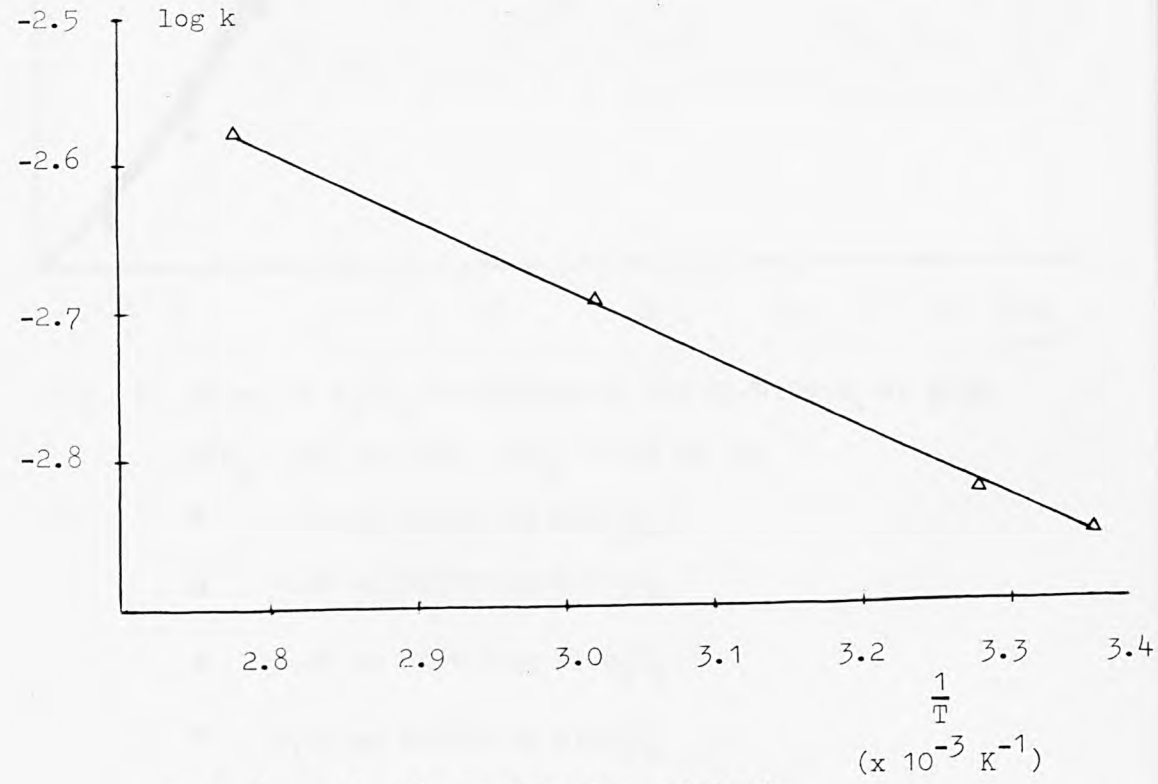

Fig. 30 Activation energy for catalytic oxidation of hydrogen using Pt.

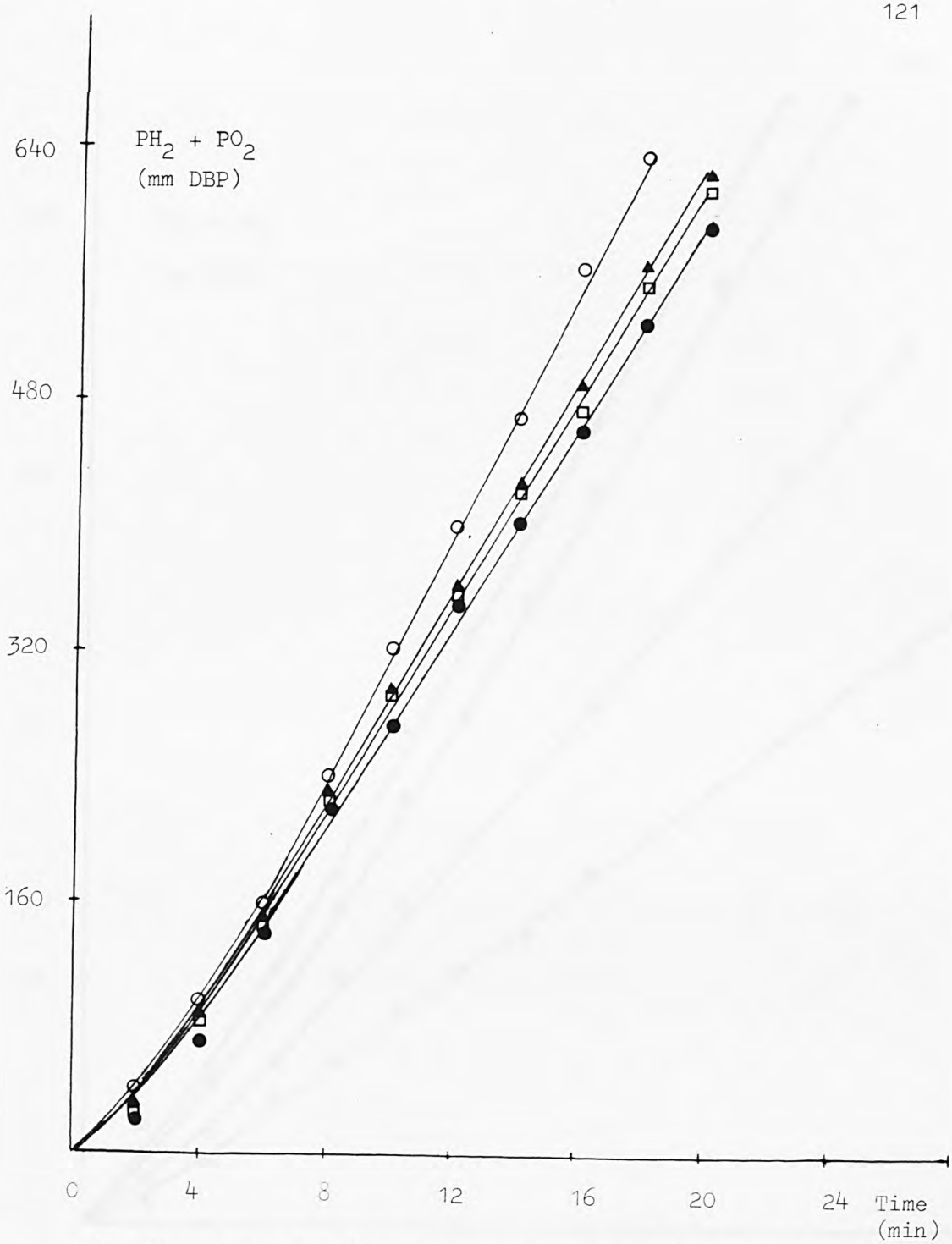

Fig. 31 Rates of H_2/O_2 recombination for $Pt/NiCo_2O_4$ at 373K, P^oH_2 = 467 mm DBP, P^oO_2 = 200 mm Hg.

- ● 0.04 mg Pt/300 mg $NiCo_2O_4$
- □ 0.06 mg Pt/300 mg $NiCo_2O_4$
- ▲ 0.08 mg Pt/300 mg $NiCo_2O_4$
- ○ 0.12 mg Pt/300 mg $NiCo_2O_4$

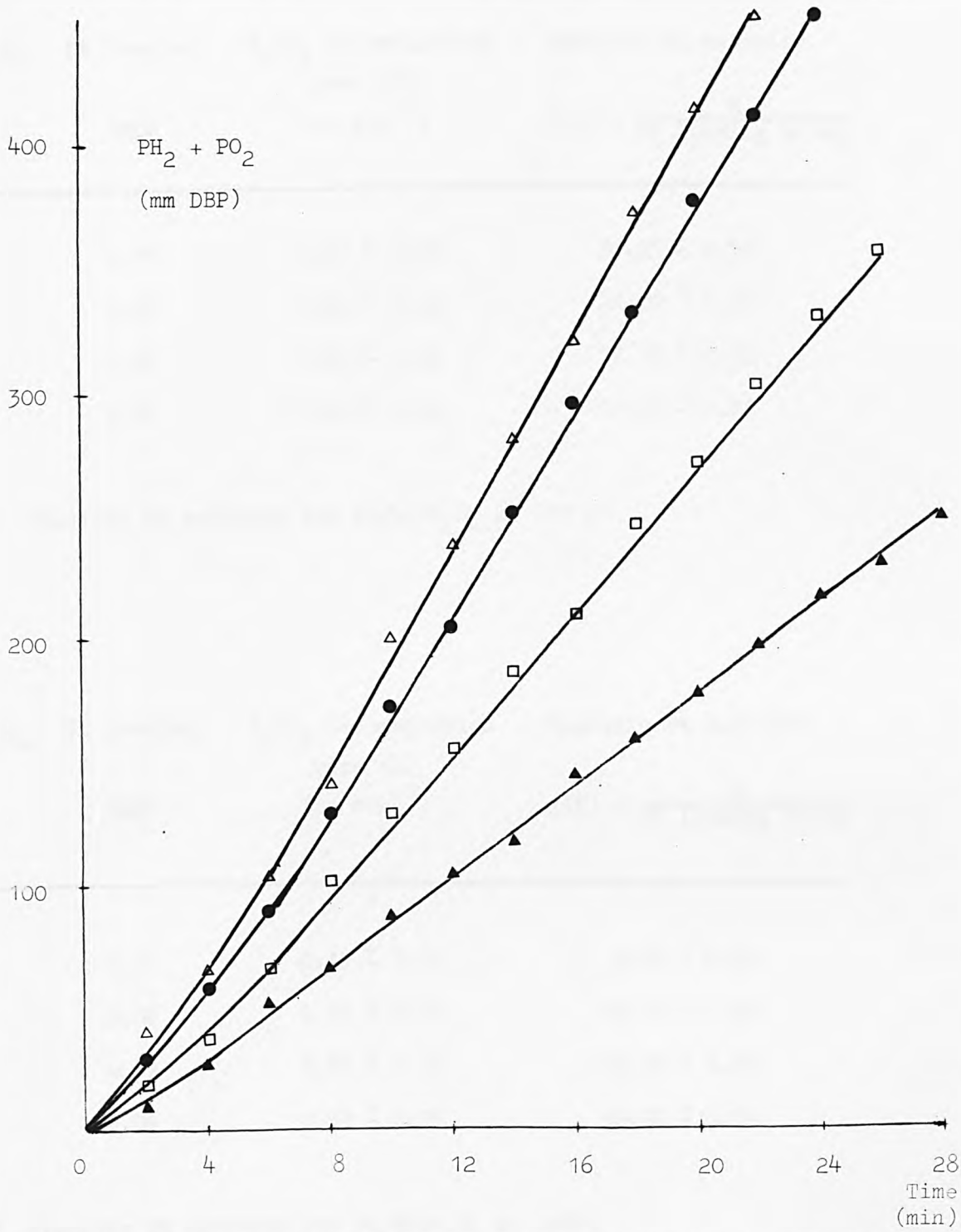

Fig. 32 Rates of H_2/O_2 recombination for $Pt/NiCo_2O_4$ at 298K, P^oH_2 = 467 mm DBP, P^oO_2 = 200 mm Hg.

▲ 0.04 mg Pt/300 mg $NiCo_2O_4$

□ 0.06 mg Pt/300 mg $NiCo_2O_4$

● 0.08 mg Pt/300 mg $NiCo_2O_4$

△ 0.12 mg Pt/300 mg $NiCo_2O_4$

$Pt/NiCo_2O_4$ (mg)	Pt loading (mg)	H_2/O_2 recombination rate (R) ($cc\ min^{-1}$)	Specific Pt activity $j(P) = \frac{R}{\text{Pt loading in mg}}$
300	0.04	1.27 ± 0.02	31.75 ± 0.50
300	0.06	1.32 ± 0.02	22.00 ± 0.33
300	0.08	1.37 ± 0.02	17.13 ± 0.25
300	0.14	1.66 ± 0.03	11.86 ± 0.21

TABLE 28 Specific Pt activity for $Pt/NiCo_2O_4$ at 373 K

$Pt/NiCo_2O_4$ (mg)	Pt loading (mg)	H_2/O_2 recombination rate (R) ($cc\ min^{-1}$)	Specific Pt activity $j(P) = \frac{R}{\text{Pt loading in mg}}$
300	0.04	0.39 ± 0.01	9.75 ± 0.25
300	0.06	0.61 ± 0.02	10.17 ± 0.33
300	0.07	0.84 ± 0.02	12.00 ± 0.29
300	0.09	0.92 ± 0.03	10.22 ± 0.34

TABLE 29 Specific Pt activity for $Pt/NiCo_2O_4$ at 298 K

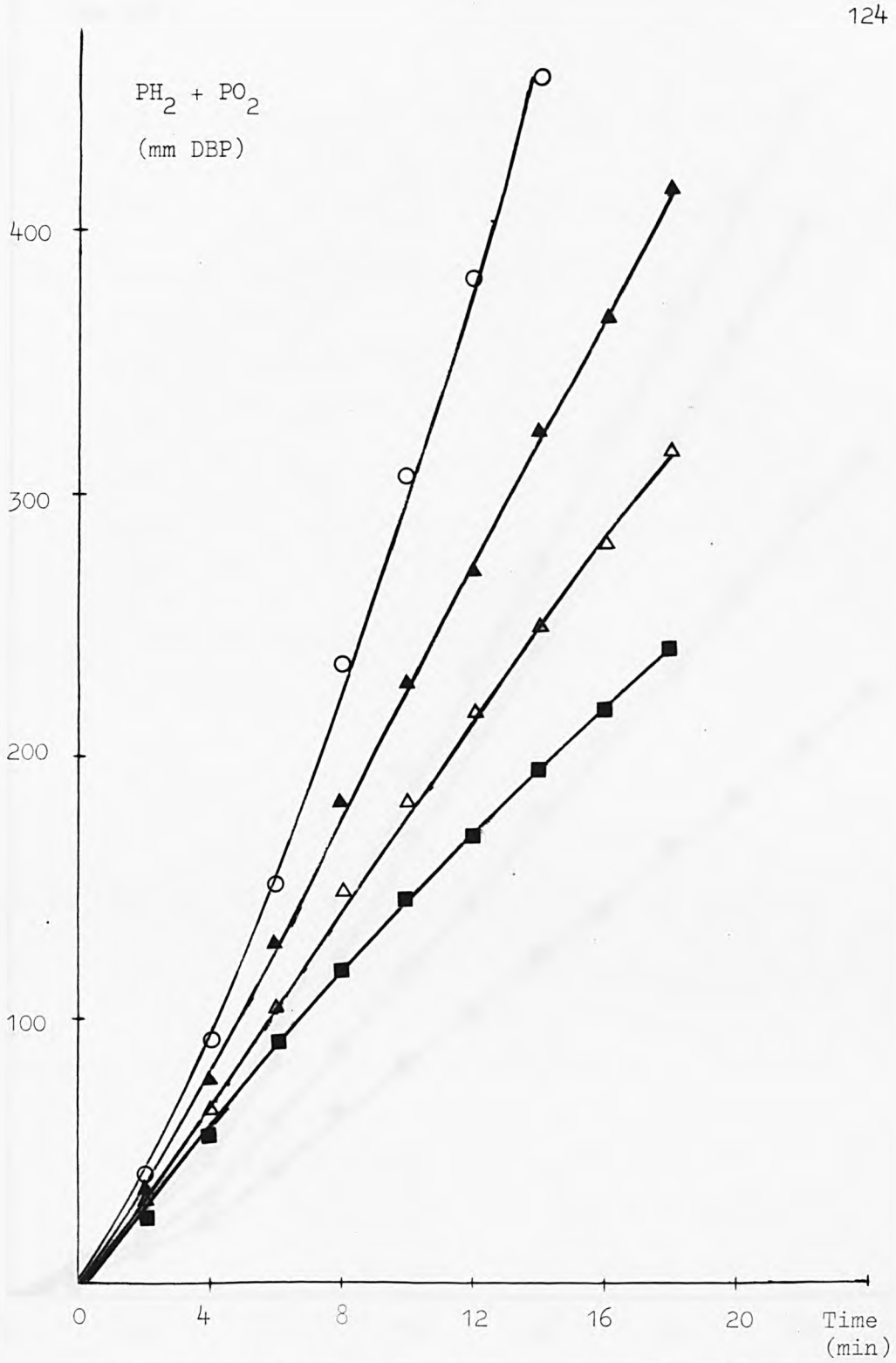

Fig. 33 Rates of H_2/O_2 recombination for Pt/glass powder at 373K, P^oH_2 = 467 mm DBP, P^oO_2 = 200 mm Hg.

■ 0.04 mg Pt/300 mg glass powder

△ 0.06 mg Pt/300 mg glass powder

▲ 0.08 mg Pt/300 mg glass powder

○ 0.12 mg Pt/300 mg glass powder

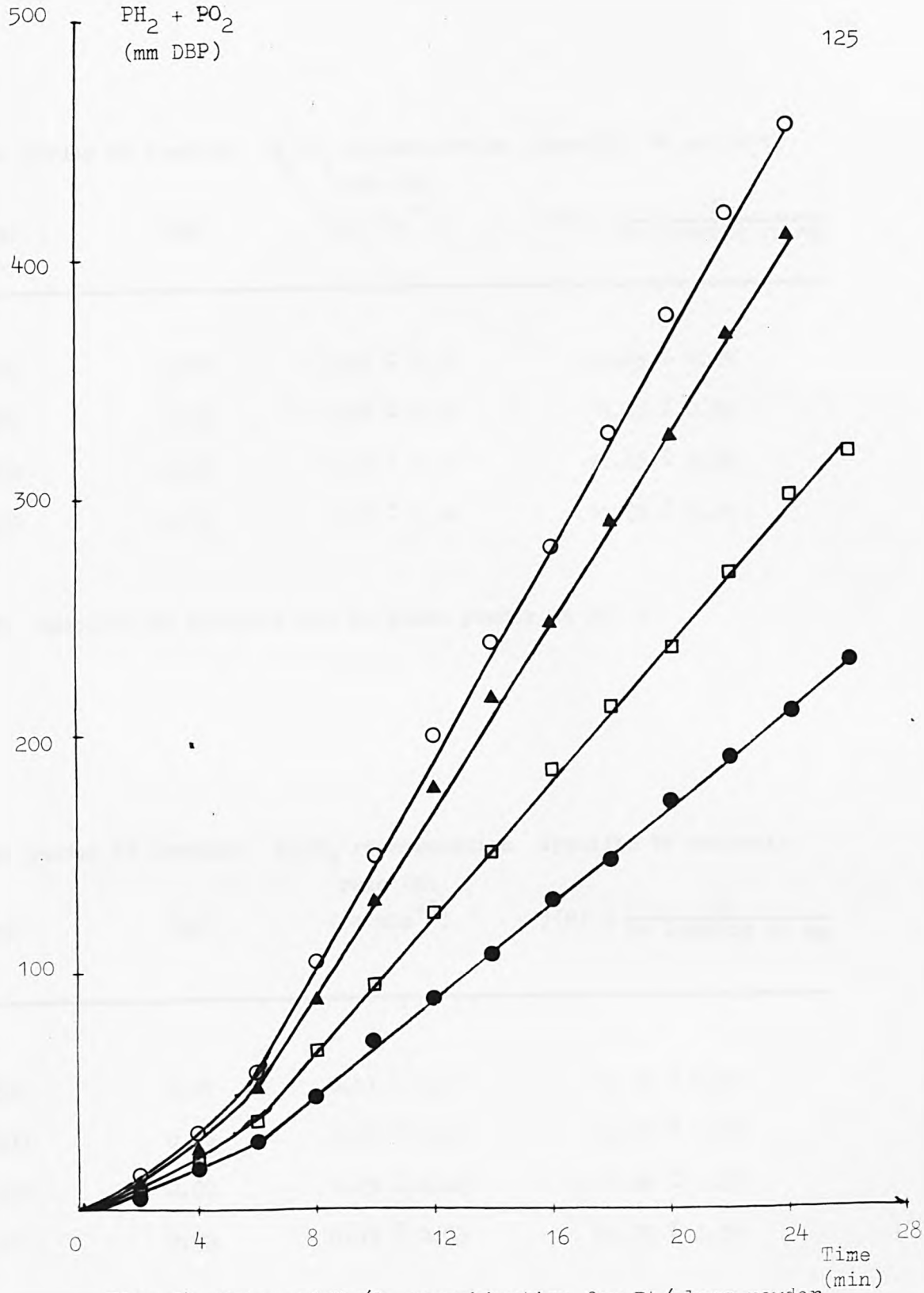

Fig. 34 Rates of H_2/O_2 recombination for Pt/glass powder at 298K, $P^{\circ}H_2$ = 467 mm DBP, $P^{\circ}O_2$ = 200 mm Hg.

- ● 0.04 mg Pt/300 mg glass powder
- □ 0.06 mg Pt/300 mg glass powder
- ▲ 0.08 mg Pt/300 mg glass powder
- ○ 0.12 mg Pt/300 mg glass powder

Pt/glass powder (mg)	Pt loading (mg)	H_2/O_2 recombination rate (R) ($cc\ min^{-1}$)	Specific Pt activity $j(P) = \frac{R}{\text{Pt loading in mg}}$
300	0.04	0.49 ± 0.01	12.25 ± 0.25
300	0.06	0.68 ± 0.03	11.33 ± 0.50
300	0.08	0.95 ± 0.03	11.88 ± 0.37
300	0.14	1.55 ± 0.04	11.07 ± 0.29

TABLE 30 Specific Pt activity for Pt/glass powder at 373 K

Pt/glass powder (mg)	Pt loading (mg)	H_2/O_2 recombination rate (R) ($cc\ min^{-1}$)	Specific Pt activity $j(P) = \frac{R}{\text{Pt loading in mg}}$
300	0.04	0.41 ± 0.01	10.25 ± 0.25
300	0.06	0.60 ± 0.02	10.00 ± 0.33
300	0.07	0.83 ± 0.02	11.86 ± 0.28
300	0.09	0.93 ± 0.03	10.33 ± 0.34

TABLE 31 Specific Pt activity for Pt/glass powder at 298 K

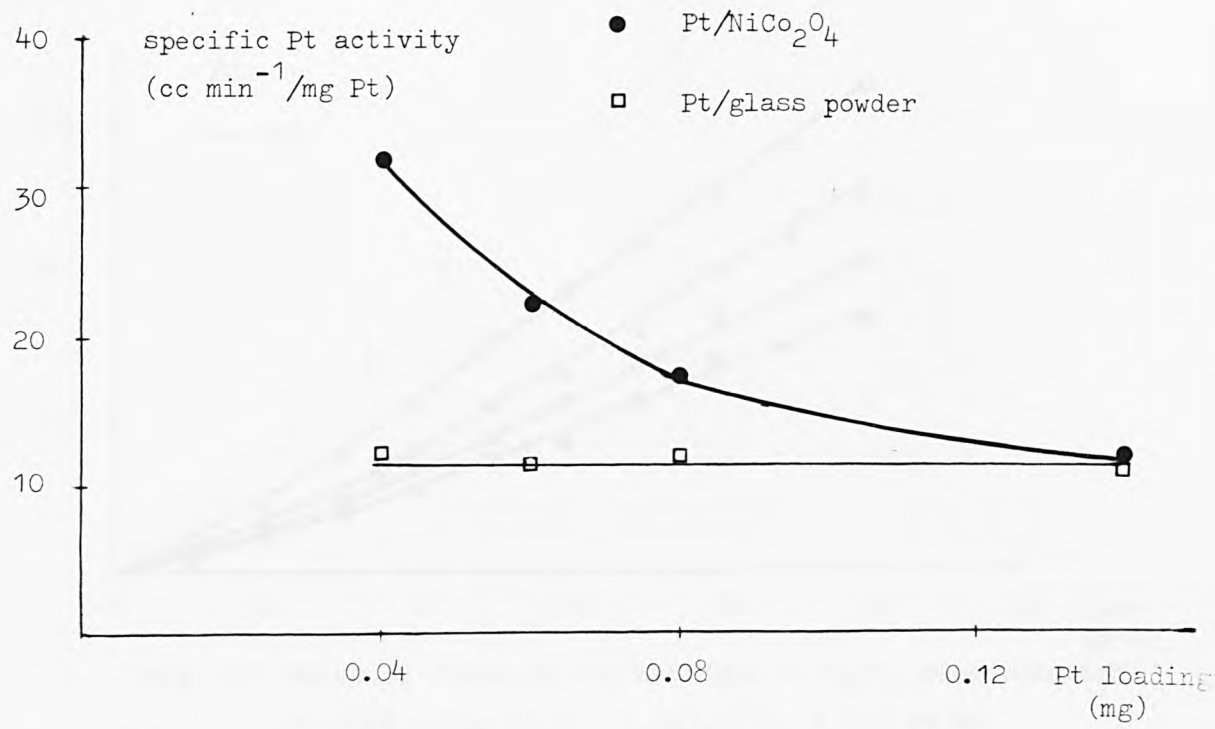

Fig. 35 Specific Pt activity Vs Pt loading at 373K.

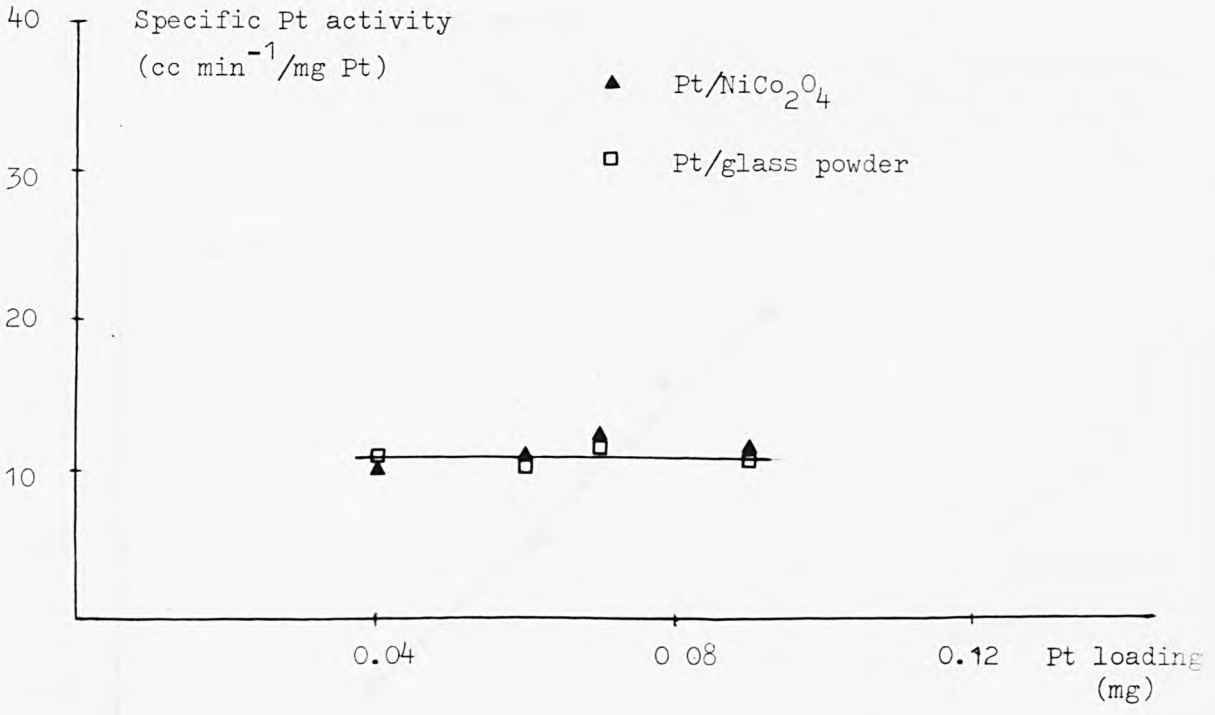

Fig. 36 Specific Pt activity Vs Pt loading at 298K.

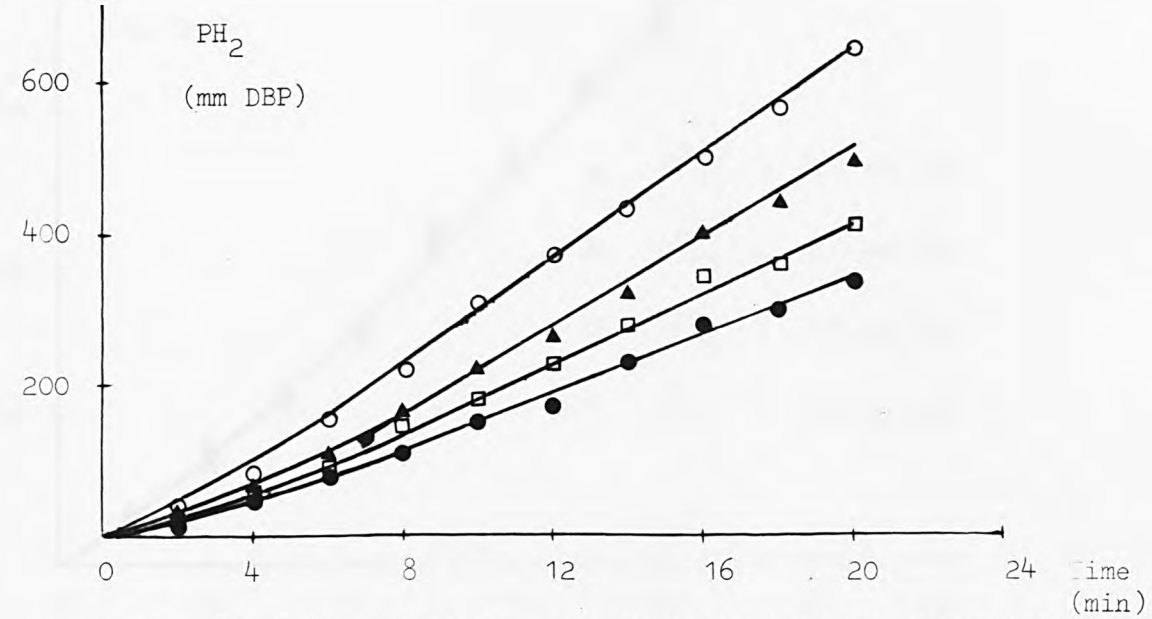

Fig. 37 Rates of reaction for hydrogen in H_2/O_2 recombination at 366K using Co_3O_4 (0.3g), P^oO_2 = 200 mm Hg.

- ● P^oH_2 = 467 mm DBP
- □ P^oH_2 = 600 mm DBP
- ▲ P^oH_2 = 734 mm DBP
- ○ P^oH_2 = 867 mm DBP

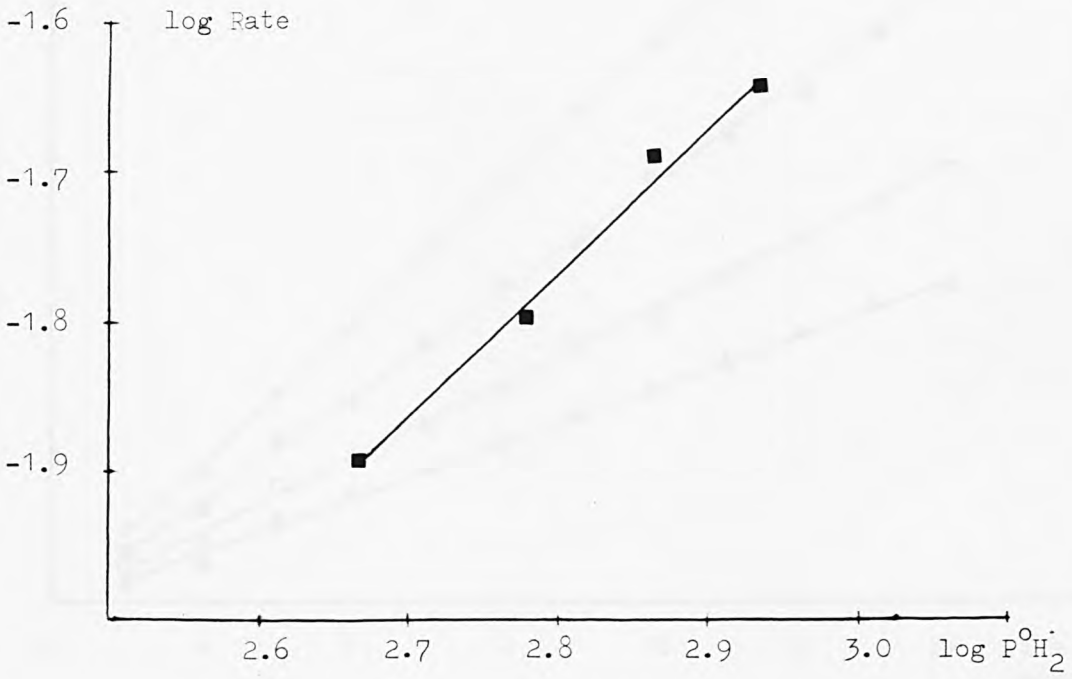

Fig. 38 Order of reaction with respect to hydrogen at 366K for Co_3O_4 .

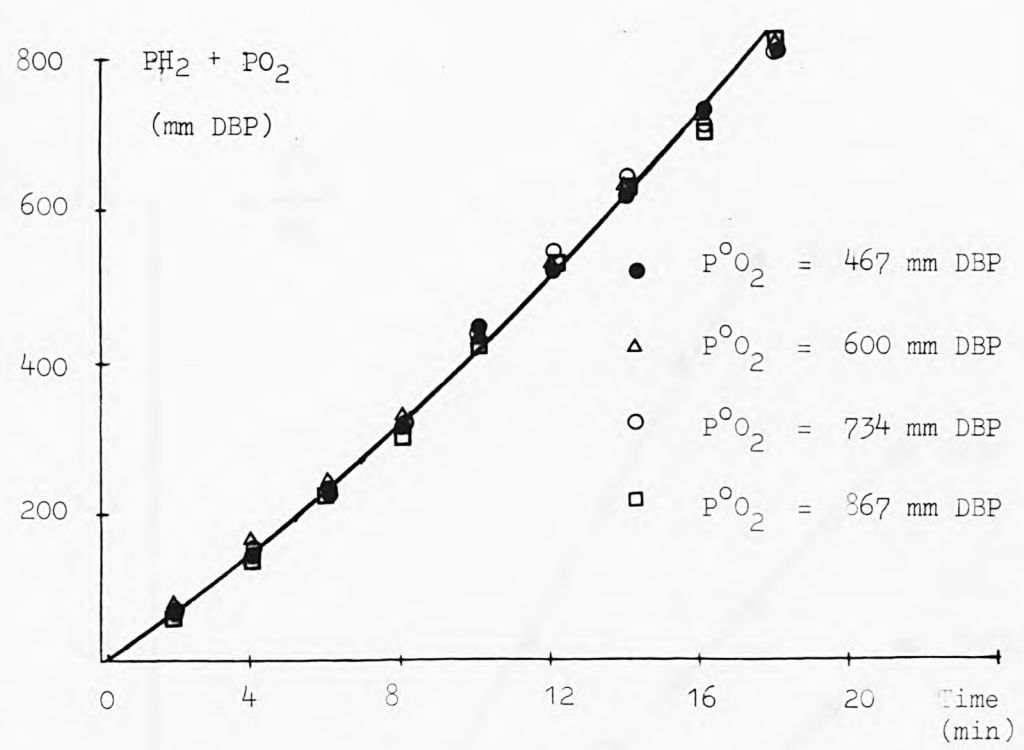

Fig. 39 Rates of H_2/O_2 recombination for Co_3O_4 at 366K, $P^{\circ}H_2$ = 130 mm Hg.

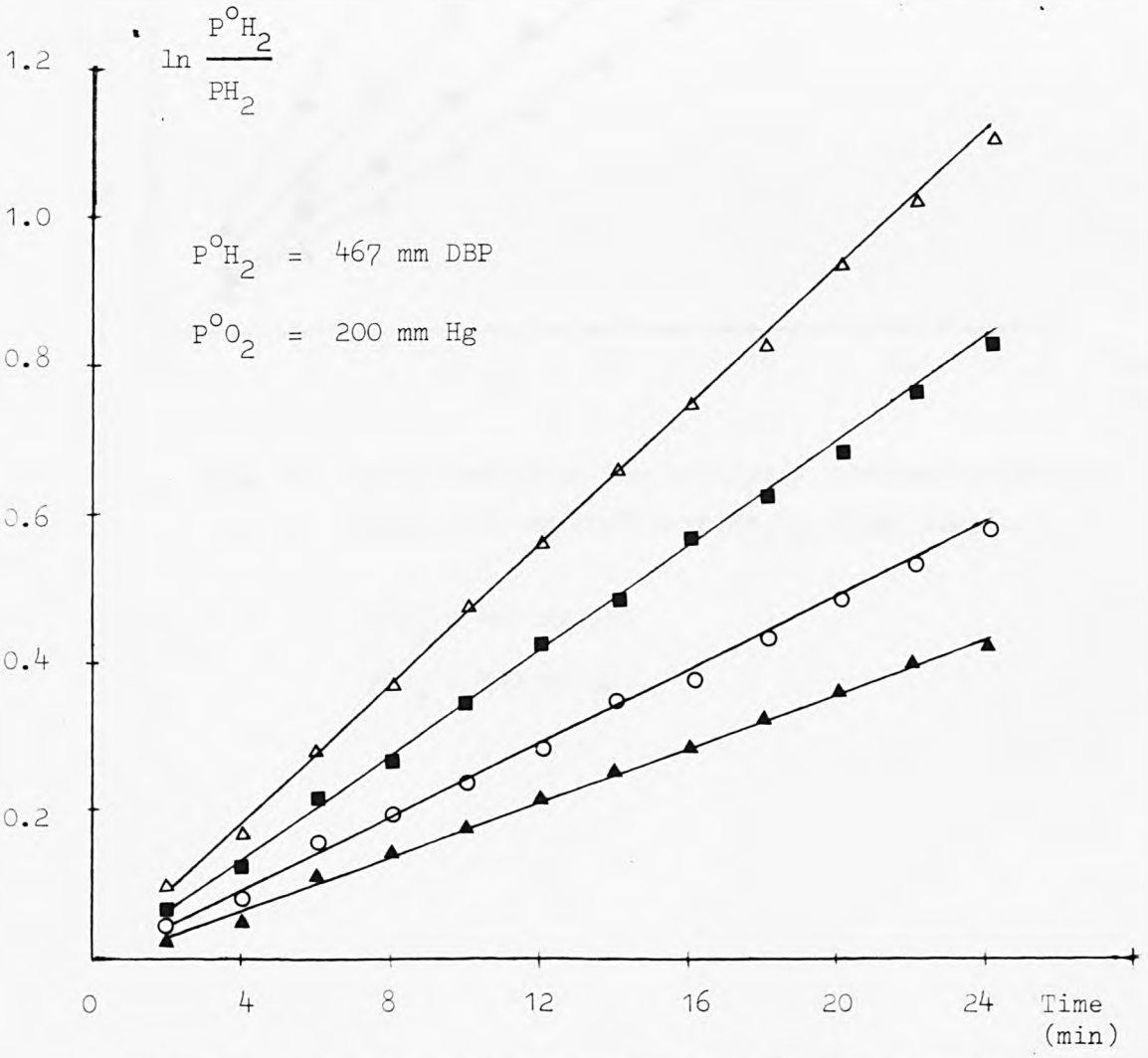

Fig. 40 Rates constants for catalytic hydrogen oxidation using Co_3O_4 .

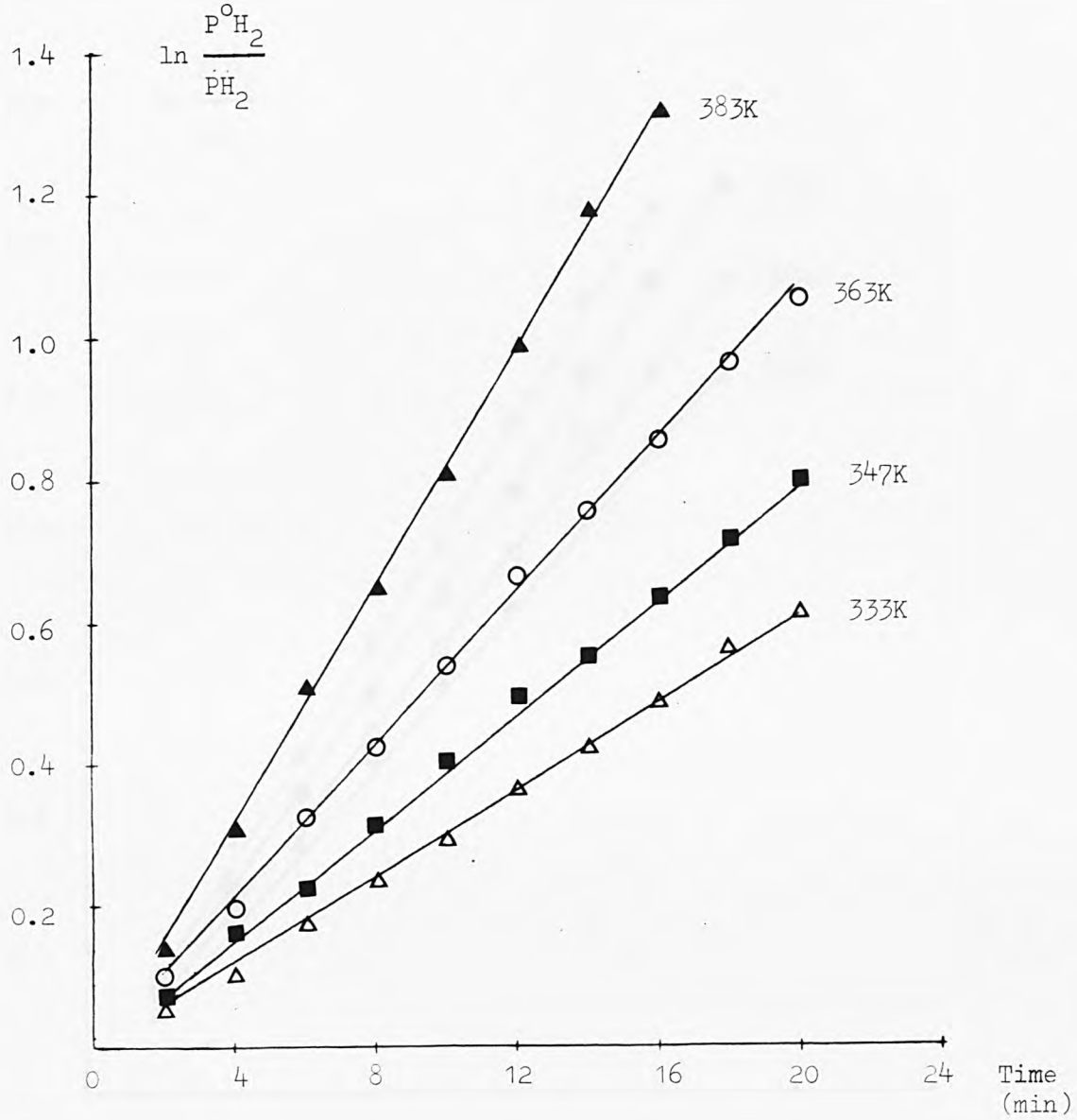

Fig. 41 Rates constants for catalytic hydrogen oxidation using 0.08 mg Pt/300 mg Co_3O_4 (high temp).

$P^{o}H_2$ = 467 mm DBP

$P^{o}O_2$ = 200 mm Hg

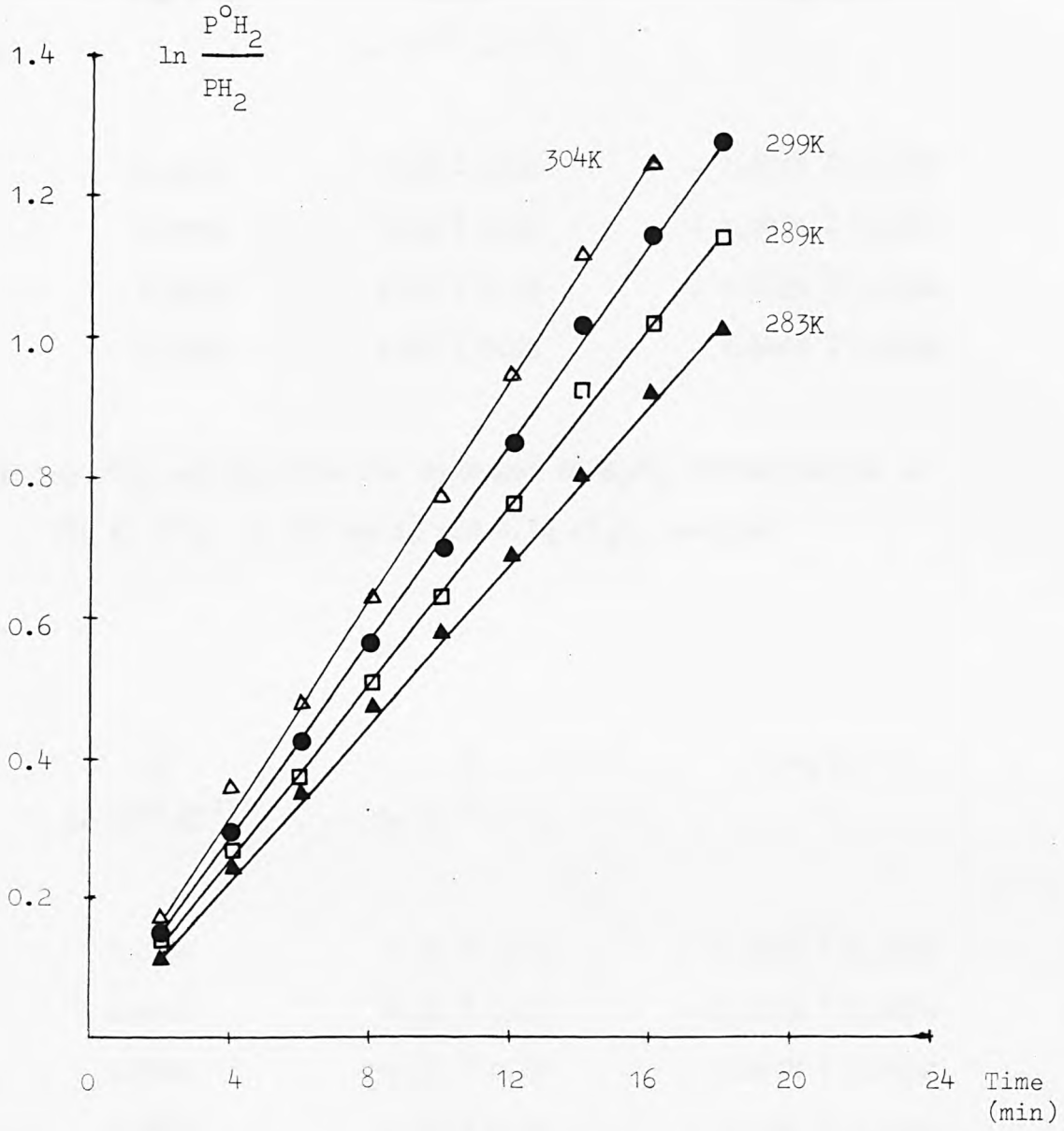

Fig. 42 Rate constants for catalytic hydrogen oxidation using 0.8 mg Pt/300 mg Co_3O_4 (low temp).

$P^{o}H_2$ = 467 mm DBP

$P^{o}O_2$ = 200 mm Hg

$P^{o}H_2$ (mm DBP)	log $P^{o}H_2$	Rate ($\times 10^{-2}$ cc s^{-1})	log Rate
467	2.6693	1.28 ± 0.02	- 1.8928 ± 0.0067
600	2.7782	1.59 ± 0.03	- 1.7986 ± 0.0081
734	2.8657	2.03 ± 0.03	- 1.6925 ± 0.0064
867	2.9380	2.28 ± 0.02	- 1.6421 ± 0.0038

TABLE 32 log $P^{o}H_2$ and log rate for hydrogen in H_2/O_2 recombination at 366 K, $P^{o}O_2$ = 200 mm Hg and 0.3g Co_3O_4 catalyst

T (K)	$\frac{1}{T}$ ($\times 10^{-3}$ K^{-1})	k ($\times 10^{-3}$ s^{-1})	log k
333	3.0030	3.00 ± 0.04	- 3.5229 ± 0.0057
339	2.9498	4.05 ± 0.07	- 3.3925 ± 0.0074
345	2.8985	5.73 ± 0.07	- 3.2418 ± 0.0052
352	2.8409	7.70 ± 0.06	- 3.1135 ± 0.0035

TABLE 33 log k at various temperatures for catalytic oxidation of hydrogen using Co_3O_4

$P^{o}H_2$ = 467 mm DBP

$P^{o}O_2$ = 200 mm Hg

T (K)	$\frac{1}{T}$ (x 10^{-3} K^{-1})	k (x 10^{-3} s^{-1})	log k
333	3.0030	4.98 ± 0.03	- 3.3028 ± 0.0026
347	2.8818	6.55 ± 0.09	- 3.1838 ± 0.0060
363	2.7548	8.78 ± 0.10	- 3.0565 ± 0.0049
383	2.6109	13.77 ± 0.14	- 2.8611 ± 0.0044

TABLE 34 log k at various temperatures for catalytic oxidation of hydrogen using 0.08 Pt/Co_3O_4

P^oH_2 = 467 mm DBP

P^oO_2 = 200 mm Hg

T (K)	$\frac{1}{T}$ (x 10^{-3} K^{-1})	k (x 10^{-3} s^{-1})	log k
283	3.5335	0.96 ± 0.02	- 3.0177 ± 0.0089
289	3.4602	1.05 ± 0.01	- 2.9788 ± 0.0041
299	3.3440	1.19 ± 0.02	- 2.9244 ± 0.0072
304	3.2894	1.27 ± 0.03	- 2.8962 ± 0.0101

TABLE 35 log k at various temperatures for catalytic oxidation of hydrogen using 1.0 mg Pt/Co_3O_4

P^oH_2 = 467 mm DBP

P^oO_2 = 200 mm Hg

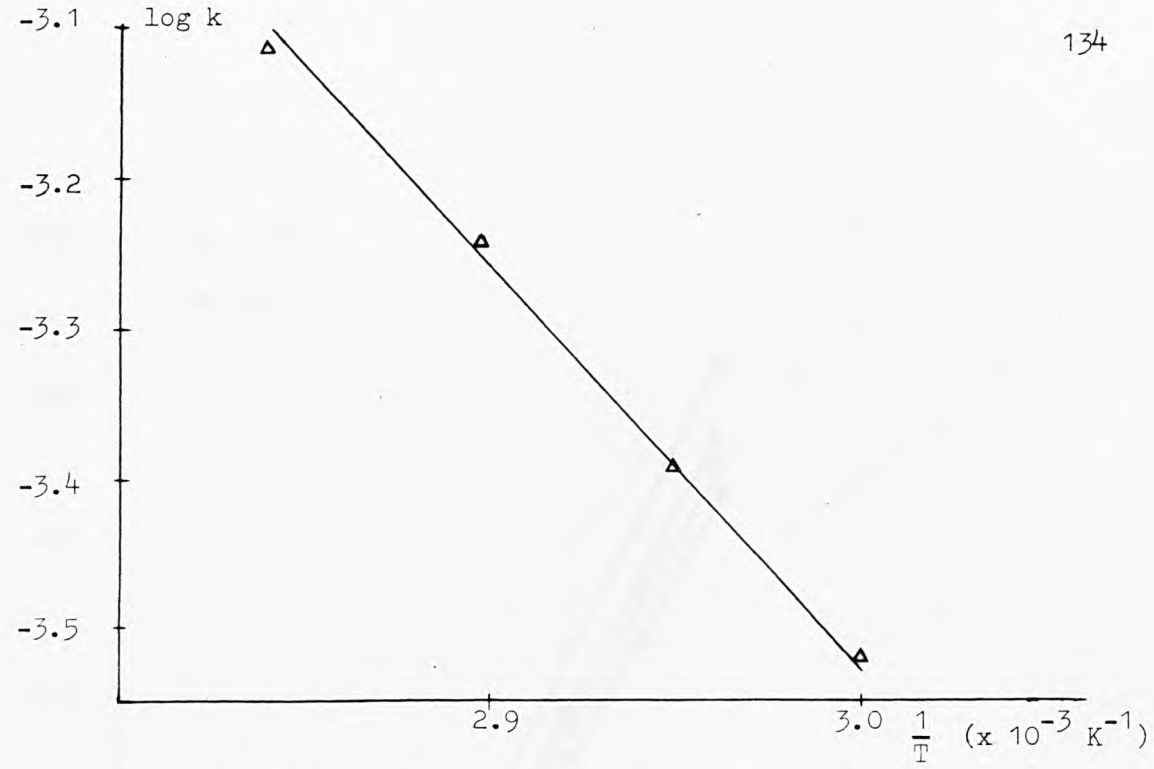

Fig. 43 Activation energy for catalytic oxidation of hydrogen using Co_3O_4.

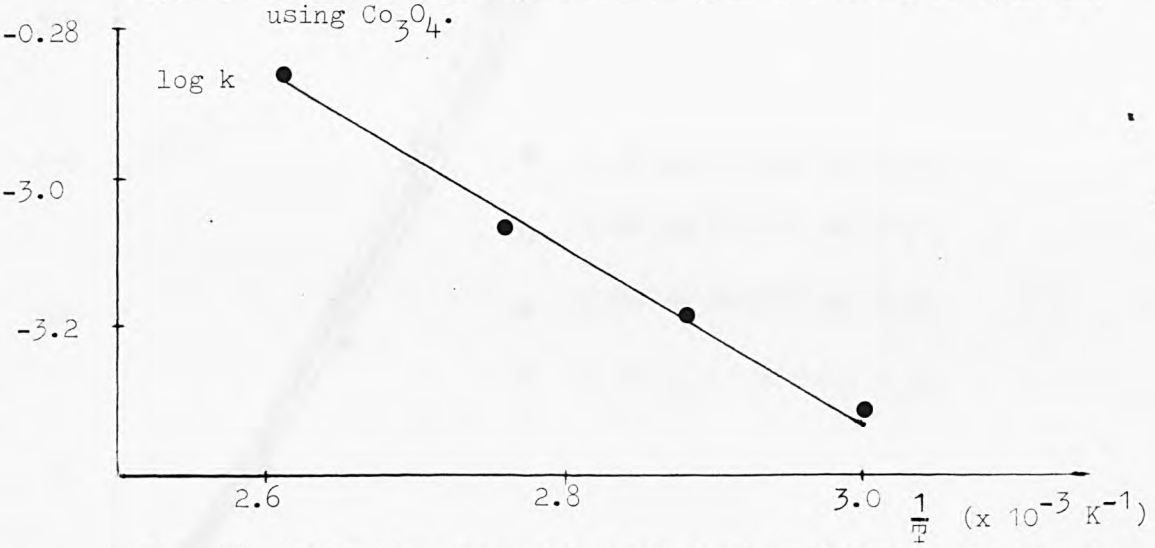

Fig. 44 Activation energy for catalytic oxidation of hydrogen using Pt/Co_3O_4 (high temp).

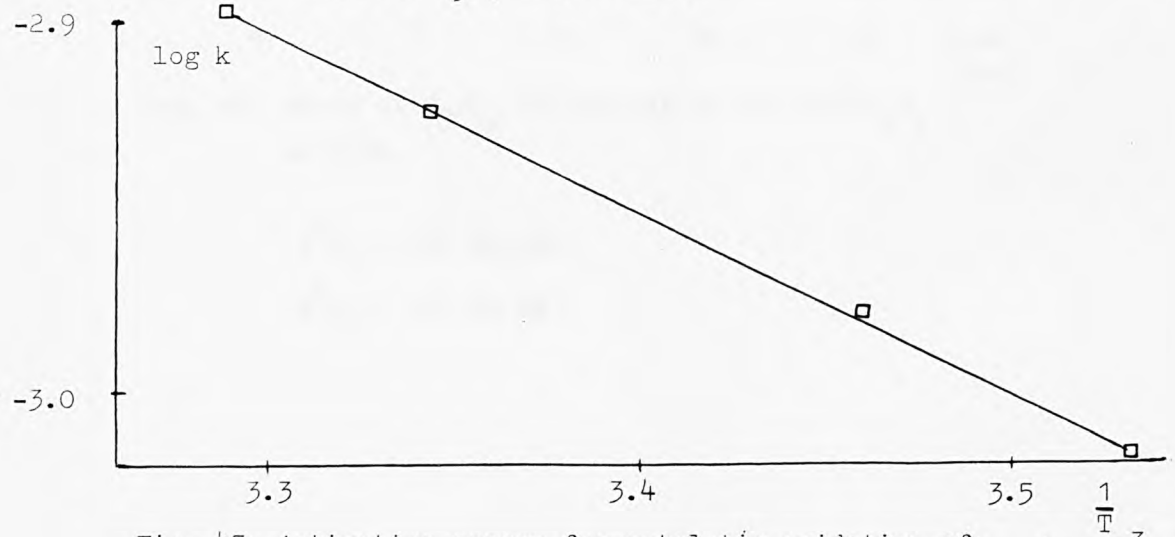

Fig. 45 Activation energy for catalytic oxidation of hydrogen using Pt/Co_3O_4 (low temp).

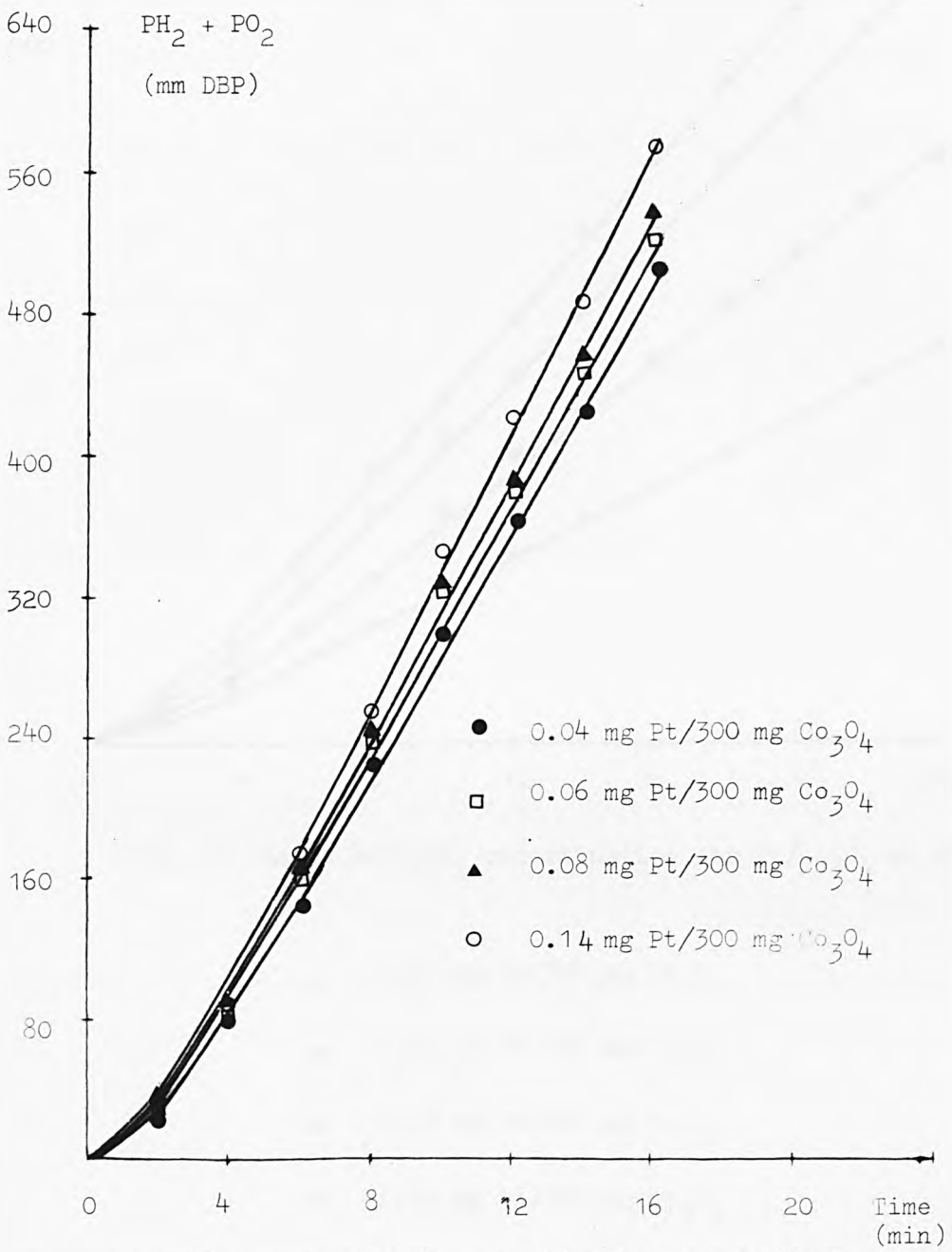

Fig. 46 Rates of H_2/O_2 recombination for Pt/Co_3O_4 at 373K.

P^oH_2 = 467 mm DBP

P^oO_2 = 200 mm Hg

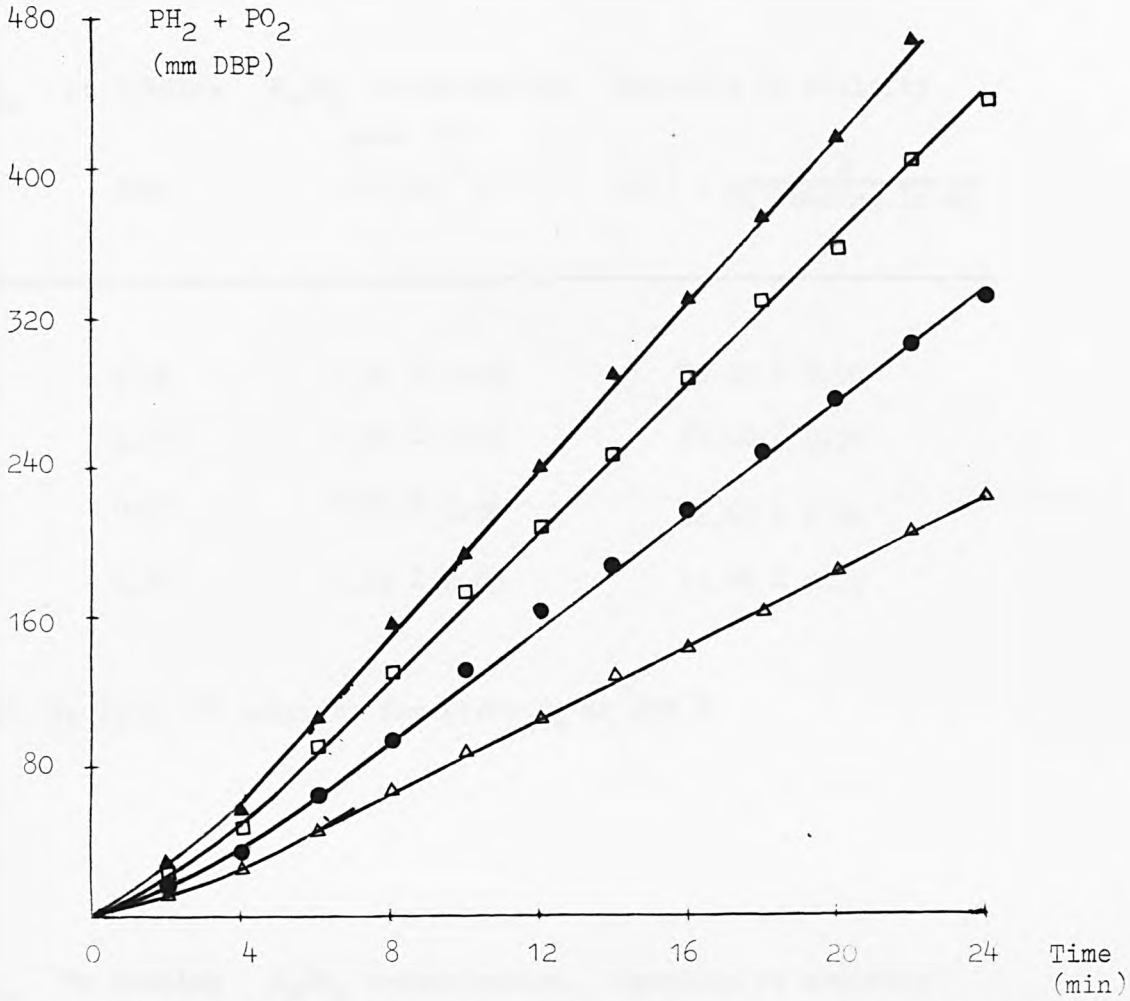

Fig. 47 Rates of H_2/O_2 recombination for Pt/Co_3O_4 at 298K.

△ 0.04 mg Pt/300 mg Co_3O_4

● 0.06 mg Pt/300 mg Co_3O_4

□ 0.07 mg Pt/300 mg Co_3O_4

▲ 0.09 mg Pt/300 mg Co_3O_4

P^oH_2 = 467 mm DBP

P^oO_2 = 200 mm Hg

Pt/Co_3O_4 (mg)	Pt loading (mg)	H_2/O_2 recombination rate (R) ($cc\ min^{-1}$)	Specific Pt activity $j(P) = \frac{R}{\text{Pt loading in mg}}$
300	0.04	1.41 ± 0.02	35.25 ± 0.50
300	0.06	1.44 ± 0.03	24.00 ± 0.50
300	0.08	1.49 ± 0.04	18.63 ± 0.50
300	0.14	1.63 ± 0.03	11.64 ± 0.22

TABLE 36 Specific Pt activity for Pt/Co_3O_4 at 373 K

Pt/Co_3O_4 (mg)	Pt loading (mg)	H_2/O_2 recombination rate (R) ($cc\ min^{-1}$)	Specific Pt activity $j(P) = \frac{R}{\text{Pt loading in mg}}$
300	0.04	0.41 ± 0.03	10.25 ± 0.75
300	0.06	0.61 ± 0.02	10.17 ± 0.33
300	0.07	0.82 ± 0.02	11.71 ± 0.29
300	0.09	0.93 ± 0.04	10.33 ± 0.45

TABLE 37 Specific Pt activity for Pt/Co_3O_4 at 298 K

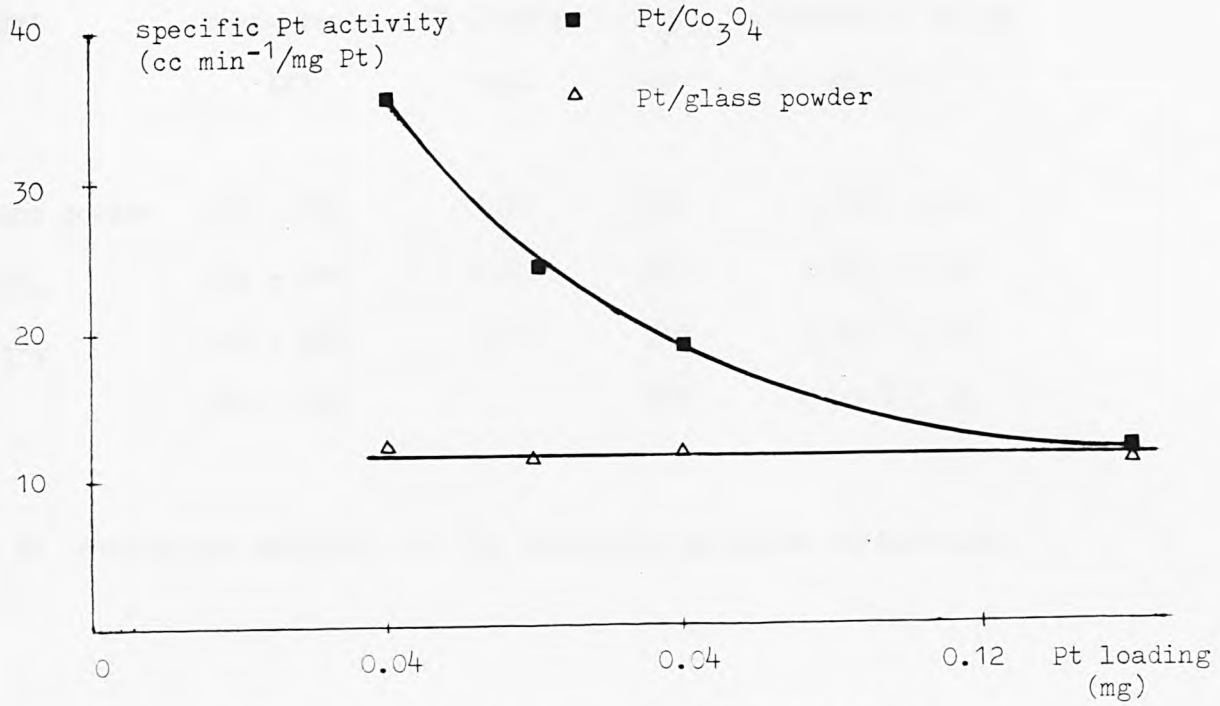

Fig. 48 Specific Pt activity Vs Pt loading at 373K.

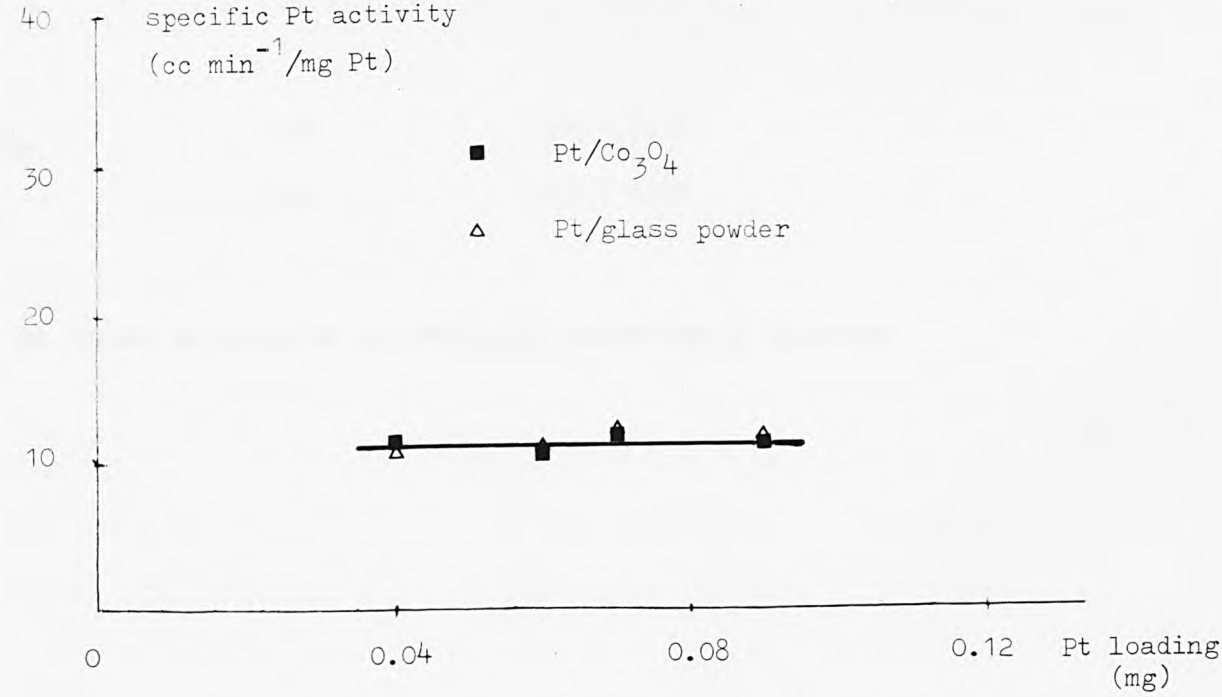

Fig. 49 Specific Pt activity Vs Pt loading at 298K.

Catalyst	Temp. range (K)	Pt loading (mg)	Co_3O_4 (mg)	Activation energy (K cal. mol^{-1})
Pt/glass powder	298 - 363	1.80	300	2.18 ± 0.05
Pt/Co_3O_4	283 - 304	0.80	300	2.23 ± 0.20
Pt/Co_3O_4	333 - 383	0.08	300	5.22 ± 0.09
Co_3O_4	333 - 352	-	300	12.05 ± 0.18

TABLE 38 Activation energies for the catalytic oxidation of hydrogen

Oxide	Temperature (K)	Order with respect to hydrogen ($^nH_2$)	Order with respect to oxygen ($^nO_2$)
$NiCo_2O_4$	418	1.04 ± 0.02	0
Co_3O_4	366	0.93 ± 0.01	0

TABLE 39 Order of reaction in catalytic oxidation of hydrogen

7.5 Results.

In catalytic oxidation of hydrogen using $NiCo_2O_4$, Table 22 and Figs. 20 & 21 show that the order of reaction with respect to H_2 is one and zero order with respect to O_2 (Fig. 22).

The rate constants for $NiCo_2O_4$, $Pt/NiCo_2O_4$ (high temp.), $Pt/NiCo_2O_4$ (low temp.) and Pt/glass powder are shown in Figs. 23 , 24 , 25 & 26 , and in Tables 23 , 24 , 25 & 26 respectively, and their respective activation energies are shown in Figs. 27 , 28 , 29 & 30 and also in Table 27.

The rates of H_2/O_2 combination/recombination for $Pt/NiCo_2O_4$ at 100° and 25°C are illustrated in Figs. 31 & 32 and in Tables 28 & 29 respectively. Likewise, the rates of H_2/O_2 recombination for Pt/glass powder at 100° and 25°C are shown in Figs. 33 & 34 and in Tables 30 & 31 respectively.

Fig. 35 demonstrates the specific Pt activities, j(P), for $Pt/NiCo_2O_4$ and Pt/glass powder at 100°C, and also in Tables 28 and 30 respectively. Fig. 36 gives the j(P) values for $Pt/NiCo_2O_4$ and Pt/glass powder at 25°C, and in Tables 21 & 31 respectively.

In the case of Co_3O_4 catalyst for H_2/O_2 recombination, Figs. 37 & 38 and Table 32 show that the order of reaction with respect to H_2 is one and zero order with respect to O_2 (Fig. 39) .

The rate constants for catalytic hydrogen oxidation using Co_3O_4 , Pt/Co_3O_4 (high temp.) and Pt/Co_3O_4 (low temp.) are shown in Figs. 40 , 41 & 42 and in Tables 33 , 34 &35 respectively, with their respective activation energies illustrated in Figs. 43 , 44 & 45.

Fig. 46 and Table 36 show the rates of H_2/O_2 recombination for Pt/Co_3O_4 at 100°C. Similarly , Fig. 47 and Table 37 illustrate the rates at 25°C .

Fig. 48 shows the specific Pt activities for Pt/Co_3O_4 and Pt/glass powder at 100°C and also at 25°C as shown in Fig. 49 . Tables 36 & 37 also give the j(P) values for Pt/Co_3O_4 at 100° and 25°C respectively.

The activation energies for Co_3O_4, Pt/glass powder and Pt/Co_3O_4 (low & high temp.) are summarized in Table 38.

Table 39 shows the orders of reaction for $NiCo_2O_4$ and Co_3O_4.

Experiments on glass powder alone reveal that H_2/O_2 recombination did not take place even at higher temperatures (e.g. 200°C).

X-ray powder diffraction analysis shows that the structures of Co_3O_4 (Table 20) and of $NiCo_2O_4$ (Table 21) remain unchanged before and after H_2/O_2 recombination.

7.6 Discussion.

To elucidate the mechanism of hydrogen and oxygen interation over $NiCo_2O_4$ and Co_3O_4 catalysts, the author measured and compared the rates, activation energies, and reaction orders of catalytic oxidation of hydrogen. For this purpose, the kinetic characteristics of the catalytic reaction of hydrogen and oxygen over Co_3O_4 were measured, and the experimental results agreed reasonably well with the published data[26].

In the catalytic reaction of hydrogen and oxygen over $NiCo_2O_4$ catalyst, the activation energies for $NiCo_2O_4$, $Pt/NiCo_2O_4$ (high temp.) , $Pt/NiCo_2O_4$ (low temp.) and Pt/glass powder are 14.38, 6.69 , 2.11 and 2.18 K cal. mol^{-1} respectively (Table 27). At lower temperatures, the support $NiCo_2O_4$ did not participate in the H_2/O_2 combination/ recombination; the distinctive feature is that the activation energy of $Pt/NiCo_2O_4$ equals to that of the Pt/glass powder (Figs. 29 , 30

and Table 27). However, at higher temperatures, the activation energy for $Pt/NiCo_2O_4$ is 6.69 Kcal. mol^{-1}, which is greater than the activation energy of Pt/glass powder (2.18 Kcal. mol^{-1}) but smaller than that of $NiCo_2O_4$ (14.38 Kcal. mol^{-1}) , indicating support participation in the H_2/O_2 interaction reaction. The results obviously demonstrate that the H_2/O_2 recombination in $NiCo_2O_4$ is ~~primary~~ due to temperature effect. This is further confirmed by the experimental results based on specific Pt activity j(P) .

The j(P) for $Pt/NiCo_2O_4$ at 100°C (Table 28 & Fig. 35) and 25°C (Table 29 & Fig. 36) together with the j(P) for Pt/glass powder at 100°C (Table 30 & Fig.35) and 25°C (Table 31 & Fig. 36) reveal that the support $NiCo_2O_4$ contributes to the H_2/O_2 recombination rate only at higher temperatures. At 100°C for example, the j(P) for $Pt/NiCo_2O_4$ increases as the Pt loading decreases as shown in Fig. 35 ; $NiCo_2O_4$ is therefore an active support, increasing the net reaction rate. In contrast, at lower temperatures (e.g. 25°C), $NiCo_2O_4$ is an inert support (Fig. 36) and takes no part in the H_2/O_2 recombination rate.

In the case of Co_3O_4 catalyst for H_2/O_2 combination/recombination, the experimental results suggest that the temperature effect also plays an important role in the H_2/O_2 interaction analogous to $NiCo_2O_4$. The j(P) for Pt/Co_3O_4 at 100° and 25°C (Tables 36,37 & Figs. 48,49), and the activation energies for Co_3O_4 and Pt/Co_3O_4 (low & high temp.) as illustrated in Table 38, have proved conclusively that Co_3O_4 only participates in H_2/O_2 interaction at higher temperatures (e.g. 80°C).

It is perhaps worthwhile to make the following observations :

Electrochemically, reduction of O_2 on $NiCo_2O_4$ has been studied by King and Tseung[32][33][119]. However, according to Tseung and Yeung[120], the spinel $NiCo_2O_4$ phase, prepared by freeze-drying and thermal treatment, has the following electronic structure :

$$Co^{2+}_{0.9}\ Co^{3+}_{0.1}\ (Ni^{2+}_{0.9}\ Ni^{3+}_{0.1}\ Co^{3+})\ O^{2-}_{3.2}\ O^{-}_{0.8}$$

where cations outside the brackets are in tetrahedral sites and those inside the brackets are in octahedral sites. The existence of loosely bound O^- on the surface is probably responsible for the high activity of $NiCo_2O_4$.

If a molecule of oxygen is introduced into the surface, the following transformations take place [111]:

$$O_2(g) \rightleftharpoons O_2(ads) \rightleftharpoons 2O^-(ads) \rightleftharpoons 2O^{2-}(s)$$

The surface oxygen of oxides[121][122][123] provides evidence in favour of an oxidation-reduction scheme in catalytic H_2/O_2 recombination over certain metal oxides. According to it, catalysis of oxidation reactions by oxide catalysts proceeds via oxidation-reduction of the catalyst surface[25-28]. The scheme suggests active participation of the catalyst surface oxygen in oxidation reactions[124][125].

The mechanism of catalytic oxidation of hydrogen on Co_3O_4 has been studied by Mamedov[26] et al ~~and showed~~ that oxidation of hydrogen on Co_3O_4 takes place by alternate reduction and oxidation of the oxide surface, with a difficult stage of reaction of hydrogen with the catalyst surface oxygen. Analogous mechanism for the catalytic

oxidation of hydrogen on $NiCo_2O_4$ is suggested based on the kinetic parameters obtained for the two oxides. Also, as mentioned earlier that the H_2/O_2 interaction takes place only at relatively high temperatures. Furthermore, X-ray powder diffraction analysis confirms such mechanism since the structure of the oxides remains unchanged before and after H_2/O_2 recombination.

For a supported metal catalyst, considerable evidence[126-130] has been suggested that hydrogen atoms chemisorbed at the metal can migrate to the catalyst support, and can participate in chemical reactions on the support.

7.7 Conclusions.

The catalytic oxidation of hydrogen by the oxide catalysts (Co_3O_4 and $NiCo_2O_4$) proceeds via oxidation-reduction of the catalyst surface. The probable mechanisms and oxidation states predicted for the synthesis of water can be illustrated as follows :

$$H_2 \longrightarrow 2H$$
$$H + O_2 \longrightarrow OH + O$$
$$O + H_2 \longrightarrow OH + H$$
$$OH + H_2 \longrightarrow H_2O + H$$

In Co_3O_4 for example, Co^{4+} may be in equilibrium with lower oxidation states in oxides which have the empirical formula of CoO and Co_3O_4[131]. For the same reasons, Co^{4+} and Ni^{3+} may be in equilibrium with $NiCo_2O_4$. The reduction of Co^{4+} and Ni^{3+} by hydrogen to Co^{3+} and Ni^{2+} respectively takes place on the oxide surface, which is reoxidised by oxygen.

CHAPTER 8

MECHANISTIC STUDIES FOR THE PROMOTIONAL EFFECT ON FREEZE-DRIED STRONTIUM-DOPED LANTHANUM COBALT OXIDE FOR HYDROGEN AND OXYGEN RECOMBINATION.

CHAPTER 8

8 MECHANISTIC STUDIES FOR THE PROMOTIONAL EFFECT ON FREEZE-DRIED STRONTIUM-DOPED LANTHANUM COBALT OXIDE FOR HYDROGEN AND OXYGEN RECOMBINATION.

8.1 Perovskites.

The unit cell of perovskite has a general formula ABO_3 , where A denotes a large ion such as Ca^{2+}, Ba^{2+}, Pb^{2+}, Cd^{2+}, La^{3+}, Pr^{3+}, Nd^{3+} and B represents a small ion like Al^{3+}, Mn^{3+}, Fe^{3+}, Ti^{4+}, Mn^{4+} etc. The A ions are located at the corners of the unit cell, the B ions are at the centre of the cube with six oxygen ions distributed around it octahedrally, and the oxygen ions occupy the midpoints of all faces[132][133]. An early study on the compounds ABO_3 by Zachariasen [134] showed that the majority had the perovskite structure. The preparation and characteristics of perovskites have been investigated by a number of authors[134-148]. However, Goldschmidt and Hauptmann[142], who prepared the compounds ABO_3 and studied their general structure type, revealed the influence of ionic radii as the determining factors. Goldschmidt[132][143] suggested that the perovskite structure is stable when the parameter t, approximately equals unity, where t is called the "tolerance factor" and is defined by

$$t = \frac{(r_A + r_O)}{(r_B + r_O)\sqrt{2}}$$

where r_A, r_B and r_O denote respectively the radii of ions A, B and O .

In 1950 , Ashkam[144] et al prepared the compound $LaCoO_3$, indexed by X-ray diffraction as a rhombohedrally-distorted cubic structure with a pseudocubic cell edge a = 3.82 Å, and Jonker[145] described

the $LaCoO_3$ perovskite structure with eight molecules per unit cell. The properties of $LaCoO_3$ have also been investigated by other authors[146-151]. The mixed crystals of lanthanum hypomanganite, $LaMnO_3$ and various manganites, for examples, $LaMnO_3$ - $SrMnO_3$ and $LaMnO_3$ - $CaMnO_3$ etc. have been examined[152]; and various compositions (1 - x)$LaMnO_3$ - x$SrMnO_3$ were observed, all samples are well-conducting semiconductors.

Strontium-doped $LaCoO_3$ was first studied by Jonker and Van Santen[133], and the properties of perovskites of the first-row transition metals have also been considered by Jonker[152][153] et al.

8.2 Preparation.

$La_{0.5}Sr_{0.5}CoO_3$ was prepared using the stoichiometric cation quantities, the starting materials were "Analar" hydrated salts $La(NO_3)_3.6H_2O$. $Co(NO_3)_2.6H_2O$ and $Sr(NO_3)_2$. The details of the freeze-drying techniques for the preparation of $La_{0.5}Sr_{0.5}CoO_3$ are described in section 3.3.2.2.1 , except the catalyst was sintered in O_2 at 600°C for 10h.

8.3 Characterization.

8.3.1 X-ray Analysis.

X-ray powder diffraction was performed on $La_{0.5}Sr_{0.5}CoO_3$ before and after H_2/O_2 recombination using radiation from a Mo cathode (section 4.5.1) . In general, the d-values agree well with those obtained by other workers. $La_{0.5}Sr_{0.5}CoO_3$ was also characterized for its BET specific surface area (27.2 m^2/g) .

8.3.2 Electrical Conductivity.

Fig. 50 shows a section through a cylindrical die for conductivity measurements. The extreme faces of the die were held between the jaws of a tensometer, with which the pressure was increased manually.

The technique involved a weighed amount of the powdered sample introduced into a specially-designed cylindrical steel die, which had a 1 cm diameter inner Teflon sleeve. The height of the pressed powder bed was then determined and its conductivity measured. All the measurements were made at 25°C. The conductivity for $La_{0.5}Sr_{0.5}CoO_3$ was 0.12 Ohm^{-1} cm^{-1} .

8.4 Experimental.

For $La_{0.5}Sr_{0.5}CoO_3$, the kinetic parameters for catalytic H_2/O_2 combination/recombination were determined using the method outlined in section 7.4.1 and Fig. 19 . Similarly, the specific Pt activity at 135° and 25°C was obtained according to the procedure described in section 7.4.3 .

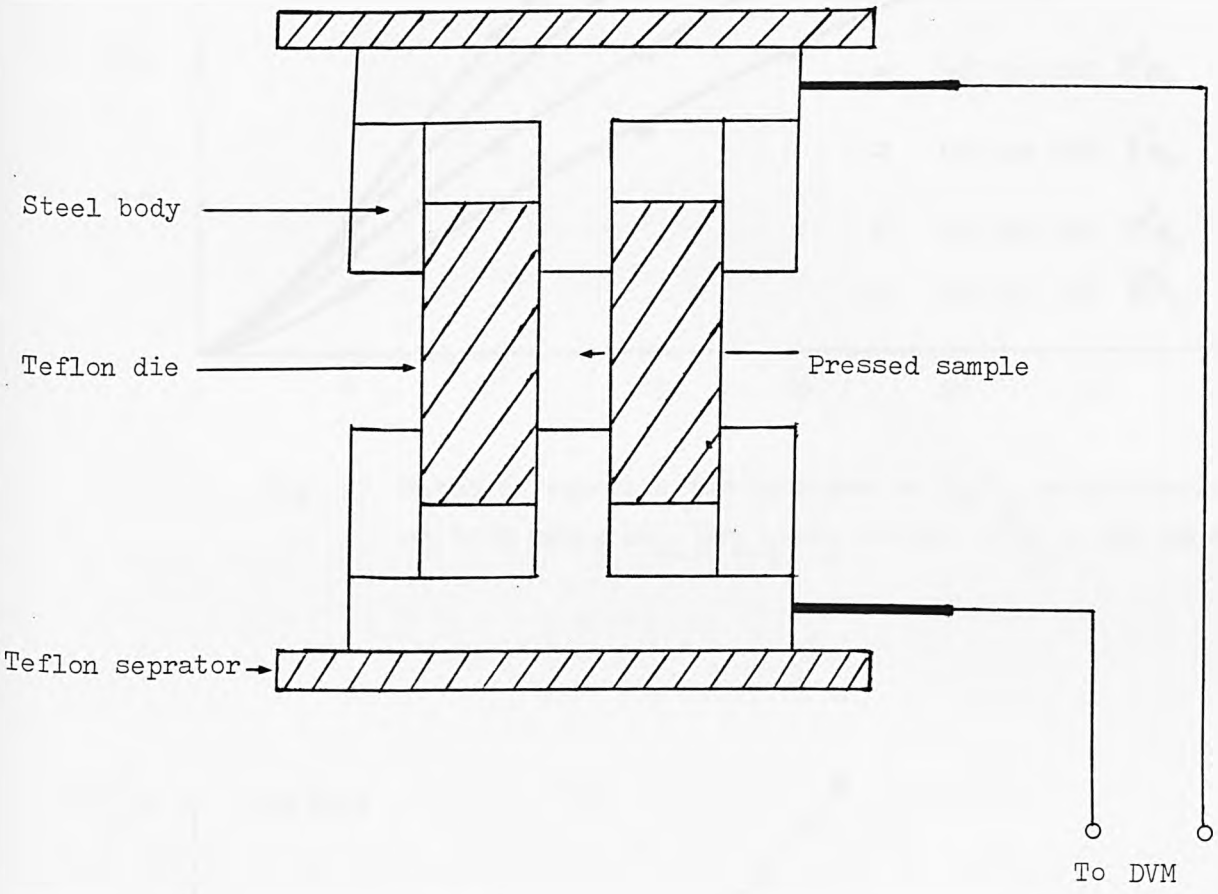

Fig. 50 Section through cylindrical die for conductivity measurement.

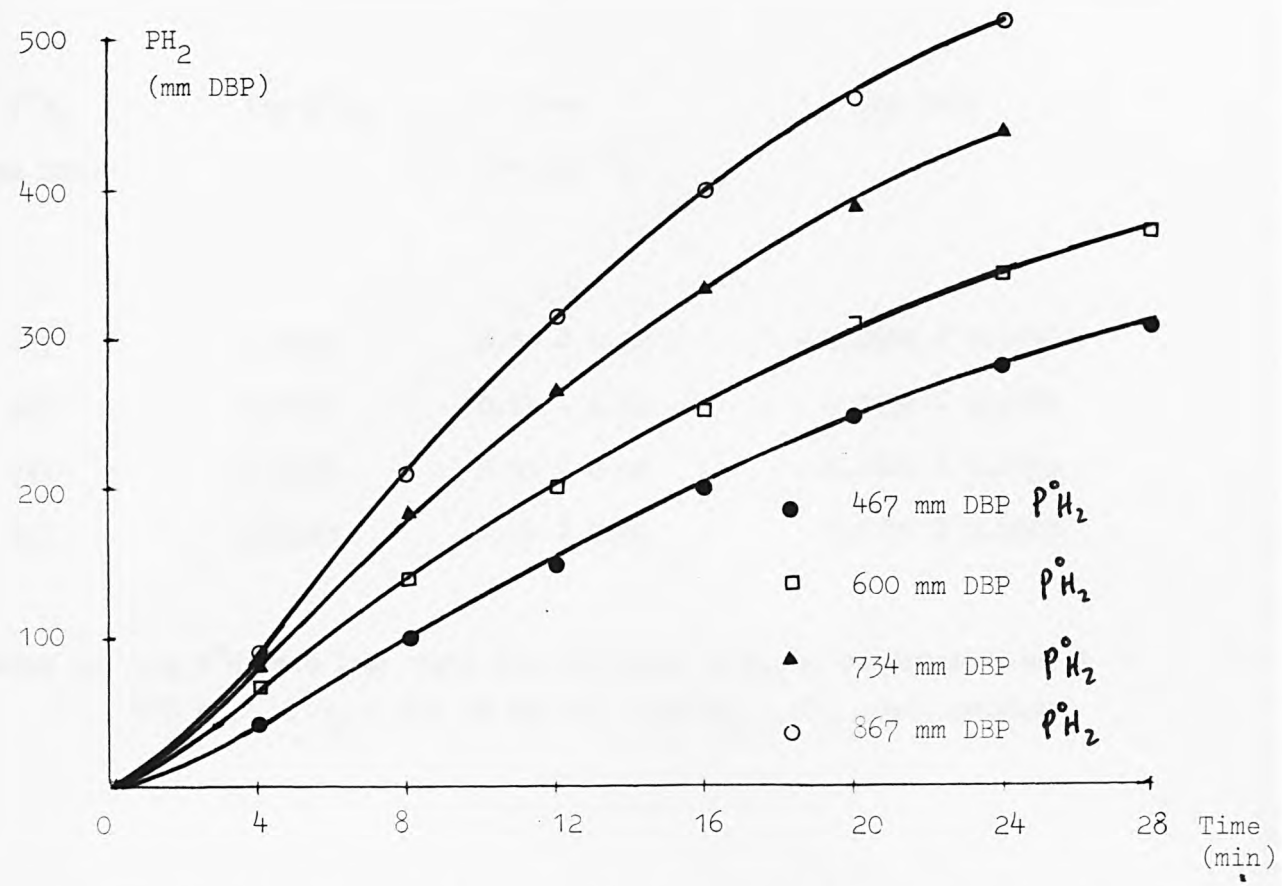

Fig. 51 Rates of reaction for hydrogen in H_2/O_2 recombination at 418K using $La_{0.5}Sr_{0.5}CoO_3$ (0.3g), $P^\circ O_2$ = 200 mm Hg.

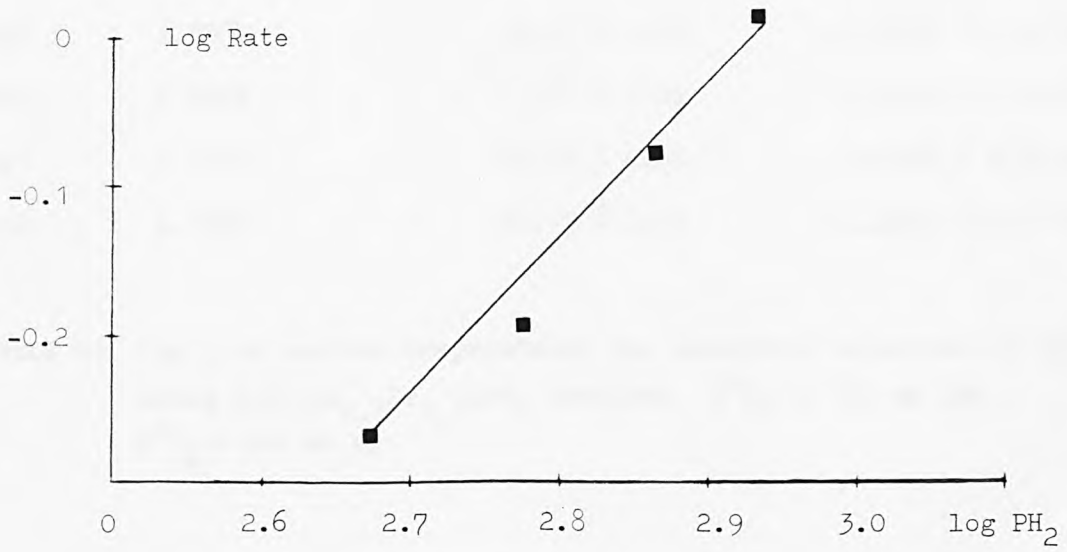

Fig. 52 Order of reaction with respect to hydrogen at 418K for $La_{0.5}Sr_{0.5}CoO_3$.

$P^{o}H_2$ (mm DBP)	$\log P^{o}H_2$	Rate (cc min^{-1})	log Rate
467	2.6693	0.54 ± 0.02	- 0.2676 ± 0.0158
600	2.7782	0.64 ± 0.02	- 0.1938 ± 0.0134
734	2.8657	0.83 ± 0.02	- 0.0809 ± 0.0103
867	2.9380	1.04 ± 0.02	0.0170 ± 0.0083

TABLE 40 log $P^{o}H_2$ and log rate for hydrogen in H_2/O_2 recombination at 418 K , $P^{o}O_2$ = 200 mm Hg and 0.3g $La_{0.5}Sr_{0.5}CoO_3$ catalyst

T (K)	$\frac{1}{T}$ (x 10^{-3} K^{-1})	k (x 10^{-4} S^{-1})	log K
428	2.3364	6.17 ± 0.02	- 3.2097 ± 0.0014
442	2.2624	11.17 ± 0.05	- 2.9520 ± 0.0020
451	2.2172	17.83 ± 0.05	- 2.7488 ± 0.0012
458	2.1834	22.17 ± 0.07	- 2.6542 ± 0.0013

TABLE 41 log k at various temperatures for catalytic oxidation of hydrogen using 0.3g $La_{0.5}Sr_{0.5}CoO_3$ catalyst $P^{o}H_2$ = 467 mm DBP , $P^{o}O_2$ = 200 mm Hg

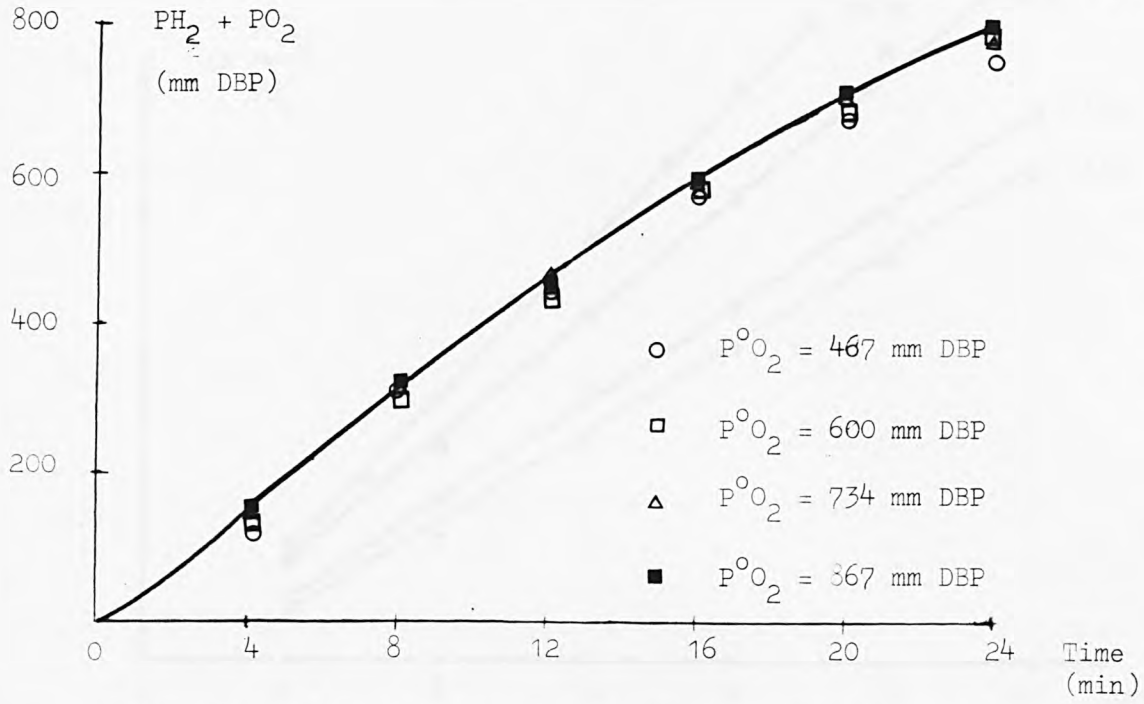

Fig. 53 Rates of H_2/O_2 recombination for $La_{0.5}Sr_{0.5}CoO_3$ at 418, $P^{\circ}H_2$ = 130 mm Hg.

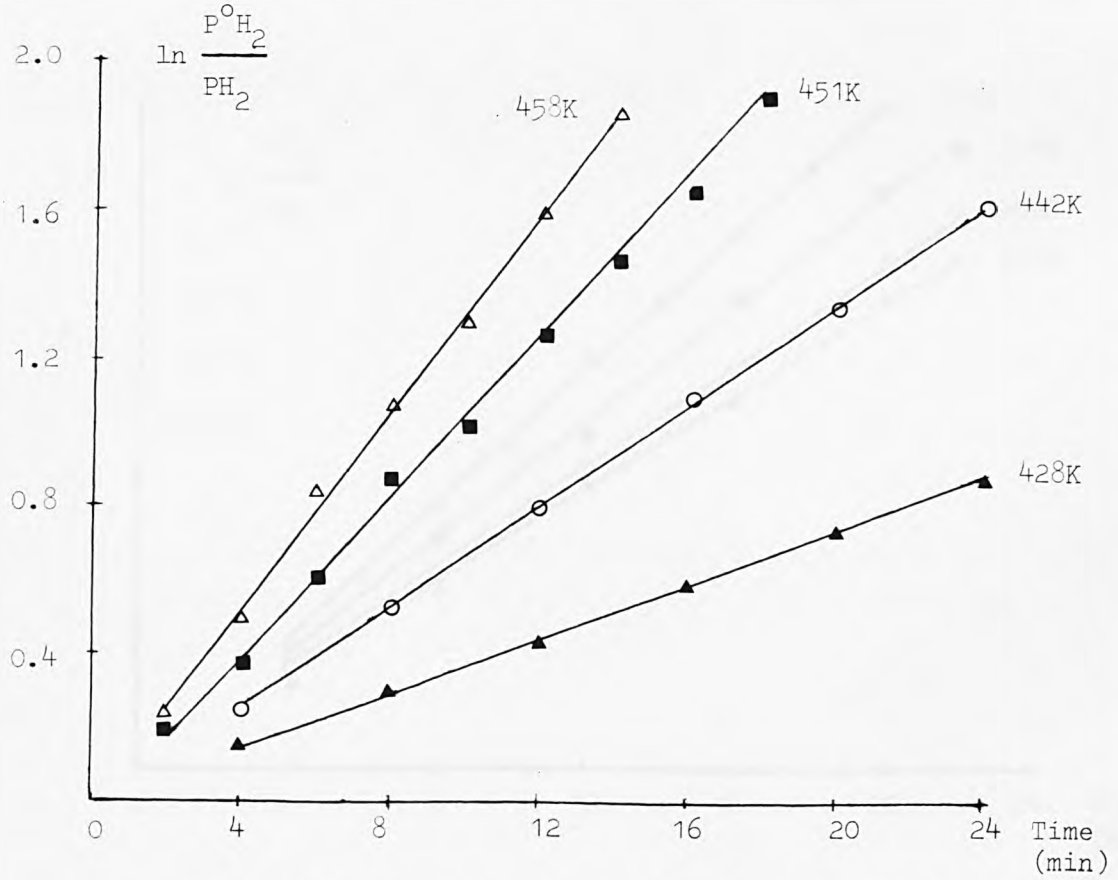

Fig. 54 Rate constants for catalytic hydrogen oxidation using $La_{0.5}Sr_{0.5}CoO_3$ (0.3g), $P^{\circ}H_2$ = 467 mm DBP, $P^{\circ}O_2$ = 200 mm Hg.

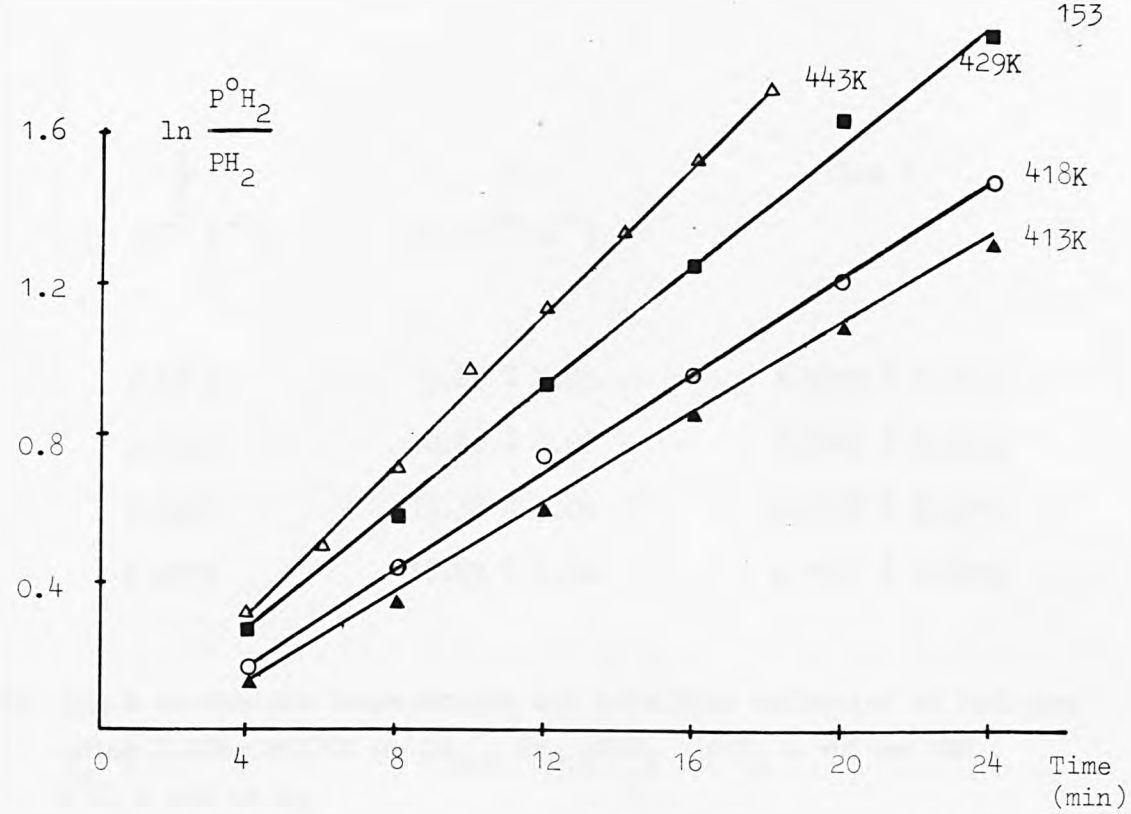

Fig. 55 Rate constants for catalytic hydrogen oxidation using 0.1mg Pt/300 mg $La_{0.5}Sr_{0.5}CoO_3$ (high temp).
$P^{o}H_2$ = 467 mm DBP, $P^{o}O_2$ = 200 mm Hg.

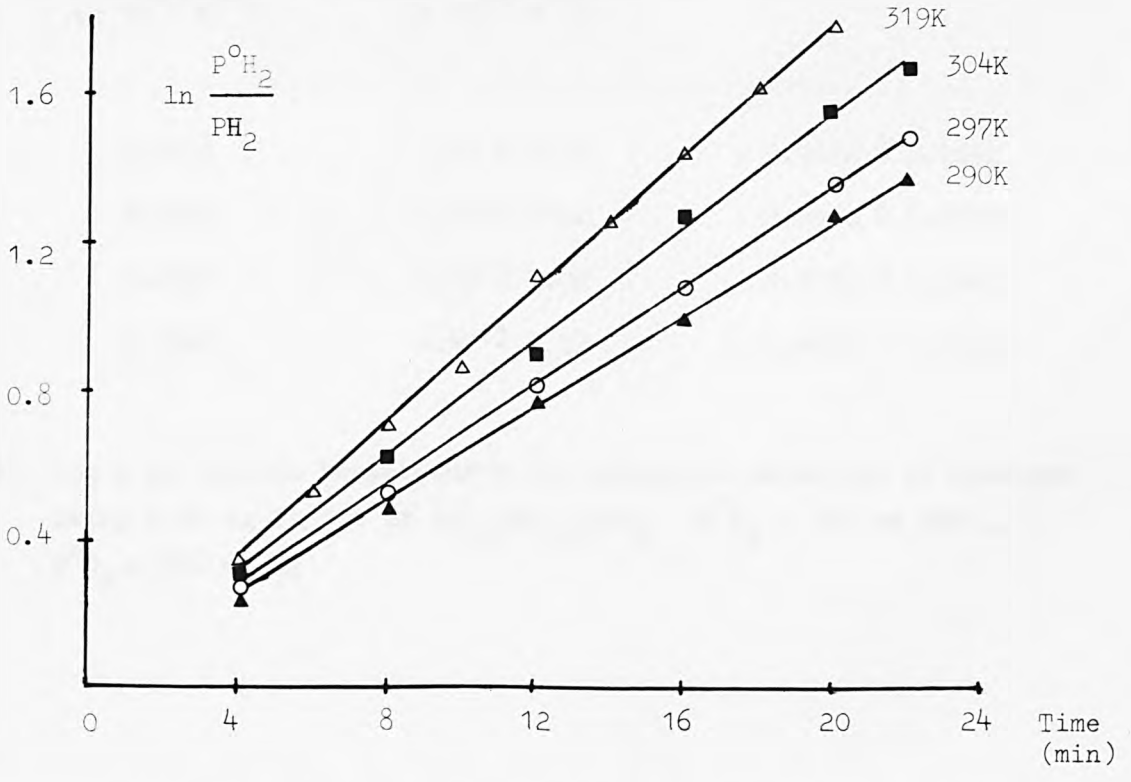

Fig. 56 Rate constants for catalytic hydrogen oxidation using 0.80mg Pt/300 mg $La_{0.5}Sr_{0.5}CoO_3$ (low temp).
$P^{o}H_2$ = 467 mm DBP, $P^{o}O_2$ = 200 mm Hg.

T (K)	$\frac{1}{T}$ ($\times 10^{-3}$ K^{-1})	k ($\times 10^{-4}$ s^{-1})	log k
413	2.4213	9.88 ± 0.03	- 3.0052 ± 0.0013
418	2.3923	10.60 ± 0.06	- 2.9747 ± 0.0025
429	2.3310	13.38 ± 0.04	- 2.8736 ± 0.0014
443	2.2573	16.67 ± 0.06	- 2.7781 ± 0.0016

TABLE 42 log k at various temperatures for catalytic oxidation of hydrogen using 0.10mg Pt/300 mg $La_{0.5}Sr_{0.5}CoO_3$ P^oH_2 = 467 mm DBP , P^oO_2 = 200 mm Hg

T (K)	$\frac{1}{T}$ ($\times 10^{-3}$ K^{-1})	k ($\times 10^{-3}$ s^{-1})	log k
290	3.4482	1.04 ± 0.01	- 2.9830 ± 0.0042
297	3.3670	1.14 ± 0.02	- 2.9430 ± 0.0075
304	3.2894	1.28 ± 0.02	- 2.8928 ± 0.0067
319	3.1347	1.47 ± 0.02	- 2.8327 ± 0.0059

TABLE 43 log k at various temperatures for catalytic oxidation of hydrogen using 0.80 mg Pt/300 mg $La_{0.5}Sr_{0.5}CoO_3$ P^oH_2 = 467 mm DBP , P^oO_2 = 200 mm Hg

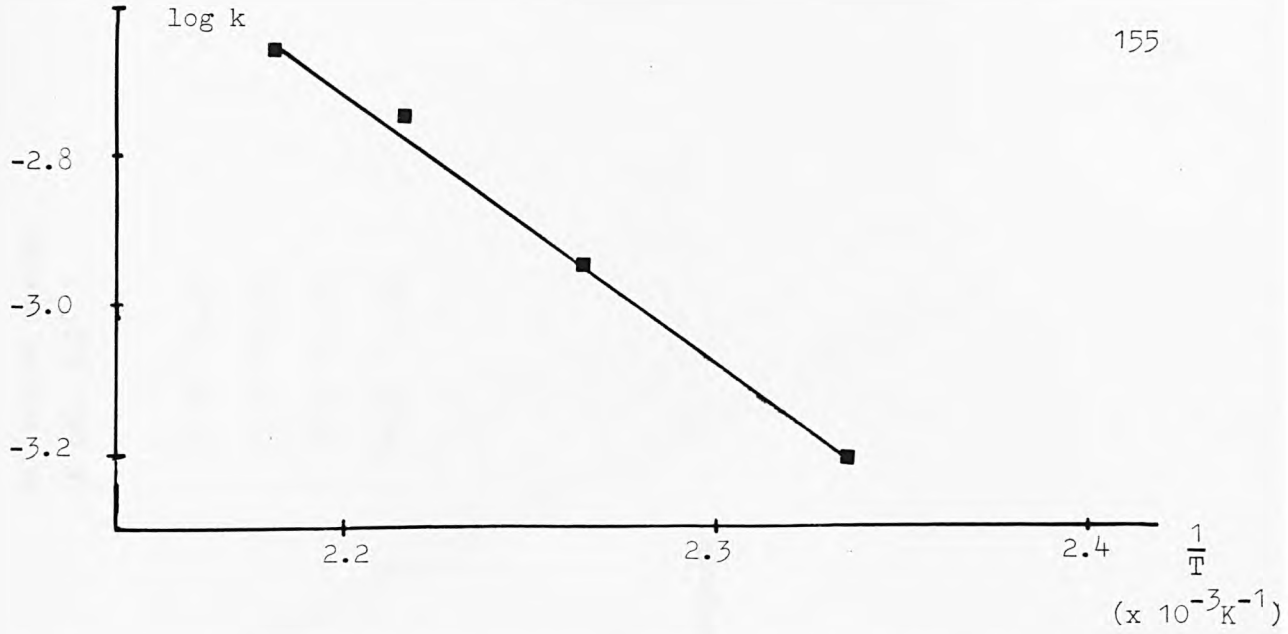

Fig. 57 Activation energy for catalytic oxidation of hydrogen using $La_{0.5}Sr_{0.5}CoO_3$

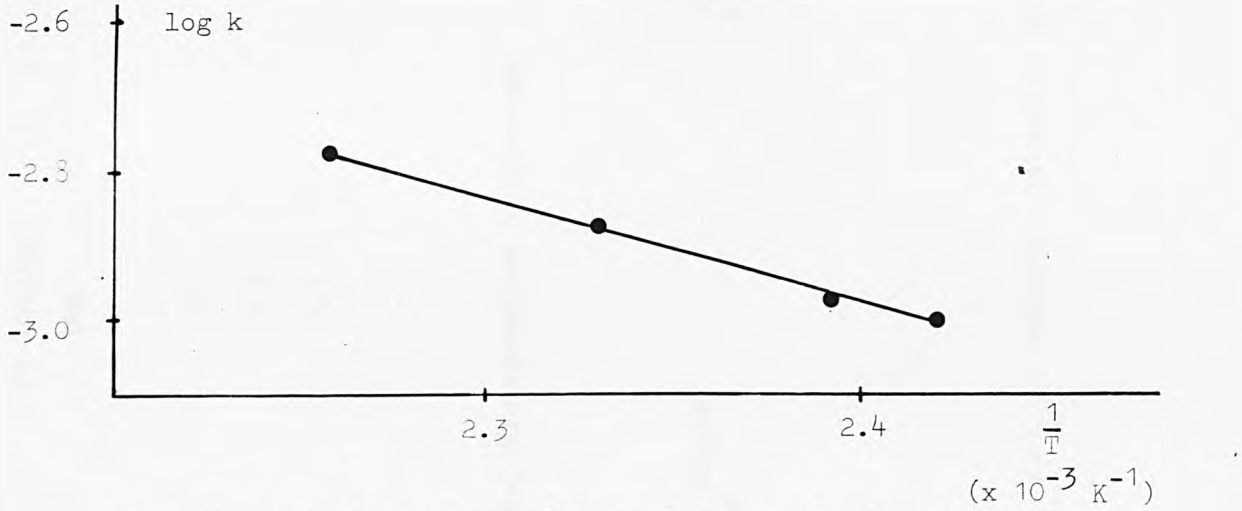

Fig. 58 Activation energy for catalytic oxidation of hydrogen using $Pt/La_{0.5}Sr_{0.5}CoO_3$ (high temp).

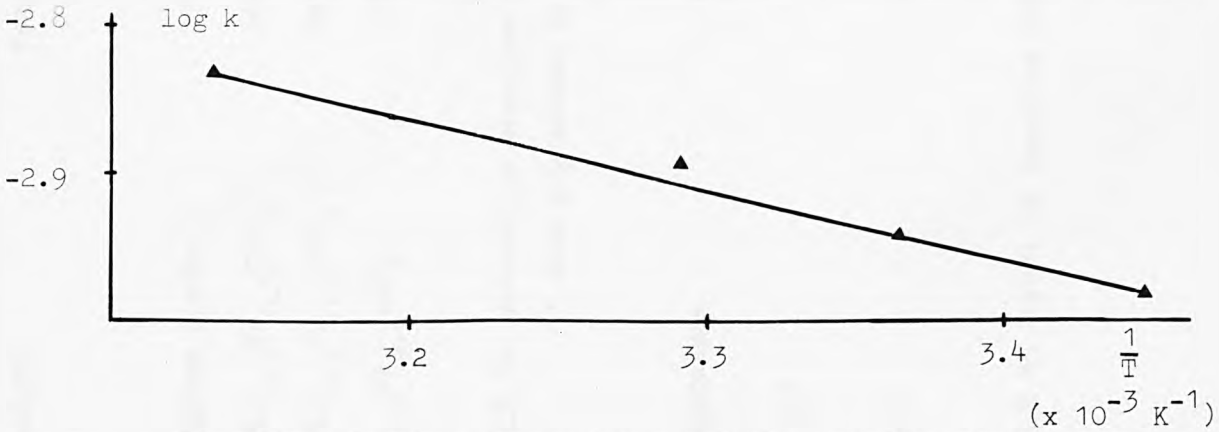

Fig. 59 Activation energy for catalytic oxidation of hydrogen using $Pt/La_{0.5}Sr_{0.5}CoO_3$ (low temp).

Catalyst	Temp. range (K)	Pt loading (mg)	$La_{0.5}Sr_{0.5}CoO_3$ (mg)	Activation energy (K cal. mol^{-1})
Pt/glass powder *	298 - 363	1.8	-	2.18 ± 0.05
$Pt/La_{0.5}Sr_{0.5}CoO_3$	290 - 319	0.8	300	2.21 ± 0.10
$Pt/La_{0.5}Sr_{0.5}CoO_3$	413 - 443	0.1	300	6.45 ± 0.10
$La_{0.5}Sr_{0.5}CoO_3$	428 - 458	-	300	16.69 ± 0.25

TABLE 44 Activation energies for the catalytic oxidation of hydrogen

* Data reproduced in Table 27

Temperature (K)	Order with respect to hydrogen ($^nH_2$)	Order with respect to oxygen ($^nO_2$)
418	1.04 ± 0.07	0

TABLE 45 Order of reaction for $La_{0.5}Sr_{0.5}CoO_3$ in catalytic oxidation of hydrogen

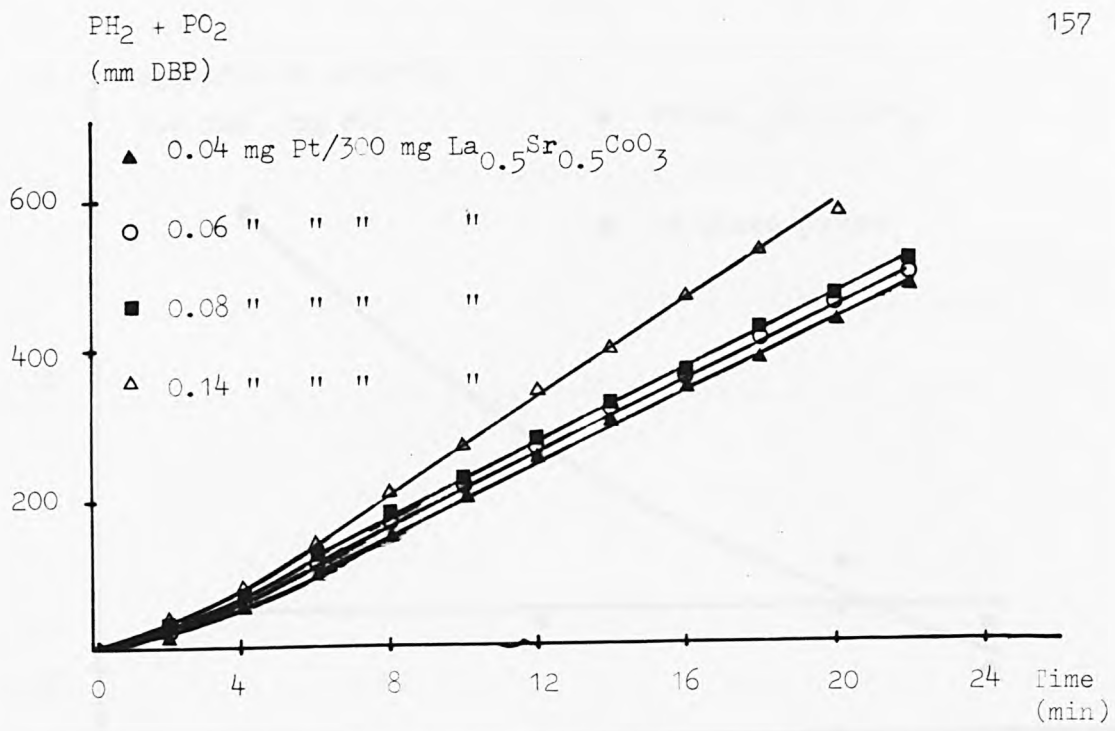

Fig. 60 Rate of H_2/O_2 recombination for $Pt/La_{0.5}Sr_{0.5}CoO_3$ at 408K. P^oH_2 = 467 mm DBP, P^oO_2 = 200 mm Hg.

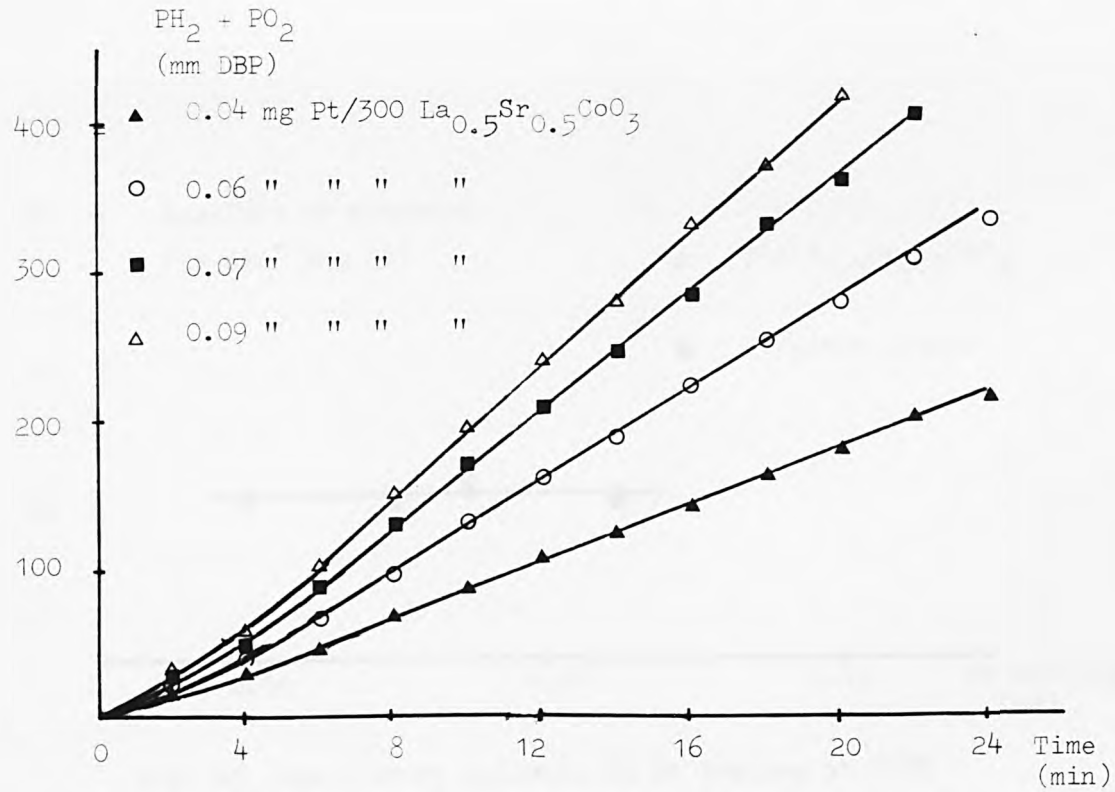

Fig. 61 Rate of H_2/O_2 recombination for $Pt/La_{0.5}Sr_{0.5}CoO_3$ at 298K. P^oH_2 = 467 mm DBP, P^oO_2 = 200 mm Hg.

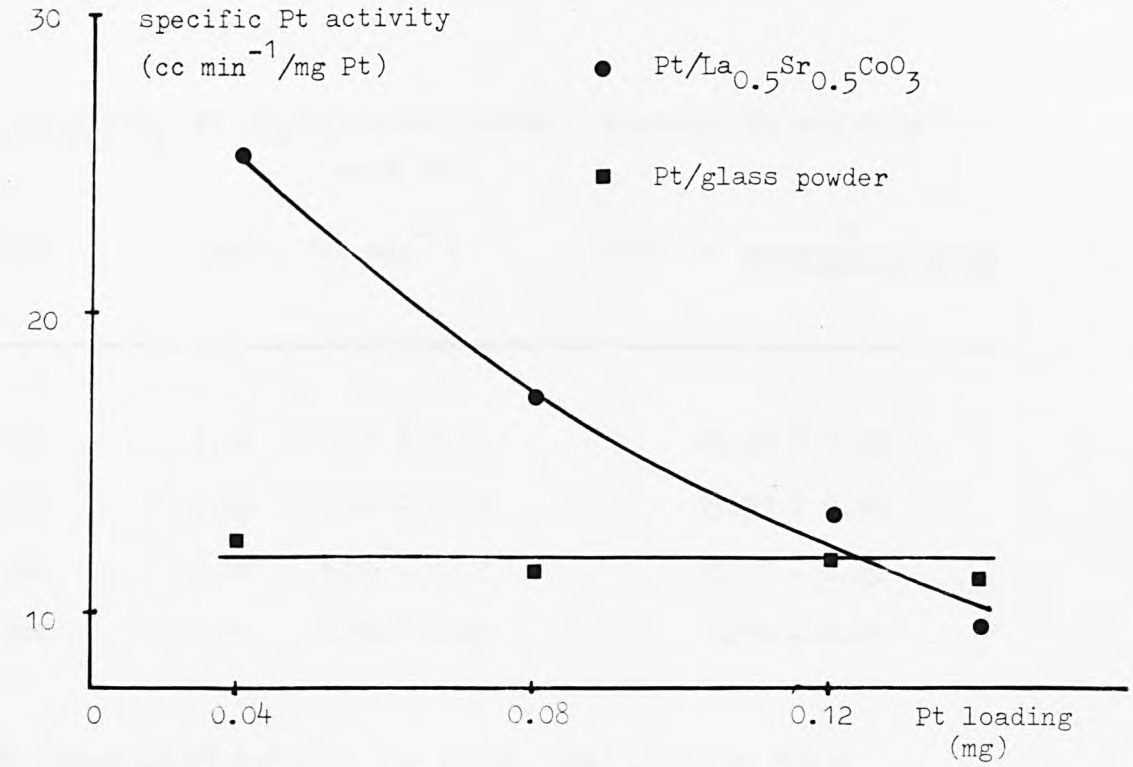

Fig. 62 Specific Pt Activity Vs Pt loading at 408K
(Data for Pt/glass powder is given in Table 30).

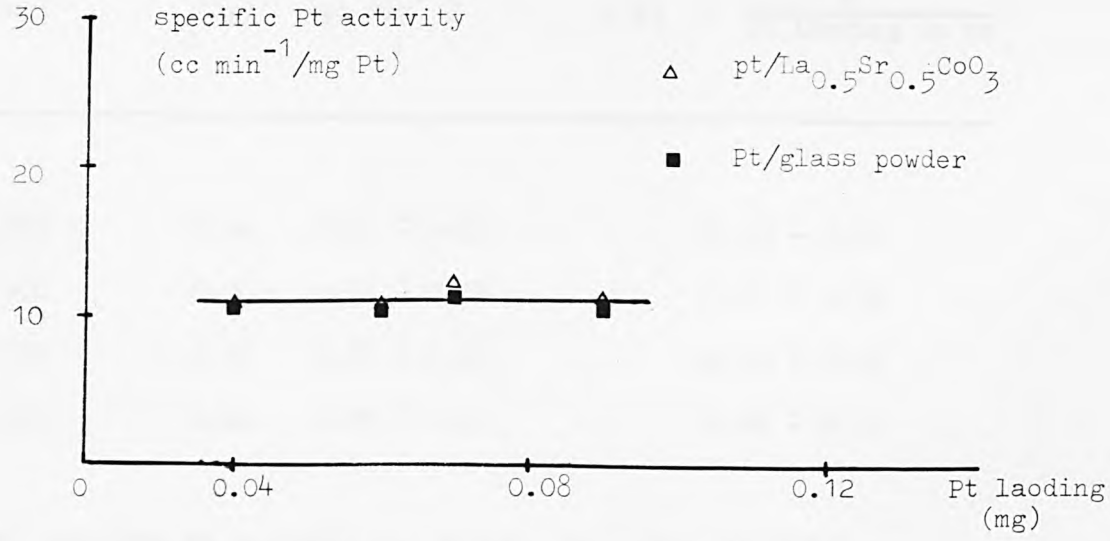

Fig. 63 Specific Pt activity Vs Pt loaidng at 298K
(Data for Pt/glass powder is given in Table 31).

$Pt/La_{0.5}Sr_{0.5}CoO_3$ (mg)	Pt (mg)	H_2/O_2 recombination rate (R) ($cc\ min^{-1}$)	Specific Pt activity $j(P) = \frac{R}{\text{Pt loading in mg}}$
300	0.04	1.01 ± 0.01	25.25 ± 0.25
300	0.06	1.04 ± 0.02	17.33 ± 0.34
300	0.08	1.08 ± 0.02	13.50 ± 0.25
300	0.14	1.33 ± 0.03	9.50 ± 0.21

TABLE 46 Specific Pt activity for $Pt/La_{0.5}Sr_{0.5}CoO_3$ at 408 K

$Pt/La_{0.5}Sr_{0.5}CoO_3$ (mg)	pt (mg)	H_2/O_2 recombination rate (R) ($cc\ min^{-1}$)	Specific Pt activity $j(P) = \frac{R}{\text{Pt loading in mg}}$
300	0.04	0.41 ± 0.02	10.25 ± 0.50
300	0.06	0.61 ± 0.02	10.17 ± 0.33
300	0.07	0.86 ± 0.03	12.29 ± 0.42
300	0.09	0.95 ± 0.03	10.56 ± 0.33

TABLE 47 Specific Pt activity for $Pt/La_{0.5}Sr_{0.5}CoO_3$ at 298 K

$La_{0.5}Sr_{0.5}CoO_3$* d-value (Å)	Intensity (I/I_o)	$La_{0.5}Sr_{0.5}CoO_3$** d-value (Å)	Intensity (I/I_o)
3.84	M	3.84	M
2.73	VS	2.73	VS
2.70	VS	2.70	VS
2.22	M	2.22	M
2.19	W	2.19	W
1.92	S	1.92	S
1.57	VW	1.57	VW

TABLE 48 X-ray powder diffraction data for strontium - doped lanthanum cobalt oxide

VS = Very strong
S = strong
M = medium
W = weak
VW = Very weak

* $La_{0.5}Sr_{0.5}CoO_3$ before H_2/O_2 recombination

** $La_{0.5}Sr_{0.5}CoO_3$ after H_2/O_2 recombination

8.5 Results.

In the H_2/O_2 recombination using $La_{0.5}Sr_{0.5}CoO_3$ catalyst at 135°C , Figs. 51 & 52 and Table 40 illustrate that the order of reaction with respect to H_2 is one and zero order with respect to O_2 (Fig. 53) .

The rate constants for $La_{0.5}Sr_{0.5}CoO_3$, $Pt/La_{0.5}Sr_{0.5}CoO_3$ (high temp.) and $Pt/La_{0.5}Sr_{0.5}CoO_3$ (low temp.) are shown in Figs. 54, 55 & 56 and in Tables 41, 42 & 43 respectively, and their respective activation energies are shown in Figs. 57, 58 & 59 . For comparative purposes, the activation energies for Pt/glass powder, $Pt/La_{0.5}Sr_{0.5}CoO_3$ and $La_{0.5}Sr_{0.5}CoO_3$ are summarized in Table 44. The results indicate the dependence of temperature for H_2/O_2 recombination over $La_{0.5}Sr_{0.5}CoO_3$ catalyst. Table 45 shows the overall order of reaction.

The rates of H_2/O_2 recombination for $Pt/La_{0.5}Sr_{0.5}CoO_3$ at 135° and 25°C are shown in Fig. 60 & Table 46 and Fig. 61 & Table 47 respectively. Thus, the specific Pt activities j(P) for $Pt/La_{0.5}Sr_{0.5}CoO_3$ and Pt/glass powder at 135°C (Fig. 62 & Table 46) and 25°C (Fig. 63 & Table 47) show conclusively that the support $La_{0.5}Sr_{0.5}CoO_3$ did not participate in H_2/O_2 interaction at low temperatures (e.g. 25°C).

X-ray analysis of $La_{0.5}Sr_{0.5}CoO_3$ reveals that its structure remains unaltered after H_2/O_2 recombination (Table 48), and oxide reduction did not take place. This is true since the reaction takes place by alternate reduction and oxidation of the oxide surface.

8.6 Discussion.

From Table 44, it could be tentatively suggested that the support $La_{0.5}Sr_{0.5}CoO_3$ participating in the H_2/O_2 recombination only when the reaction temperature was raised significantly high (e.g. 130°C).

The specific Pt activity for $Pt/La_{0.5}Sr_{0.5}CoO_3$ (Figs. 63 & 63) is independent of variations in the Pt loading when the temperature is relatively high (135°C). The experimental evidence thus favours an explanation of the temperature effect for H_2/O_2 combination/recombination using $La_{0.5}Sr_{0.5}CoO_3$ catalyst at atmospheric pressure.

Recalling the results of Chapter 7, the promotional effect of platinized $NiCo_2O_4$ and Co_3O_4 for H_2/O_2 recombination is in fact temperature dependence. However, a considerable advantage could be gained from a general survey of the reaction temperature for the three oxides. For example, at 70°C, their relative catalytic activity is as follows :

$$Co_3O_4 > NiCo_2O_4 > La_{0.5}Sr_{0.5}CoO_3$$

The difference in activity is probably due to the different concentration of cobalt ions in each oxide and/or surface area effect. These will form part of the investigations considered in Chapter 9.

The catalytic oxidation of hydrogen by $La_{0.5}Sr_{0.5}CoO_3$ takes place by oxidation-reduction of the oxide surface. The scheme is supported by X-ray analysis of the catalyst before and after H_2/O_2 recombination as shown in Table 48 . The possible mechanisms for water synthesis from hydrogen and oxygen are therefore similar to those outlined in section 7.7 .

Generally, the catalysed reaction between hydrogen and oxygen has been extensively studied by a number of authors[154-158]. But the mechanism[159] of the hydrogen/oxygen reaction is probably not fully understood even today.

Finally, the 50% Sr-doped $LaCoO_3$ was chosen for this study, is

mainly due to the fact that the high-temperature gas-phase heterogeneous catalysis for $La_{0.5}Sr_{0.5}CoO_3$ has been reported to be superior for oxygen reduction[160], and the work on Sr-doped lanthanum cobalt oxide by Tseung and Bevan[161].

CHAPTER 9

CATALYTIC ACTIVITY OF LITHIUM DOPED COBALT OXIDE.

CHAPTER 9

9 CATALYTIC ACTIVITY OF LITHIATED DOPED COBALT OXIDE.

9.1 Introduction.

The use of various lithiated Co_3O_4 is to study the factors affecting the catalytic activity towards H_2/O_2 combination/recombination. The important parameters such as the specific surface area of catalyst, dopant concentration and conductivity will be examined. Generally, the introduction of lithium ion into oxide lattice (e.g. Co_3O_4) tends to increase the specific conductivity significantly. Using the freeze-dried preparative method, the catalytic activities of Co_3O_4 and lithiated Co_3O_4 will be compared under the same experimental conditions.

9.2 Preparation.

Four different concentration of dopants in Li-doped Co_3O_4 were prepared by freeze-drying method as described in section 3.3.2.2.1. Each sample of Li-doped Co_3O_4 was prepared using the stoichiometric cation quantities and the starting materials were "Analar" hydrated salts, e.g. $Co(NO_3)_2.6H_2O$ and $LiNO_3.3H_2O$. All samples were sintered in air at 500°C for 10h . The preparation of each sample took about one week.

9.3 Characterization.

9.3.1 BET Surface Area and X-ray Analysis.

The specific surface areas of the Li-doped Co_3O_4 samples were determined by BET techniques (section 4.5.2) and all results are

shown in Table 51.

The X-ray powder diffraction patterns however show that the d-spacings of Li-doped Co_3O_4 are similar to those fo Co_3O_4 (see Table 12) , demonstrating the addition of Li^+ into lattices does not affect the spinel phase of Co_3O_4 .

9.3.2 Atomic Absorption.

It was not possible to differentiate between samples of varying Li content by reference to their X-ray powder diffraction patterns.

Li-doped Co_3O_4 is very resistant to dilute acids but dissolves in concentrated acids. In contrast, the free lithium is soluble in dilute acetic acid at 60^oC . Therefore, by boiling Li-doped Co_3O_4 under reflux in aqua regia it can be completely dissolved. Atomic absorption (AA) was then used to analyse the lithium concentration in the various solutions. The AA instrument was pre-calibrated.

After removing the free lithium, 0.25g of Li-doped Co_3O_4 was heated in aqua regia at $\sim 100^oC$. The solution was then diluted to 250 cc in a volumetric flask before analysis.

9.3.3 Electrical Conductivity.

The conductivity of Li-doped Co_3O_4 was measured using the method outlined in section 8.3.2 . In general, the conductivity increases proportionally with dopant concentration.

9.4 Experimental.

The freeze-dried Li-doped Co_3O_4 samples were used as H_2/O_2 recombination catalysts. At a given temperature (e.g. 88^oC) and atmospheric pressure, the rates of H_2/O_2 recombination were determined using the procedure fully described in section 7.4.1 .

Li-doped Co_3O_4 (atomic %)	Conc. of Li in $Li_xCo_{3-x}O_4$ (Wt %)
0	0.000
1	0.087
2	0.175
4	0.356
6	0.540
8	0.735
10	0.924

TABLE 49 Wt % of Li in Li-doped Co_3O_4 (theoretical)

Conc. of Li in $Li_xCo_{3-x}O_4$ (Wt %)	Li-doped Co_3O_4 (atomic %)
0	0
0.078	0.8
0.255	2.8
0.735	8.0

TABLE 50 Atomic % doping in Li-doped Co_3O_4

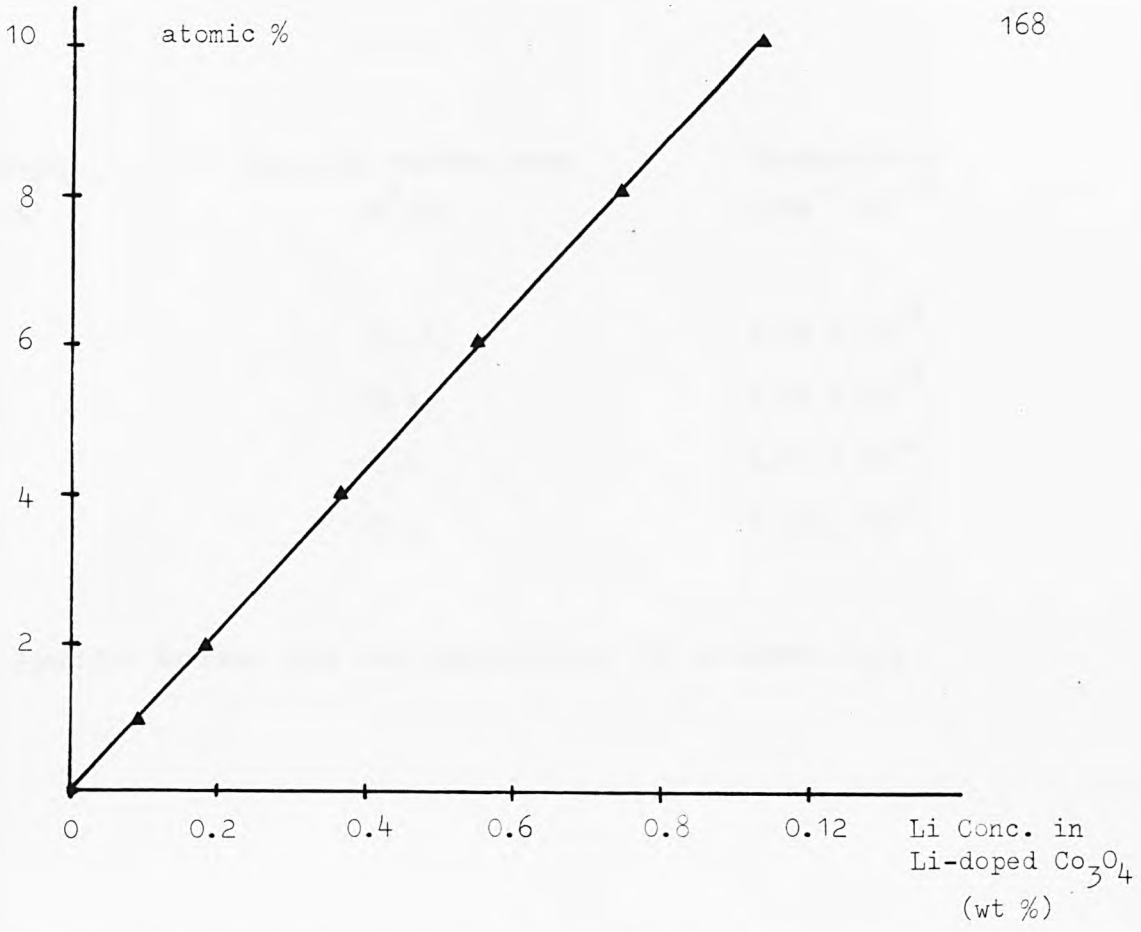

Fig. 64 Calibration graph for the determination of atomic % in Li-doped Co_3O_4.

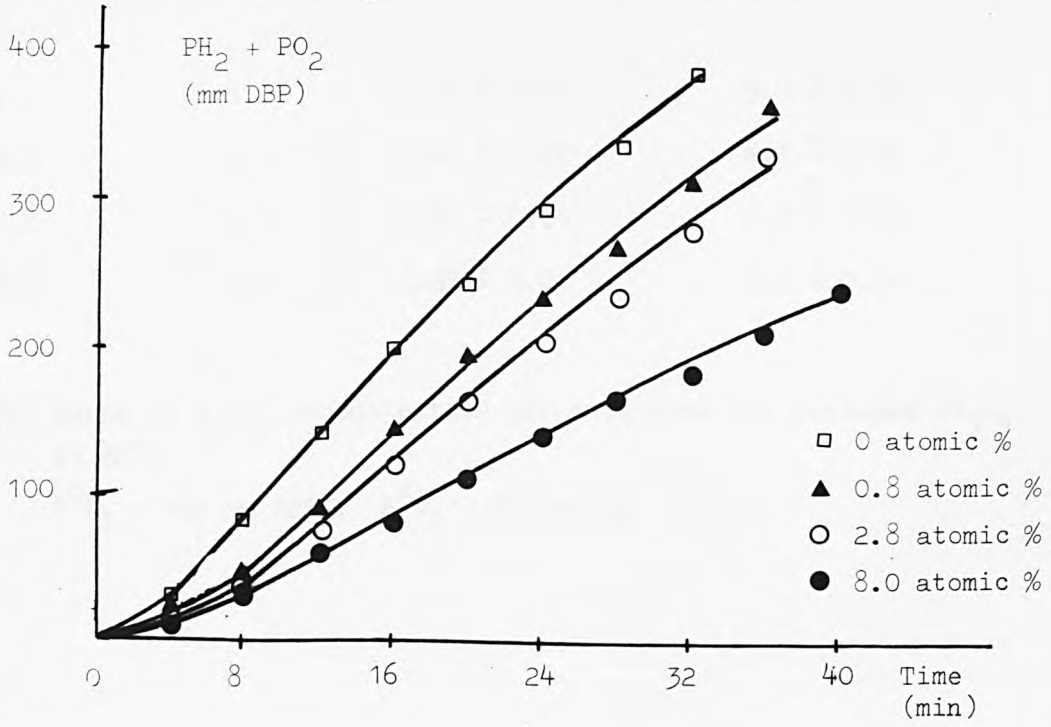

Fig. 65 Rates of H_2/O_2 recombination for Li-doped Co_3O_4 at 88°C, P^oH_2 = 467 mm DBP, P^oO_2 = 200 mm Hg.

Li-doped Co_3O_4 (atomic %)	Specific surface area (m^2/g)	Conductivity ($ohm^{-1}\ cm^{-1}$)
0	20.5	2.04×10^{-3}
0.8	19.8	1.05×10^{-2}
2.8	18.6	4.01×10^{-2}
8.0	17.2	1.53×10^{-1}

TABLE 51 Specific surface area and conductivity of Li-doped Co_3O_4

Li-doped Co_3O_4 (atomic %)	Surface area (SA) ($m^2/0.3g$)	Rate of H_2/O_2 recombination (R) ($cc\ min^{-1}$)	$\frac{(R)}{(SA)}$ ($\times 10^{-2} cc\ min^{-1}\ m^{-2}$)
0	6.2	0.56 ± 0.01	9.0 ± 0.02
0.8	5.9	0.48 ± 0.02	8.1 ± 0.04
2.8	5.6	0.38 ± 0.01	6.8 ± 0.02
8.0	5.2	0.27 ± 0.01	5.2 ± 0.02

TABLE 52 Rates of H_2/O_2 recombination per unit area for Li-doped Co_3O_4 at $88^\circ C$

$P^\circ H_2 = 467$ mm DBP , $P^\circ O_2 = 200$ mm Hg

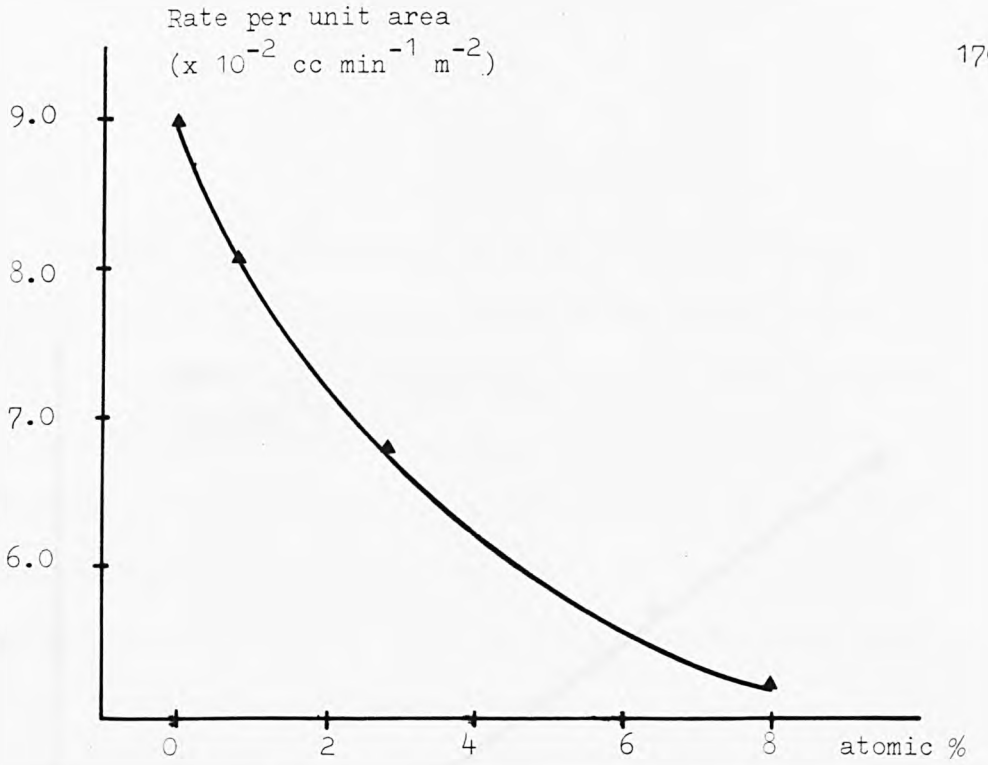

Fig. 66 Rate of H_2/O_2 recombination per unit area Vs atomic % of Li in Li-doped Co_3O_4 at 88°C.

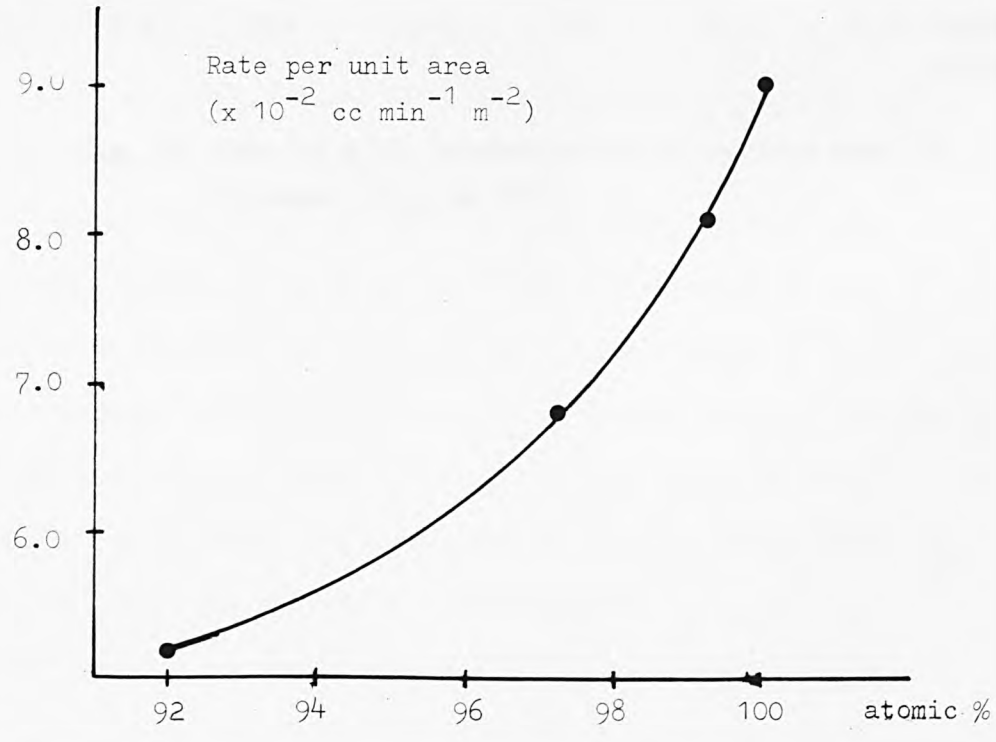

Fig. 67 Rate of H_2/O_2 recombination per unit area Vs atomic % of Co in Li-doped Co_3O_4 at 88°C.

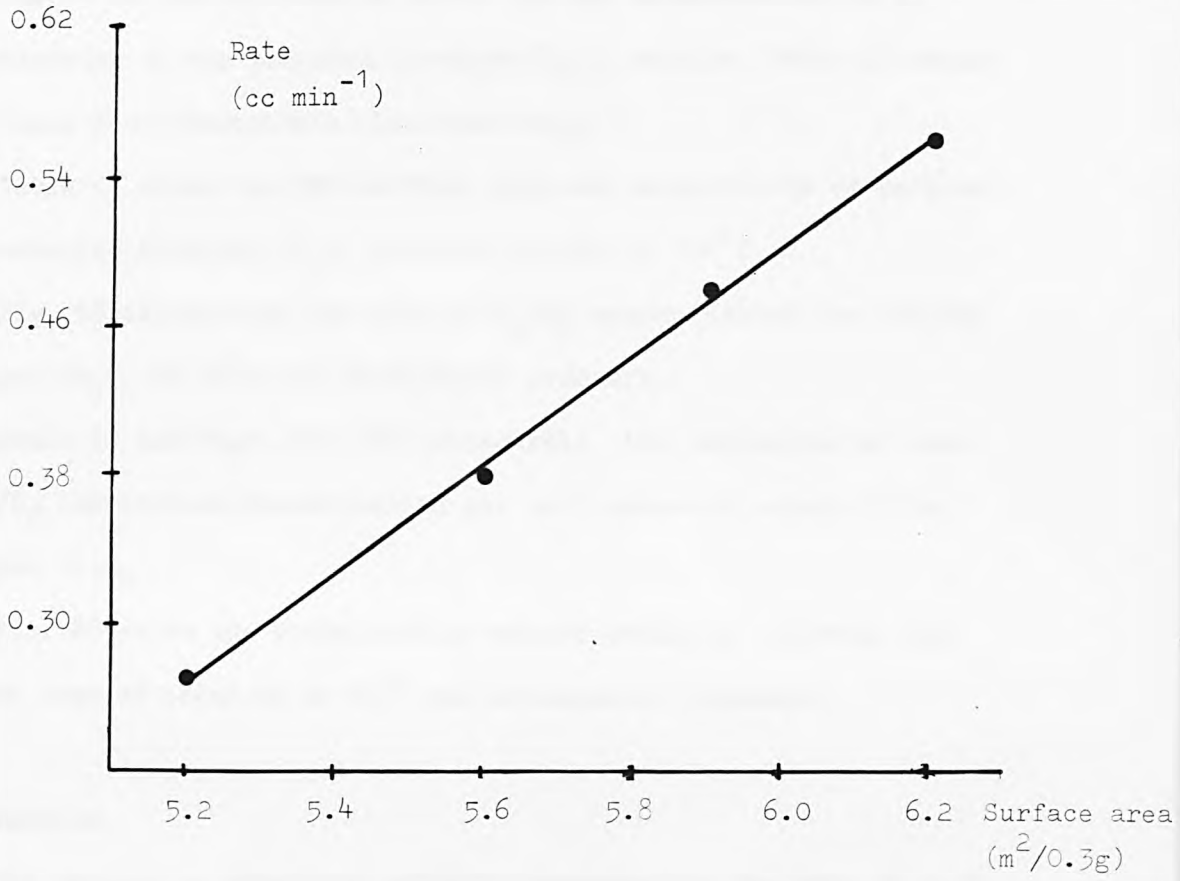

Fig. 68 Rate of H_2/O_2 recombination Vs surface area of Li-doped Co_3O_4 at 88°C.

9.5 Results.

Table 49 shows the theoretical wt % of Li in Li-doped Co_3O_4 and Fig. 64 is the calibration curve for the determination of Li concentration in the prepared Li-doped Co_3O_4 samples. Table 50 shows the atomic % of freeze-dried Li-doped Co_3O_4 .

Table 51 shows the BET surface area and conductivity of various freezed-dried Li-doped Co_3O_4 sintered in air at 500^oC .

Fig. 65 illustrates the rate of H_2/O_2 recombination for various Li-doped Co_3O_4 at 88^oC and atmospheric pressure.

Table 52 and Figs. 66 & 67 demonstrate the variations of rate of H_2/O_2 combination/recombination per unit area with atomic % in Li-doped Co_3O_4 .

Fig. 68 shows the relationship between catalytic activity and surface area of catalyst at 88^oC and atmospheric pressure.

9.6 Discussion.

The decline in catalytic activity (measured by the rate of H_2/O_2 recombination) for Li-doped Co_3O_4 could be attributed to the effect of catalyst surface area (Fig. 68) and/or cobalt ion concentration.

When the Co ion in Co_3O_4 is progressively replaced by Li ion, the activity also decreases as shown in Table 52 and Figs. 66 & 67. However, the decrease in catalytic activity is not directly proportional to the change in Co concentration (Fig. 67) . This could be due to the influence of Co^{2+} and/or Co^{3+} ions, as in lithiated Co_3O_4 some Co^{2+} become Co^{3+} in order to restore charge neutrality.

At higher lithium concentration, comparatively more Co^{2+} being promoted to Co^{3+} resulting in further decrease in catalytic activity (Table 52). It appears that the Co^{2+} is important in this reaction,

indicating the oxidation of Co^{2+} by oxygen is slow. This is true in the case of Co_3O_4 as show by Mamedov[26] et al that the interaction of hydrogen and oxygen takes place by alternate reduction and oxidation of the oxide surface at high temperatures (e.g. 70°C for Co_3O_4), with a difficult stage of reaction of hydrogen with the catalyst oxygen. Surface reactions are usually carried out at temperatures high enough to obtain rapid rates of reaction[162].

The results thus show conclusively that the catalytic activity of lithiated Co_3O_4 depends on :

(a) specific surface area

(b) dopant concentration and

(c) the influence of Co^{2+} and/or Co^{3+} ions.

This investigation has demonstrated that the activity of Co_3O_4 is greater than that of lithiated Co_3O_4 under the experimental conditions.

CHAPTER 10

GENERAL CONCLUSIONS AND RECOMMENDATIONS FOR FUTURE WORK.

10.1 The Life and Reliability of Catalysts.

10.2 Modification of Hydrocaps.

10.3 Promotional Effect of Metal Oxide Support.

10.4 Suggestions for Future Work.

CHAPTER 10

10 GENERAL CONCLUSIONS AND RECOMMENDATIONS FOR FUTURE WORK.

10.1 The Life and Reliability of Catalysts.

The hydrogen/oxygen recombination catalysts in the commercial hydrocaps fixed to a secondary battery tend to suffer from " start-up " problems. This is particularly severe when the catalyst ages and eventually ceases to function normally. The problem is solved principally by the incorporation of a valve system to isolate the catalyst from the free-space during off charge period. In this way, any water arising out of the slow reaction of residual hydrogen and oxygen on the surface of the catalyst is effectly kept to minimum.

Generally, catalyst failure is due to flooding by a thin film of water on the catalyst surface since catalytic activity was fully restored after the catalyst had been dried in an oven.

The life of catalysts is further optimised by avoiding water vapour being condensed on the catalyst. This arises from the gradual evaporation of water droplets on standing. Several water droplets were normally found lying on the sides of the hydrocap. However, the use of high surface area NiO as packing material is :

(a) capable of adsorbing water vapour from its surrounding by capillary condensation so as to reduce condensation of water on the catalyst, and

(b) itself capable of catalysing H_2/O_2 recombination at low temperatures (e.g. $50^{\circ}C$) .

The results show conclusively that after each charging cycle the catalyst in hydrocap fixed to a secondary battery remains dry and its activity restored.

10.2 Modification of Hydrocaps.

The modified hydrocaps consist of small apertures for the ingress of air and thus oxygen to the catalyst bed. This is especially useful in situations where there is a shortage of oxygen. Not only such invention is suitable for battery systems but also in cases where hydrogen is to be removed from a gas stream.

10.3 Promotional Effect of Metal Oxide Support.

The catalyst " start-up " problem has been successfully solved, and a specially designed hydrocap to provide an external source of oxygen as already noted. The Pd or Pt dispersed on metal oxides (e.g. $Pt/NiCo_2O_4$) exhibit pronounced catalytic activity than the commercially used catalyst, Pd/Al_2O_3 . Mechanistic studies demonstrate that the metal oxides as active support only participate in H_2/O_2 recombination at high temperatures, and the reaction takes place by alternate reduction and oxidation of the catalyst surface.

From the above discussion, not only the life and reliability of the catalyst can be improved but also its efficiency can be increased substantially by using an active support. For examples, platinized Co_3O_4 or $NiCo_2O_4$.

10.4 Suggestions for Furture Work.

Further developments could include :

(a) to evaluate other metal oxides for H_2/O_2 interaction activity, particularly at low temperatures.

(b) to investigate the effect of different oxidation states of cations (metal oxides) involved in H_2/O_2 recombination.

REFERENCES

1. C.A.Hampel, The Encyclopedia of Electrochemistry, P92, Reinhold Publishing Corporation, New York (1964).

2. J.O'M. Bockris, B.E.Conway, E.Yeager and R.E.White, Comprehensive Treatise of Electrochemistry, 3 , P372 , Plenum Press, New York (1981).

3. D.H.Collins, Power Sources 5, P218 , Academic Press Inc. Ltd., London (1975).

4. Oldham British Patent No. 1181399 (1970).

5. Ibid.; No. 1181400 (1970).

6. J.Thompson, Power Sources 8, P532 , Academic Press Inc. Ltd., London (1980).

7. Oldham British Patent No. 1188952 (1970).

8. B.S.Hobbs and A.C.C.Tseung , J.Electrochem. Soc., 119 , 580 (1972).

9. Ibid.; 120 , 766 (1973).

10. B.S.Hobbs and A.C.C.Tseung, Nature, 222 , 556 (1969).

11. M.Ladacki, T.J.Houser and R.W.Roberts, J.Catal., 4 , 239 (1965).

12. G.K.Boreskov, M.G.Sliniko and A.G.Filippova, Dokl. Akad. Nauk SSSR, 92 , 353 (1953).

13. T.J.Jennings, H.H.Voge and W.E.Armstrong, J.Catal., 24 , 493 (1972).

14. G.K.Boreskov, J.Chim. Phys., 51 , 759 (1954) ; Chem. Abstr., 49 , 7350 (1955).

15. G.K.Boreskov, M.G.Sliniko and V.S.Chesalova, Zh. Fiz. Khim., 30 , 2787 (1956) ; Chem. Abstr. 51 , 13539 (1957).

16. I.Langmuir, J.Am.Chem. Soc., 37, 1165 (1915).

17. D.E.Mears and R.C.Hansford, J.Catal., 9 , 125 (1967).

18. V.E.Ostrovskii, Kinetika i Kataliz, 8 , 371 (1967).

19. G.A.Somorjai, The Structure and Chemistry of Solid Surfaces, PP51.1 - 51.10 , John Wiley & Son, Inc., London (1969).

20. J.F.Read, Can., J.Chem., 50 , 490 (1972).

21. J.F.Read and R.E.Conrad, J.Phys. Chem., 76 , 2199 (1972).

22. J.F.Read, L.G.Dunfield, R.M.Shreve and E.A.Spinney, J.Catal., 33 , 335 (1974).

23. T.T.Bakumenko, Kinetika i Kataliz, 6 , 61 (1965).

24. T.T.Bakumenko and I.T.Chashechnikova, Ibid.; 10 , 651 (1969).

25. E.A.Madedov, V.V.Popovskii and G.K.Boreskov, Ibid.; 11 , 799 (1970).

26. Ibid.; 11 , 807 (1970).

27. N.N.Bulgakov, Z.R.Ismagilov, V.V.Popovskii and G.K.Boreskov, Ibid.; 11 , 520 (1970).

28. E.A.Mamedov, V.V.Popovskii and G.K.Boreskov, Ibid.; 10 , 697 (1969).

29. U.S.Patent 2687449 (1954).

30. A.C.C.Tseung, T.M.Ho and C.Elbeik, Prov. Brit. Pat. Application No. 8228577.

31. G.I.Brown, Introduction to Physical Chemistry, P355 , Longmans, London (1964).

32. W.J.King and A.C.C.Tseung, Electrochim . Acta, 19 , 485 (1974).

33. Ibid.; 19 , 493 (1974).

34. A.C.C.Tseung, J.Electrochem. 125 , 1660 (1978).

35. G.C.Bond, Catalysis by Metals, PP 4-6 , Academic Press, London (1962).

36. Ibid.; PP 105 - 108 .

37. Ibid.; PP 447 - 450 .

38. Ibid.; PP 39 - 44 .

39. A.J.B.Robertson, Catalysis of Gas Reaction by Metals, P101, Logos Press Ltd., London (1970).

40. G.C.A. Schuit and L.L.Van Reijen, Adv. Catal., 10 , 243 (1958).

41. I.E. Adadurov, I.I.Rivlin and N.M.Kovalev, J.Phys. Chem., 8 , 147 (1936).

42. E.B.Maxted and S.Akhtar, J.Chem. Soc., 1995 (1960).

43. G.C.Bond, Catalysis by Metals, PP 173 - 174, Academic Press, London (1962).

44. W.A.Bone and R.V.Wheeler, Phil. Trans., 206 , 1 (1906).

45. H.G.Tanner and G.B.Taylor, J.Am. Chem. Soc. 53 , 1289 (1931).

46. S.J.Stephens, J.Phys. Chem. 63 , 188 (1959).

47. G.I.Brown, Introduction to Physical Chemistry, PP 545 - 548, Longmans, London (1964).

48. G.W.Castellan, Physical Chemistry, PP 118 - 131, Addison- Wesley Publishing Company, Inc., London (~~9164~~ 1964).

49. Ibid.; PP 152 - 165 .

50. T.M.Lowry and A.C.Cavell, Intermediate Chemistry, PP 549 - 553, Macmillan and Co. Ltd., London (1968).

51. G.W.Castellan, Physical Chemistry, PP 559 - 579, Addison-Wesley Publishing Company, Inc., London (1964).

52. F.Prescott, Intermediate Chemistry, P. 17, University Tutorial Press Ltd., Cambridge (1965).

53. I.Langmuir, J.Am. Chem Soc., 34 , 860 (1912).

54. Ibid.; 38 , 2221 (1916).

55. Ibid.; 40 , 1361 (1918).

56. M.Bodenstein and C.G.Fink, Z.Phys. Chem., 60 , 46 (1907).

57. " Hydrocaps " manufactured by the Hydro-Catylator Corporation, Florida.

58. A.C.C.Tseung and H.L.Bevan , J.Mater. Sci., 5 , 604 (1970).

59. D.B.Hibbert and A.C.C.Tseung, IBid.; 14 , 2665 (1979).

60. V.Ponec, Z.Knor and S.Černy, Adsorption on Solids, P372 , Butterworth Group, London (1974).

61. S.J.Gregg and K.S.W.Sing, Adsorption, Surface Area and Porosity, P130 , Academic Press, London (1982).

62. V.Ponec, Z.Knor and S.Černy, Adsorption on Solids, PP 402 - 404 , Butterworth Group, London (1974).

63. S.J.Gregg and K.S.W.Sing, Adsorption, Surface Area and Pososity, PP 111 - 123 , Academic Press, London (1982).

64. A.W.Adamson, Physical Chemistry of Surfaces, PP 616 - 620, John Wiley & Sons, U.S.A. (1976).

65. E.A.Boucher, J.Mater. Sci., 11 , 1734 (1976).

66. A.A.Liabastre and C.Orr, J.Colloid Interface Sci., 64 , 1 (1978).

67. S.J.Gregg and K.S.W.Sing, Adsorption, Surface Area and Porosity, P 175 , Academic Press, London (1982).

68. E.W.Washburn, Proc. Nat. Acad. Sci., U.S.A., 7 , 115 (1921).

69. F.A.Bettelheim, Experimental Physical Chemistry, PP 368 - 377, W.B.Saunders Company, London (1971).

70. S.Brunauer, P.H.Emmett and E.Teller, J.Am. Chem. Soc., 60 , 309 (1938).

71. S.Brunauer, L.S.Deming, W.E.Deming and E.Teller, Ibid.; 62 1723 (1940).

72. P.H.Emmett and S.Brunauer, Ibid.; 59 , 1553 (1937).

73. P.H.Emmett, Advan. Colloid Sci., 1 , 1 (1942).

74. S.J.Gregg and K.S.W.Sing, Adsorption, Surface Area and Porosity, P26 , Academic Press, London (1982).

75. J.E.Huheey, Inorganic Chemistry, PP 318 - 319 , Harper & Row, Publishers, London (~~9172~~ 1972).

76. H.J. Emeleus and A.G.Sharpe, Modern Aspects of Inorganic Chemistry, PP 57 - 58 , Routledge & Kegan Paul, London (1973).

77. A.Kozawa, Denki Kagaku, 46 , 416 (1978).

78. A.Kozawa, J.Electrochem. Soc., 123 , 1193 (1976).

79. A.Kozawa, U.S.Patent 3893870 (1975).

80. A.Kozawa and K.V.Kordesch, Electrochim. Acta, 26 , 1489 (1981).

81. A.Kozawa and K.V.Kordesch, U.S.Patent 4224384 (1980).

82. A.Kozawa, Denki Kagaku, 44 , 572 (1976).

83. N.C.Cahoon and M.P.Korver, J.Electrochem. Soc., 106 , 745 (1959).

84. G.S.Bell and R. Huber, Ibid.; 111 , 1 (1964).

85. A.Kozawa and J.F.Yeager, Ibid.; 112 , 959 (1965).

86. A.Kozawa, Ibid.; 123 , 1193 (1976).

87. A.Kozawa and R.A.Powers, Ibid.; 113 , 870 (1966).

88. A.Kozawa and R.A.Powers, J.Chem. Ed., 49 , 587 (1972).

89. A.Kozawa and R.A.Powers, J.Electrochem. Soc., 115 , 122 (1968).

90. A.Kozawa and J.F.Yeager, Ibid.; 115 , 1003 (1968)

91. S.A.Abbaro, A.C.C.Tseung and D.B.Hibbert, Ibid.; 127 , 1106 (1980).

92. A.C.C.Tseung and L.L.Wong, J.App. Electrochem. 2 , 211 (1972).

93. W.A.Pliskin and R.P.Eischens, Zeitschrift fur Physikalische Chemie Neue Folge, Bd. 24, s. 11 -23 (1960).

94. K.F.Bouhoffer and A.Farkas, Trans. Faraday Soc., 28 , 242 (1932).

95. T.Takaishi, Z.Physik. Chem., 14 , 164 (~~9158~~ 1958).

96. W.M.H.Sachtler and G.J.H.Dorgelo, Z.Physik. Chim., 25 , 69 (1960).

97. R.Suhrmaun, G.Wedler and H.Gentsch, Z.Physik. Che., 17 , 350 (1958).

98. P.H.Lewis, J.Phys.Chem., 67 , 2151 (1963).

99. M.Boudart, J.Am. Chem. Soc., 74 , 3556 (1952).

100. K.Christmann, G.Ertl and T.Pignet, Surf. Sci., 54 ,365 (1976).

101. A.M.Baro, H.Ibach and H.D.Bruckmann, Ibid.; 88 , 384 (1979).

102. P.R.Norton and P.J.Richards, Ibid.; 44 , 129 (1974).

103. J.G.Aston, E.S.J.Tomezsko and R.A.Fisher, JR., J.Am. Chem. Soc., 86 , 2097 (1964).

104. J.L.Gland, G.B.Fisher and E.B.Kollin, J.Catal., 77 263 (1982).

105. A.J.B.Robertson, Catalysis of Gas Reaction by Metals, P12 , Lagos Press Ltd., London (1970).

106. P.Sabatier, Catalysis in Organic Chemistry, P40 , The Library Press Ltd., London (9123).

107. A.Eucken and W.Hunsmann, Z.Physik. Chem., 44 , 163 (1961).

108. J.H.Espenson, Chemical Kinetics and Reaction Mechanisms, P1 , MeGraw - Hill Book Company, London (1981).

109. T.J.Gray and P.W.Darby, J.Phys. Chem., 60 , 209 (1956).

110. J.F.Read, W.H.Bouma and S.E.Robertson, J.Catal., 19 , 1 (1970).

111. G.V.Antoshin, Kh. M. Minachev and M.E.Lokhuary, J.Catal., 22 , 1 (1971).

112. J.H.Espenson, Chemical Kinetics and Reaction Mechanism, PP 5-7 , McGraw - Hill Book Company, London (1981).

113. G.M.Harris, Chemical Kinetics, PP 41 - 43 , D.C.Heath and Company, U.S.A. (1966).

114. G.I.Brown, Introduction to Physical Chemistry, PP 336 - 339 , Longmans, London (1964).

115. F.A Bettelheim , Experimental Physical Chemistry, P270 , W.B.Sauders Company, London (1971).

116. G.W.Castellan, Physical Chemistry, PP 602 - 607 , Addison - Wesley Pyblishing Company, Inc., London (1964).

117. G.I.Brown, Introduction to Physical Chemistry, PP 322-324, Longmans, London (1964).

118. F.A.Bettelheim, Experimental Physical Chemistry, P281, W.B.Saunders Company, London (1971).

119. W.J.King and A.C.C. Tseung, Brit. Pat., 1461764 (1977).

120. A.C.C. Tseung and K.L.K.Yeung, J.Electrochem. Soc., 125, 1003(1978).

121. E.R.S.Winter, Advan. Catal. Relat. Subj., 10, 196 (1958).

122. G.K.Boreskov, Ibid.; 15, 285 (1964).

123. E.R.S. Winter, J.Chem.Soc., A, 2891 (1969).

124. J.Komuro, H.Yamamoto and T.Kwan, Bull. Chem. Soc. Jap., 36, 1532 (1963).

125. V.A.Roiter and G.I.Golodetz, Ukr. Khim. Zh., 29, 667 (1963).

126. S.Khoobiar, J.Phys. Chem., 68, 411 (1964).

127. J.E.Benson, H.W.Kohn and M.Boudart, J.Catal., 5, 305 (1966).

128. K.M.Sancier and S.H.Inami, Ibid.; 11, 135 (1968).

129. W.Verhoeven and B.~~G.R.H.~~Demon, Acad. Sci. Ser., C262, 33 (1966).

130. K.M.Sancier , J.Catal., 23, 298 (1971).

131. R.A.Gardner, Ibid.; 10, 290 (1968).

132. G.H.Jonker and J.H.Van Santen, Physica,16, 337 (1950).

133. Ibid.; 19, 120 (1953).

134. W.H.Zachariasen, Skrift. Norske . Viden, Akad. Oslo, I.Nat. Naturv. Klasse, 4, 1 (1928).

135. I.Naray - Szabo, Naturwissenschaften, 31, 202 (1943).

136. H.D.Megaw, Proc. Phys.Soc., 58, 133 (1946).

137. S.Roberts, Phys. Review, 76, 1215 (1949).

138. Ibid.; 81, 865 (1951).

139. B.T.Matthias, Phys. Review, 75, 1771 (1949).

140. Ibid.; 76, 430 (1949).

141. F.Galasso and J.Pyle, Inorg. Chem., 2, 482 (1963).

142. V.M.Goldschmidt and H.Hauptmann, Nachr. Ges. Wiss. Gott. Math. - Phys. KI (1932).

143. V.N.Goldschmidt, Geochemische Verteilungsgesetze der Elemente, VII, VIII (1927 - 1928).

144. F.Ashkam, I.Fankuchen and R.Ward, J.Am. Chem. Soc., 72, 3799 (1950).

145. G.H.Jonker, Philips Research Reports, 24, 1 (1969).

146. P.M.Raccah and J.B.Goodenough, Phys. Rev., 155, 932 (1967).

147. J.B.Goodenough, J.Phys. Chem. Solids,6, 287 (1958).

148. C.S.Naiman, R.Gilmore and B.D.Bartolo, J.Appl. Phys., 36, 1074 (1965).

149. G.Blasse, Ibid.; 36 , 879 (1965).

150. G.H.Jonker, Ibid.; 37 , 1424 (1966).

151. R.R.Heikes, R.C.Miller and R.Mazelsky, Physica, 30, 1600 (1964).

152. J.H.Van Santen and G.H.Jonker, Ibid.; 16, 559 (1950).

153. G.H.Jonker Ibid,;22, 707 (1956).

154. F.E.Belles and M.R.Lauver, J.Chem. Phys., 40, 415 (1964).

155. J.E.Benson, H.S.Hwang and M.Boudart, J.Catal., 30, 146 (1973).

156. A.Amariglio and H.Amariglio, Ibid.; 68, 86 (1981).

157. D.M.Collins, J.B.Lee and W.E.Spicer, Physical Review Letters, 35, 592 (1975).

158. I.S.Zaslonko, S.M.Kogarko and E.V.Mozzhukhin, Kinet. Katal. 10, 1197 (1969).

159. G.W.Castellan, Physical Chemistry, PP 620 - 621, Addison-Wesley Publishing Company, Inc., London (1964).

160. H.L.Bevan, Ph.D.Thesis, The City University, London (1970).

161. A.C.C. Tseung and H.L.Bevan, 138th National Meeting of Electrochem. Soc., Atlantic City, October 1970 (Extended Abstract No. 8)

162. D.Gidaspow and R.T.Ellington, A.I.Ch.E Journal., 10, 707 (1964).